




# A Review on Intense Pulsed Light Sintering Technologies for Conductive Electrodes in Printed Electronics

Yong-Rae Jang<sup>1</sup> · Sung-Jun Joo<sup>1</sup> · Ji-Hyeon Chu<sup>1</sup> · Hui-Jin Uhm<sup>1</sup> · Jong-Whi Park<sup>1</sup> · Chung-Hyeon Ryu<sup>1</sup> · Myeong-Hyeon Yu<sup>1</sup> · Hak-Sung Kim<sup>1,2</sup> 

Received: 5 July 2019 / Revised: 11 January 2020 / Accepted: 20 January 2020 / Published online: 15 February 2020  
© Korean Society for Precision Engineering 2020

## Abstract

Intense pulsed light (IPL) sintering or annealing technology has attracted tremendous attention from many researchers and a variety of industries owing to its unique features. In IPL process, the pulsed white flash-light from xenon lamp is irradiated on the target materials and converts it to the desired conductive layer. The IPL process is ambient condition and room temperature process. The irradiated IPL on the materials can induce an extremely quick heating (several milliseconds) to the certain temperature by the synergetic opto-chemical, opto-thermal phenomena without damage on the low temperature substrates such as polymer and paper. The exact mechanisms of these opto-synergetic phenomena has been intensively studied by many researchers for a decade. Also, the applications of IPL techniques have become more extensive in printed electronics. In this review, we summarized the brief history and various applications of the intense pulsed light technology to conductive electrodes as well as several applications. The IPL process can provide a paved route to revolutionary eco-benign and low-cost manufacturing process for many applications.

**Keywords** Intense pulsed light · Conductive paste · Nanoparticles · Metal · Printed electronics

## 1 Introduction

The intense pulsed light (IPL) is the short pulsed white flash-light from xenon lamp covering the entire visible light range with small portion of ultra-violet and a near infrared light as shown in Fig. 1a [1]. There have been several different terminologies to name this process such as an intense pulsed light process (IPL) [1–10], flash-light process [5, 11–43], and photonic curing or photonic sintering process [19, 27, 44–62]. In spite of different terminologies, all of them are using same tool, the milliseconds short pulsed white light from xenon lamp, where the arc plasma was generated with applying the voltage and

current between two tungsten electrodes though an inert xenon gas, followed by generating the pulsed white light [1, 2, 44]. The xenon gas has been generally used to generate IPL as it is the most efficient gas to convert the applied electrical energy to the white light with around 50% of efficiency [63]. Intense pulsed light (IPL) sintering has received the increased attention as an alternative to the conventional sintering techniques [1, 13, 16, 47, 49, 55]. The IPL irradiation from xenon lamp, which emits radiation in the range between 380 and 950 nm, encompassing the entire visible spectrum is available to sinter the metal nano particles because the plasmon resonance bands of metal NPs are in visible spectrum [64–66]. Also, it can immediately reduce the metal oxide and sinter the metal NPs within a few milliseconds at room temperature under ambient conditions [1, 3, 11, 13]. As a conventional sintering method, thermal sintering which directly applies heat to the metal nano ink was mainly used [67]. However, since this method needs high temperature to sinter metal nano inks, it was not suitable for flexible substrates made of polymers. Also, since the thermal sintering method requires a long time to sinter, oxidation occurs in the case of copper nanoparticles [68]. To solve this problem, several

---

This paper is an invited paper.

✉ Hak-Sung Kim  
kima@hanyang.ac.kr

<sup>1</sup> Department of Mechanical Convergence Engineering, Hanyang University, 17 Haengdang-Dong, Seongdong-Gu, Seoul 04763, South Korea

<sup>2</sup> Institute of Nano Science and Technology, Hanyang University, Seoul 04763, South Korea

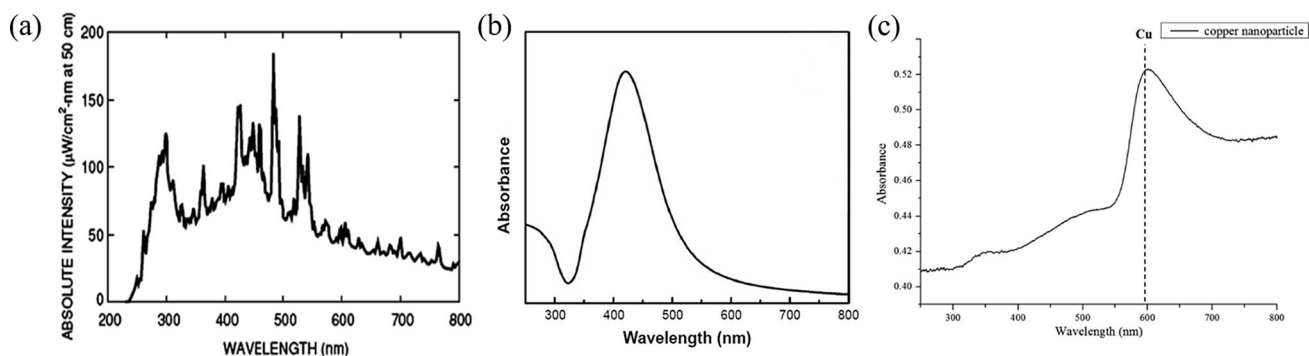


**Fig. 1** **a** Spectrum of the intense pulsed light from xenon flash lamp [1]. UV-vis spectra of **b** silver nanoparticles [92] and **c** copper nanoparticles [37] [a This article is published under an open access license © The Authors 2009; **b** This work is licensed under the Creative Commons Attribution-NonCommercial 3.0 Unported License. To

view a copy of this license, visit <https://creativecommons.org/licenses/by-nc/3.0/> or send a letter to Creative Commons, PO Box 1866, Mountain View, CA 94042, USA; **c** Reprinted with permission from Hwang et al. [37]. Copyright (2016) American Chemical Society]

sintering methods were suggested such as microwave sintering method, electric sintering method, plasma sintering method and laser sintering method [69–75]. Especially, microwave sintering process, which is also called electromagnetic heating process, has been developed to the synthesis and treatment of various nano-materials [76–80]. However, these methods still had drawbacks in that complicated equipment was required or the sintering range was narrow. Therefore, the sintering method proposed as an alternative method was intense pulsed light (IPL) sintering method. The IPL process is ambient condition and room temperature process and it can transform various organic or inorganic materials to the certain composition or crystal structure exhibiting the desired electrical/chemical/optical properties by irradiating the milliseconds pulsed white light on it. In particular, the IPL process is suitable for various materials such as polymers, metals and ceramic system [81–88]. Research for applying the IPL process to many kinds of metals and ceramic materials has been

continuously conducted, and the scope of the IPL has been expanded. In this work, researches on IPL process using metal materials and various applications were summarized and reviewed. The irradiated IPL on the target materials can induce an extremely quick heating (several milliseconds) to the certain temperature by the synergetic opto-chemical, opto-thermal phenomena between the irradiated IPL and the target materials without damage of the low temperature substrates such as a polymer and a paper. The exact mechanisms of these opto-synergetic phenomenon have been intensively studied by many researchers for a decade.

## 2 IPL Sintering of Metal Particles Ink

The usage of intense pulsed light for sintering of metal particles in printed electronics was firstly introduced by Kinney et al. in their historical patent in 1969 as shown in Fig. 2a

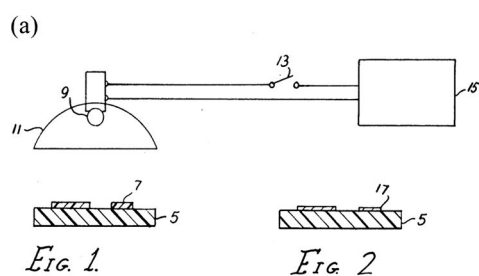
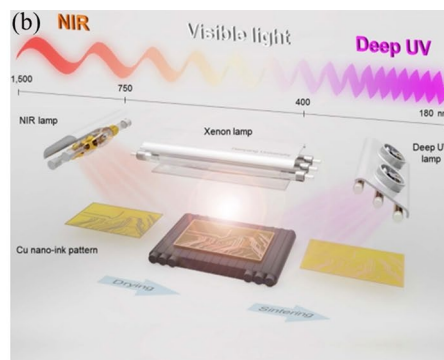


**Fig. 2** Earlier ideas and related schematics on IPL sintering **a** the schematic on first concept of IPL sintering process in U.S. patent 1969 [2]; **b** developed IPL sintering process [11]. [a Open access patent. **b** This work is licensed under the Creative Commons Attribution



4.0 International License. To view a copy of this license, visit <https://creativecommons.org/licenses/by/4.0/> or send a letter to Creative Commons, PO Box 1866, Mountain View, CA 94042, USA.]

[2]. In this patent, they showed that the IPL from xenon lamp could sinter the metal particles or metal precursors on the low-temperature polymer substrate successfully. They also showed that the reduction of the various metal oxides such as copper oxide, silver oxide and lead oxide, was even possible without the damage of the heat sensitive polymer substrate by IPL irradiation for the first time in the history. After three decades, in 2002–2003, IPL sintering of the metal nanoparticles were again reported by Miyashita et al. in their patent [89]. They reported that the nano-sized metal particles such as copper, silver and gold can be sintered on the polymer substrates by IPL irradiation on the low-temperature substrates. In 2006, Schroder et al. introduced the first commercialized R&D type IPL sintering machine in their conference paper in order to sinter metal nanoparticles [44]. After these earlier works, many studies on IPL sintering techniques for various conductive inks have been extensively conducted with developed IPL equipment and processes as shown in Fig. 2b [11].

Most metal nanoparticles show surface plasmon resonance in the visible light region electromagnetic wave [90, 91]. Therefore, IPL irradiation on metal nano inks causes localized heating on metal nanoparticles due to surface plasmon resonance. Heated metal nanoparticles are melted and connected. On the other hand, most polymer substrates absorb only in the UV region electromagnetic wave. Furthermore, pulse of IPL is too short to increase temperature of the polymer substrates, which have low thermal conductivity and high heat capacity. Thus, these phenomena make that IPL sintering method can sinter metal nanoparticles without substrate damage. For example, silver and copper nanoparticles, which are mainly used in metal nano-inks, have maximum absorption at wavelengths of 420 nm and 590 nm, respectively (Fig. 1b, c) [37, 92]. However, since the maximum absorption wavelength depends on the particle size, shape, materials and additives of the metal nano ink, it is important to irradiate electromagnetic waves of the appropriate wavelength for the high quality of the IPL-sintered conductive circuit.

## 2.1 Copper (Cu) Based Conductive Ink/Paste for IPL Sintering

Before IPL sintering technique emerged, noble metal-based (gold or silver) nanoparticles had been used in printed electronics due to their high conductivity, oxidation resistance, and low melting point [93–95]. However, cost of the noble metal based nano ink is too high to be used in commercial applications. For this reason, copper particle based ink have been proposed as an alternative way due to high electrical conductivity and cost effectiveness compared with gold or silver [96, 97]. However, most copper particles are easily oxidized at room temperature ambient condition, which makes sintering difficult [68, 98]. For these reasons, IPL

sintering method has been emerged as an alternative way. In earlier studies, Kim et al. reported the effect of IPL irradiation on copper nanoparticles ink and its mechanism in 2009 [1]. In this study, they used commercially available copper nano ink which has copper particles of 5 nm diameter uniformly dispersed in a mixed solvent of ethylene glycol and 2-methoxyethanol with PVP (poly *N*-vinylpyrrolidone) binders.

The use of nanoparticles in IPL sintering have the advantage due to its low melting temperature. The melting temperature of the metal nanoparticles dramatically decreases when the particle size decreases. It is because the nanoparticles have a high surface-to-volume ratio. According to Buffat and Borel [99], it can be calculated by using the Eq. (1):

$$T_m = T_0 \times \left( 1 - \frac{2}{\rho_s L r} \left[ \gamma_s - \gamma_1 \left( \frac{\rho_s}{\rho_1} \right)^{\frac{2}{3}} \right] \right). \quad (1)$$

The copper nano ink was printed over a 10 mm × 10 mm square area on various plastic substrates. The copper film was irradiated by IPL with various irradiation energy conditions from 20 to 50 J/cm<sup>2</sup> at room temperature and ambient condition. As shown in Fig. 3a, the sintered copper film with 40 J/cm<sup>2</sup> of IPL energy showed a dense structure with minimized resistivity at 5 μΩ cm, which is one third that of reported thermally sintered copper nano ink. In addition, IPL can sinter the copper nano ink without oxidation and any damage of plastic substrate due to the short irradiation time of 2 ms. In 2010, Ryu et al. reported the exact reduction mechanism of copper oxide shell with PVP (poly *N*-vinylpyrrolidone) during IPL sintering [3]. They found that IPL irradiation degrades PVP chains and generate the intermediate acid such as primary alcohols, secondary alcohols, carboxyl acid, and acetic acid, which reduce oxide shell of copper nanoparticles [3–5, 12, 68]. and it reduces the copper oxide shell and transform it to pure copper instantly high temperature by IPL irradiation [3].

Hwang et al. studied the IPL sintering process by varying PVP content in copper ink with light irradiation conditions [13]. A real time Wheatstone bridge electrical circuit and a high-speed data acquisition system were used to accurately monitor millisecond of IPL process as shown in Fig. 4a. It appeared that optimal amount of PVP exists for certain amount and certain size of copper nano particles [100]. Also, re-oxidation of copper particles was found by too long or too short pulse width of IPL, and optimized irradiation conditions (irradiation energy, on-time, and off time) was found depending on the amount of PVP during the in-situ resistance monitoring (Fig. 4b–e). In-depth study of amount of PVP according to copper oxide shell thickness was performed by Oh et al. [12]. In this study, it was found that appropriate copper oxide shell thickness for IPL sintering is less than 4 nm thick and the multi-pulse

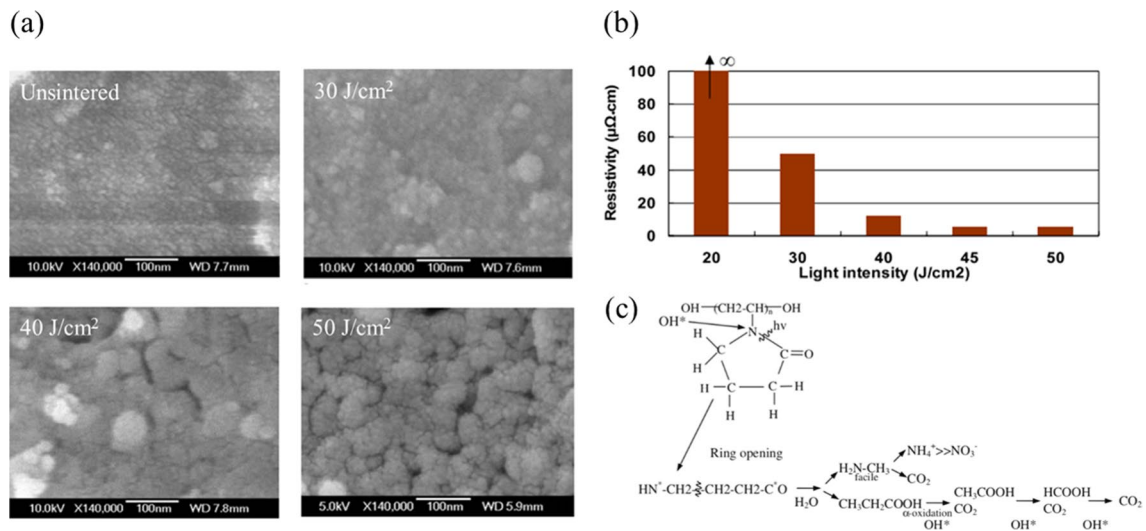


**Fig. 3** **a** SEM micrographs and **b** electrical resistivity of the sintered copper nano inks with respect to light intensity [1]. **c** The photodegradation phenomena of PVP resulting in alcohol or acid [3]. [**a**, **b** This article is published under an open access license © The Authors

2009; **c** Reprinted by permission from Springer Nature Customer Service Centre GmbH: Springer, Journal of Electronic Materials, Reactive sintering of copper nanoparticles using intense pulsed light for printed electronics, Ryu et al. 2011]

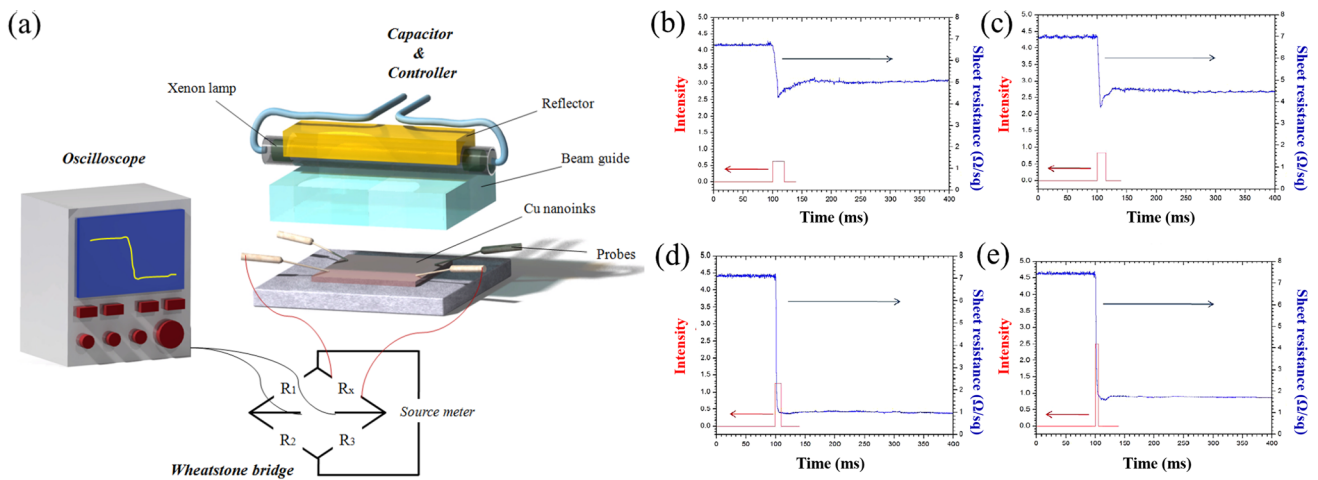


**Fig. 4** **a** Schematic diagrams of the flash-light sintering and the in situ monitoring of the sintering process of copper nano particles. In situ monitoring of the electrical sheet resistance changes of Cu nano films during the flash-light sintering process with on-times of **b** 20 ms, **c** 15 ms, **d** 10 ms, and **e** 5 ms [PVP amount: 0.3 g (weight

ratio: 0.079), irradiation energy: 12.5 J cm<sup>2</sup>, pulse number: 1] [13]. [Nanotechnology by Institute of Physics (Great Britain); American Institute of Physics Reproduced with permission of IOP Publishing in the format Journal/magazine via Copyright Clearance Center.]

pulse light irradiation can effectively reduce the thicker copper oxide shell without damaging the copper film during sintering. In addition, the effect of PVP molecular weight (MW) for the sintering of the copper nano particles was studied by Kim et al. [101]. They found that the copper nano paste were dispersed and sintered well as the PVP MW increased. It was because polymer materials induce dispersion of the solution and their functions increases with increasing MW (Fig. 5a–f).

In order to improve the electrical conductivity, the Cu NP-ink were fabricated with high solid contents adding some additive such as Cu precursor, carbon nanofibers and Cu flake by enhancing the packing density of printed Cu NP-ink pattern [14, 103, 104]. Also, the IPL sintering conditions were controlled to enhance the electrical conductivity [11–13, 16, 18, 35, 36].

The properties of copper nanoparticles paste with mixing different sized nano particles were a studied by Yu et al. [105]. In this work, bimodal copper nano particles (40

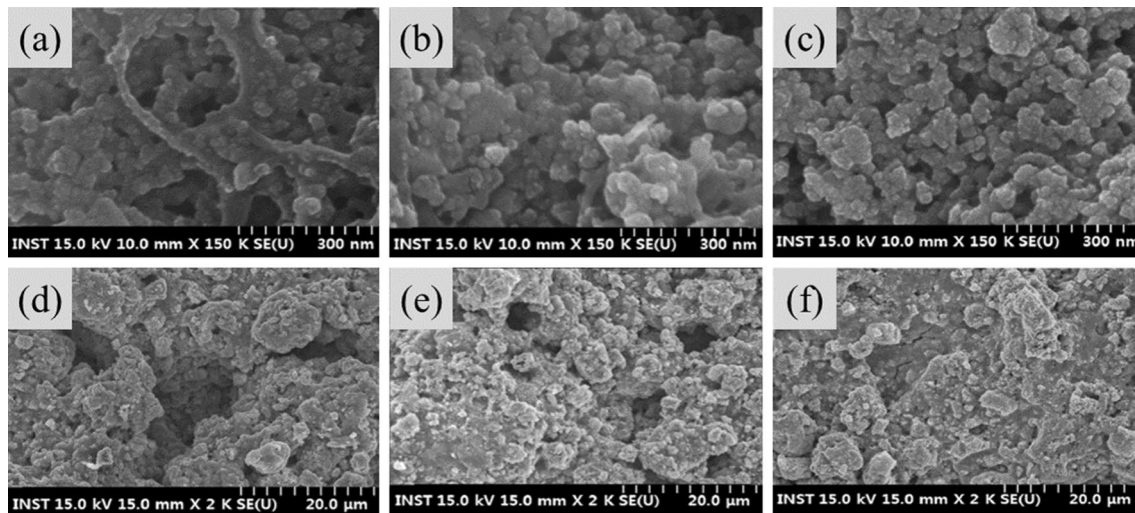


**Fig. 5** The SEM images of unsintered copper nanoparticles with the high magnification; PVP MW **a** 10,000, **b** 40,000 and **c** 55,000 and the low magnification; **d** 10,000, **e** 40,000 and **f** 55,000 [101]. [The effect of poly (*N*-vinylpyrrolidone) molecular weight on flash light

sintering of copper nanopaste, 570, Y.-J. Kim, C.-H. Ryu, S.-H. Park, H.-S. Kim, Part A, Pages 114–122, Copyright (2014), with permission from Elsevier]

and 100 nm diameter) were used to improve conductivity. Among different mixed ratios, the bimodal copper nano ink with 25:75 wt% cases sintered by IPL with multi-pulse light sintering technique was found to be optimal to sufficiently sinter bimodal copper film. The size effect of spherical copper nano particles (20–50 nm diameters) with copper micro particles (2 μm diameter) on IPL sintering was also investigated by Joo et al. (Fig. 6a) [14]. The resistivity of copper micro particles film was higher than that of copper nano particles film because melting temperature of micro particles is much higher than that of nano particles. Interestingly, the mixed copper nano/micro inks with different ratio of copper nano/micro particles were found to have lower resistivity than that of only nano ink or micro ink. Among various mixing ratio, copper nano/micro inks with 50:50 wt% ratio could induce much lowest resistivity than among all other cases due to denser necking structure and smaller pores as shown in Fig. 6a. Similarly, the study using a mixture of copper micro flake and copper nano particle was also reported (Fig. 6c–e) [106]. The film printed with the paste containing bimodal particle and flake could be sintered at a much lower temperature, and the presence of flakes could suppress the formation of cracks during sintering. In addition, flakes have a large number of contact points between the fillers and result in more electrical conduction paths (Fig. 6c–e). As a result, the higher electrical conductivity could be achieved than bimodal with fewer contact points using only particles of spherical type.

As other way for improving the conductivity of the copper electrode, copper precursors ink was studied. Copper precursors are generally used to generate copper nanoparticles

and have been used in various studies. Especially, Patil, S. A. et al. demonstrate a simple, convenient and low cost synthesis method for Cu nanoparticles through the reduction of copper salt in ethylene glycol using rongalite as novel reducing agent as well as capping agent and IPL sintering technique used to archive conductive electrode pattern for printing electrode [107]. There was also an attempt to fabricate green electrodes using cellulose nanocrystals (CNC), graphene nanoplatelets (GNP) and copper precursors via IPL sintering process [108]. However, when used with conductive materials such as copper nano, the copper precursor can also improve the IPL sintering process efficiency. Araki et al. demonstrated the IPL sintering of Cu salt (Cu formate/acetate/oleate) precursor ink based on the ink's light absorption ability [56]. From the relationship between the ratios of C/Cu and the required sintering energy, it is possible to ascertain that integral absorbance coefficients are strongly correlated with the IPL sintering behavior. Finally, the wires formed by sintered Cu formate ink showed a 56 μΩ cm resistivity. Wang et al. demonstrated the IPL sintering of Cu ion ink (Fig. 7a–c) [102]. The Cu ion ink was fabricated using formic acid, citric acid, NH<sub>4</sub>OH and Cu(OH)<sub>2</sub> and it was printed on PI substrate using inkjet printing. The printed Cu ion ink was IPL sintered with 40 J/cm<sup>2</sup> energy. The Cu-patterned film after sintering showed outstanding electrical resistivity 5.27 μΩ cm. Rosen et al. report on using IPL irradiation for obtaining conductive patterns from ink composed of submicron particles of Cu formate, a Cu precursor that has a self-reduction property [109]. Decomposition of Cu formate can be done by IPL irradiation and is affected both by the mode of energy application and the properties of the

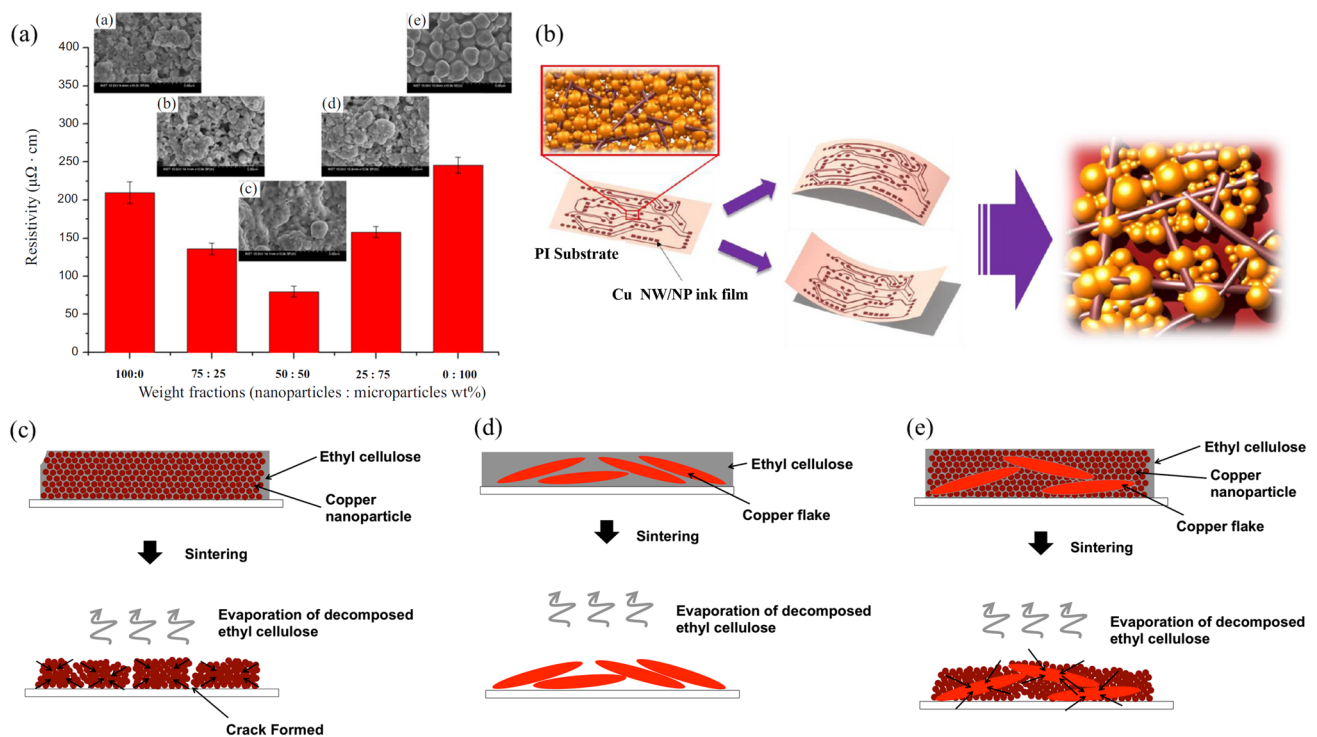


**Fig. 6** **a** The sheet resistance of IPL sintered Cu film with several weight fractions of Cu nano and microparticles and SEM images of the IPL sintered Cu films with different weight fractions [14]. **b** A schematic illustration of the improved reliability of IPL sintered Cu NW/NP ink film under outer bending (tension) and inner bending (compression) conditions [110]. Schematic diagram of sintering for paste consisting of **c** copper nano particles; **d** copper flakes; and **e** a mixture of copper nanoparticles and flakes [106]. [**a** Nanotechnology

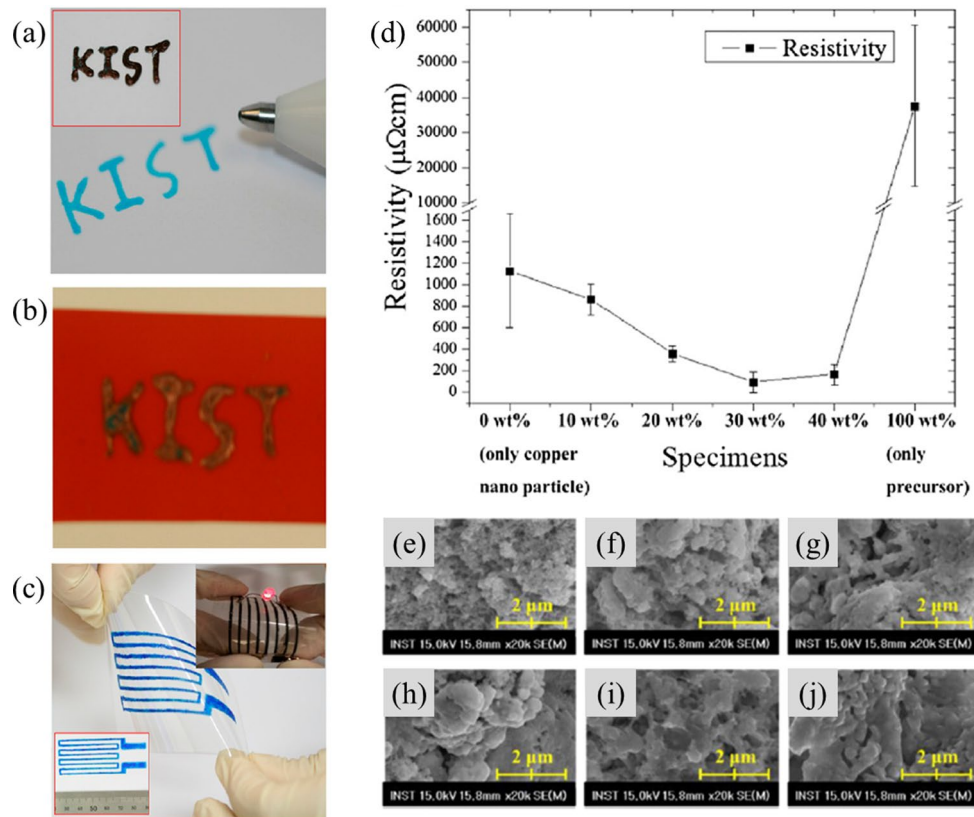
by Institute of Physics (Great Britain); American Institute of Physics Reproduced with permission of IOP Publishing in the format Journal/magazine via Copyright Clearance Center; **b** Reprinted with permission from Joo et al. [110]. Copyright (2015) American Chemical Society; **c** Reprinted by permission from Springer Nature Customer Service Centre GmbH: Springer, Journal of Materials Science, Copper pastes using bimodal particles for flexible printed electronics, Tam et al. [105]]

printed precursor layer. Chung et al. also studied the applicability of the copper precursors ink (e.g., copper(II) chloride, copper(II) nitrate trihydrate, copper(II) sulfate pentahydrate and copper(II) trifluoroacetylacetonate) with the copper nanoparticles in IPL sintering [15]. It was found that different precursor absorbed the different light wavelength region and the decomposition temperature was changed according to the kind of the precursor. As shown in Fig. 7d–j, the addition of the precursor could reduce the pores among the copper according to increase necking.

In addition, Rosen et al. Added copper nano wire and CNT to improve not only conductivity but also mechanical properties. To improve the light absorption, carbon nanotubes were added to the ink and the electrical conductance was improved about 2 times after IPL sintering process [109]. A study with similar effects was also performed by Hwang et al. (Fig. 8a–c) [110]. In this work, they found that optimum CNT weight fractions could improve the conductivity and fatigue resistance of copper nanoparticle ink films by IPL sintering process. In a study reported by Joo et al., copper nano wires was added to copper nano particle inks to improve the electrical conductivity and reliability under

repeatable mechanical fatigue in tension and compression conditions (Fig. 6b) [111]. As a result, the cracks among copper nano particles could be reduced with increasing wt% of copper nano wires, resulting in increased densification and mechanical flexibility of sintered copper nano particle and copper nano wire networks (Fig. 6b).

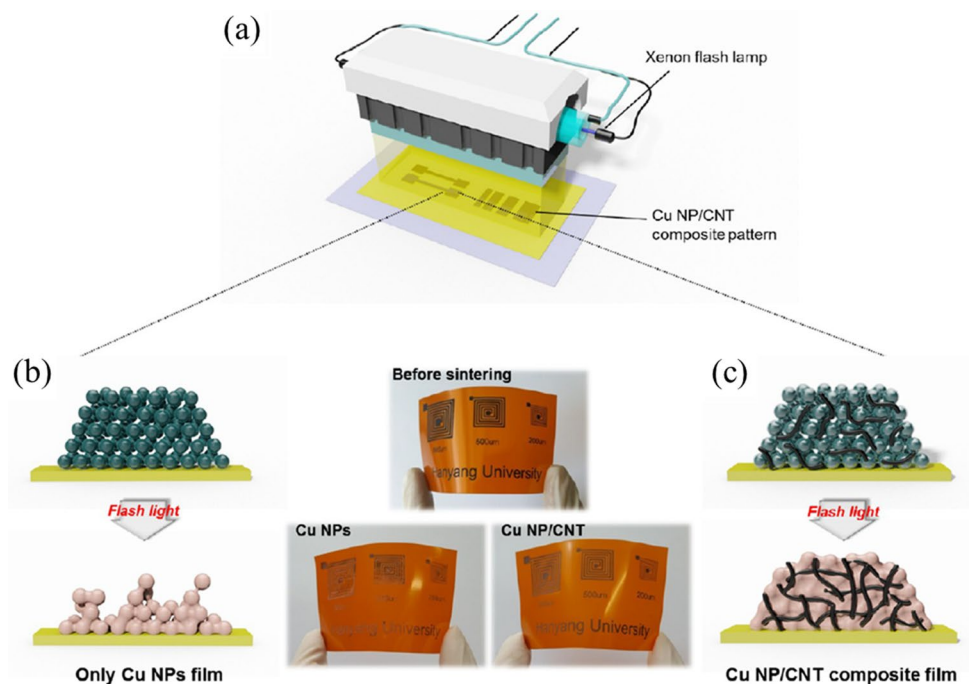
In order to enhance the electrical conductivity, many researchers intensively controlled the sintering conditions and performed the IPL sintering combined with other process. Yu et al. demonstrated the multi-pulsed IPL sintering of bimodal Cu NP-ink for enhancing the electrical conductivity (Fig. 9a) [112]. They experimentally showed the stepwise sintering phenomena of the Cu particles ink with multi-pulsed light sintering process using in-situ resistance measurement setup. Ryu et al. also performed the two-step IPL sintering of Cu NP-ink for high electrical conductivity [36]. They demonstrated that the two-step sintering could enhance the conductivity of the Cu NP-ink film than the one-step sintering process. The optimized two-step IPL sintered ( $12 \text{ J/cm}^2$  preheating followed by  $7 \text{ J/cm}^2$  main sintering) Cu pattern showed  $3.81 \mu\Omega \text{ cm}$  resistivity, which is approximately 2.3 times of that of bulk Cu. Two-step



**Fig. 7** Patterns of the ion ink printed using a roller-ball pen: **a** PET substrate (inset: IPL treated), **b** PI substrate (IPL treated), and **c** PET substrate (inset, upper right: IPL treated) [102]. **d** The resistivity of sintered hybrid copper patterns for copper(II) nitrate trihydrate weight ratio and the SEM image of sintered hybrid copper patterns for weight fraction of copper(II) nitrate trihydrate of **e** 0 wt%, **f** 10 wt%, **g** 20 wt%, **h** 30 wt%, **i** 40 wt%, and **j** 100 wt% (irradiation energy: 10 J/

$\text{cm}^2$ , pulse duration: 10 ms, pulse number: 1) [15]. [a–c Reprinted with permission from Wang et al. [101]. Copyright (2013) American Chemical Society; d–j Reprinted from Flash light sintered copper precursor/nanoparticle pattern with high electrical conductivity and low porosity for printed electronics, Volume 580, W.-H. Chung, H.-J. Hwang, H.-S. Kim, Pages 61–70, Copyright (2015), with permission from Elsevier]

**Fig. 8** Schematics of the IPL sintering system (a), and the shape change comparison of Cu NPs film only (b) and Cu NP/CNT composite film (c) after IPL irradiation [110]. [Reprinted with permission from Hwang et al. [109]. Copyright (2015) American Chemical Society]



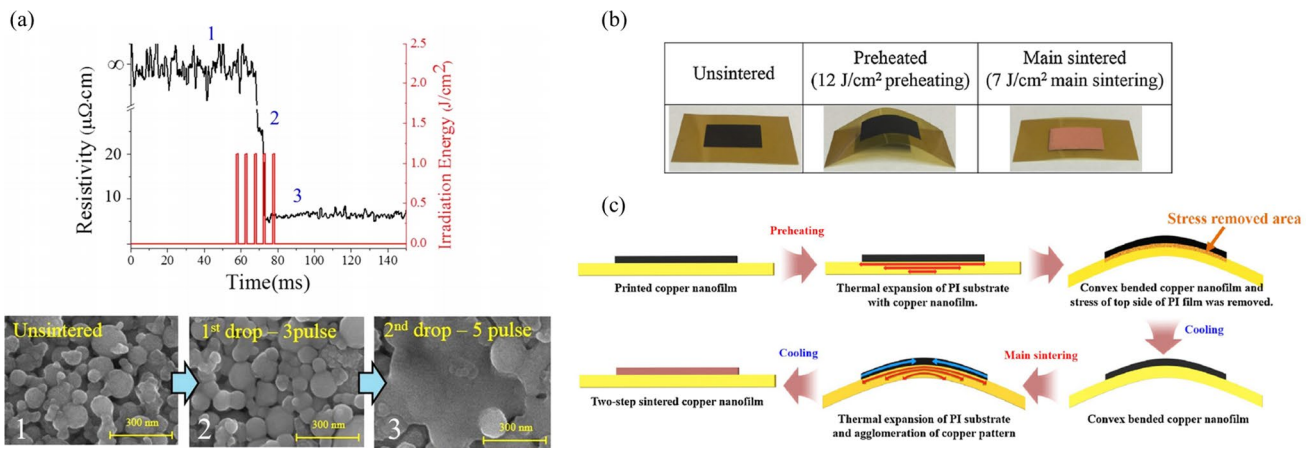


**Fig. 9** **a** SEM images of IPL sintered Cu nano-ink with respect to the pulse number: 1 is unsintered state, 2 is SEM image at 1st drop (after 3 pulse irradiation), and 3 is SEM image at 3rd drop (after 5 pulse irradiation) (irradiation energy:  $6 \text{ J/cm}^2$ , pulse duration: 1 ms, pulse interval: 4 ms and pulse number: 5) [112]. **b** The optical images and **c** schematic diagrams of substrate warpage reduction during two-step IPL sintering process [36]. [a Nanotechnology by Institute of Phys-

ics (Great Britain); American Institute of Physics Reproduced with permission of IOP Publishing in the format Journal/magazine via Copyright Clearance Center; **b, c** Reprinted from Two-step flash light sintering of copper nanoparticle ink to remove substrate warpage, Volume 384, C.-H. Ryu, S.-J. Joo, H.-S. Kim, Pages 182–191, Copyright (2016), with permission from Elsevier]

sintering method was also employed to prevent the warpage of the substrate after IPL sintering [36]. As a result, it was found that a two-step sintering method could sinter the copper electrode on a  $50 \mu\text{m}$  thick PI substrate without warpage (Fig. 9b, c).

Furthermore, Ryu et al. Studied the IPL sintering of copper nano / micro ink by changing the sintering condition in order to reduce the warpage of the substrate [113]. Figure 10a shows the schematics of the IPL sintering system with vacuum heating plate. The vacuum pressure for substrate holding was fixed to 0.2 MPa, and the heating temperature was varied from 25 to  $200 \text{ }^\circ\text{C}$ . When the substrate

heating was applied to the substrate, IPL irradiation was conducted to the specimen after stabilization of specimen temperature. Figure 10b explains the substrate vacuum holding and heating effect on IPL sintering and substrate warpage. In this study, the warpage was differently generated with respect to the heating temperature. When the Cu NP/MP-ink film was IPL sintered with only vacuum condition, significant temperature difference in Cu layer occurred. This temperature difference results in poor morphology of sintered bottom part Cu NP/MP-ink film due to insufficient heat energy. On the other hand, the IPL with heating vacuum holding condition IPL sintered the Cu layer with

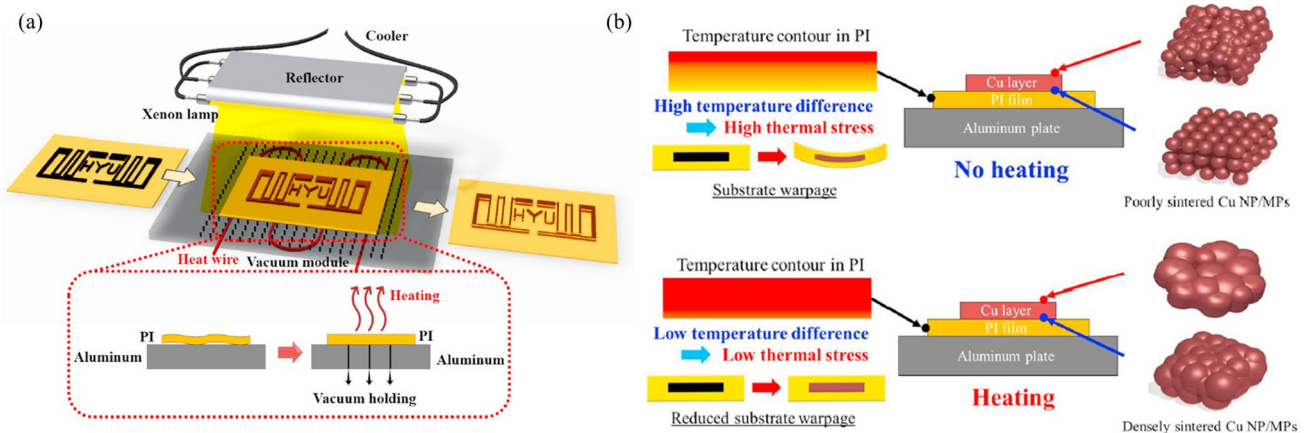


**Fig. 10** **a** Schematic of IPL sintering system with vacuum heating module. Inset figure express substrate heating and vacuum holding. **b** The schematic diagrams of substrate warpage reduction during the

IPL sintering with substrate vacuum heating [113]. [Reprinted from Ryu et al. [112], Copyright (2019), with permission from Elsevier]



low temperature difference, allowing dense structure about top- and bottom-part of Cu layer. Also, low temperature difference in PI layer resulted in reduced warpage after IPL sintering.

To improve the conductivity of the sintered Cu ink, the wavelength of the IPL was controlled or additional light sources were used together during IPL sintering process by several researchers [11, 37]. Hwang et al. reported IPL sintering process combined with deep-UV and NIR irradiation for highly conductive Cu NP-ink (Fig. 11a) [11]. The resistivity of IPL sintered Cu NP-ink film with NIR irradiation was lower than that of only IPL irradiation case. It was noteworthy that deep UV irradiation during IPL sintering could further enhance the reduction and sintering of the Cu oxide shell, because the PVP coating layer was decomposed more effectively under deep UV irradiation. A study was also conducted to improve the quality of the sintered copper nanoparticles by controlling the wavelength range of the light to be irradiated using a band-pass filter (Fig. 11b–d) [37]. The copper nanoparticles were effectively sintered by intensive irradiation in the wavelength range near 590 nm, (from 500 to 600 nm) which is the absorption wavelength of the copper nanoparticles.

Park et al. fabricated highly functioning electrodes composed of Cu, Ni, and Cu/Cu<sub>10</sub>Sn<sub>3</sub> core/shell nanoparticles on PI substrate (Fig. 12a). The IPL sintered ink showed a resistivity of 49  $\mu\Omega$  cm and normalized resistance variation of around 1 after long-term 85/85 test. Also, these electrical properties were also showed well on PET substrates by formation of an thin film Ag NPs layer, which resulted in 53.8  $\mu\Omega$ ·cm with little increase of resistance under 85/85 test [114]. Meanwhile, Son et al. fabricated 1-octanethiol coated Cu nanoparticles (NPs) for prevent oxidation of pure Cu surface (Fig. 12b, c). It showed improved long-term stability against oxidation and durability, sintered Cu patterns showed almost no resistance change over 2 months in the air and 1000 cycles of bending (bending radius: 2.5 mm) [38].

IPL sintering of Cu NPs on silicon wafer substrate has been regarded to be difficult due to its high thermal conductivity ( $k$ ) compared to polymer substrates such as PI. To solve this problem, Hwang et al. applied multiple pulsed IPL to sinter bimodal Cu NPs on silicon wafer (Fig. 13). It was demonstrated that the multi-pulse with 30 pulses and artificial oxidation of Cu NPs were necessary to successfully sinter the Cu NPs on silicon wafer, showing a resistivity of 9.37  $\mu\Omega$  cm [39].

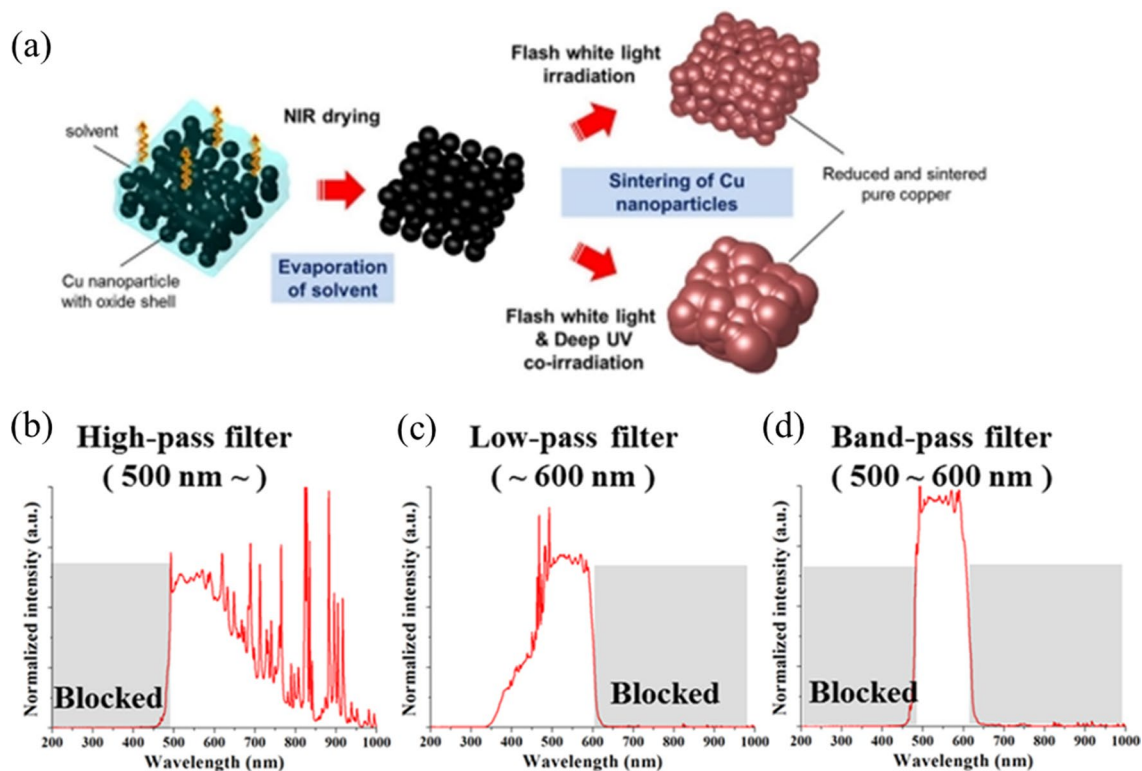


**Fig. 11** **a** The morphology change of Cu nanoparticles in nano-ink during the photonic drying and sintering process [11]. Wavelength spectrum of the IPL **b** with 500 nm high-pass filter, **c** with 600 nm low-pass filter, and **d** 500–600 nm band-pass filter [37]. [a This work is licensed under the Creative Commons Attribution 4.0 Interna-

tional License. To view a copy of this license, visit <https://creativecommons.org/licenses/by/4.0/> or send a letter to Creative Commons, PO Box 1866, Mountain View, CA 94042, USA; **b–d** Reprinted with permission from Hwang et al. [37]. Copyright (2016) American Chemical Society]

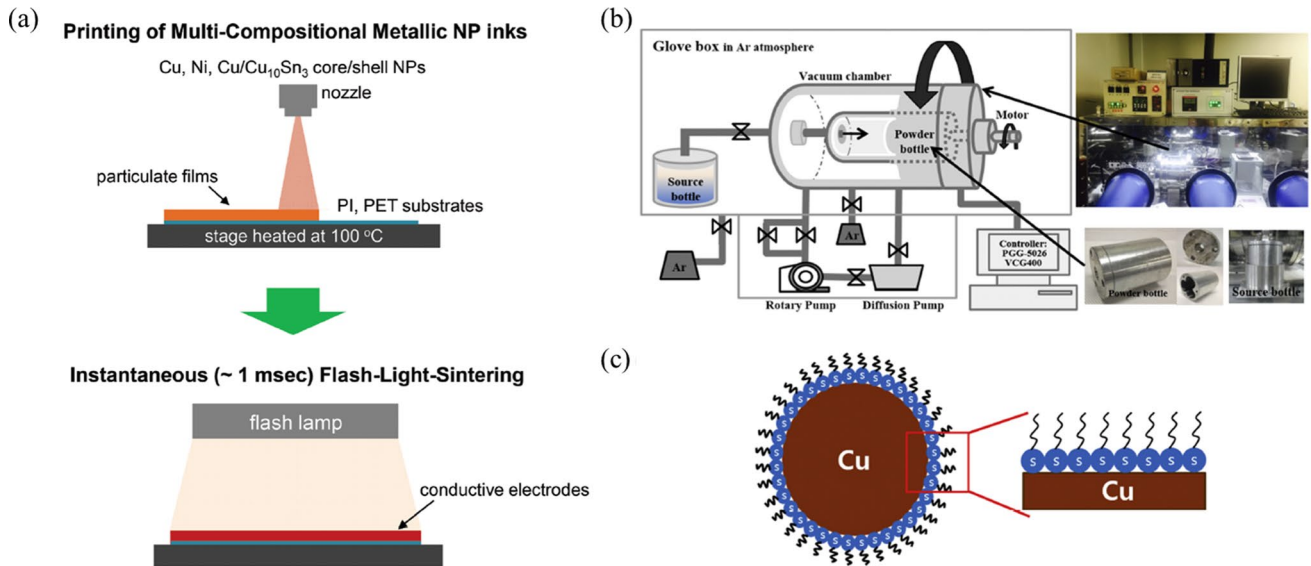
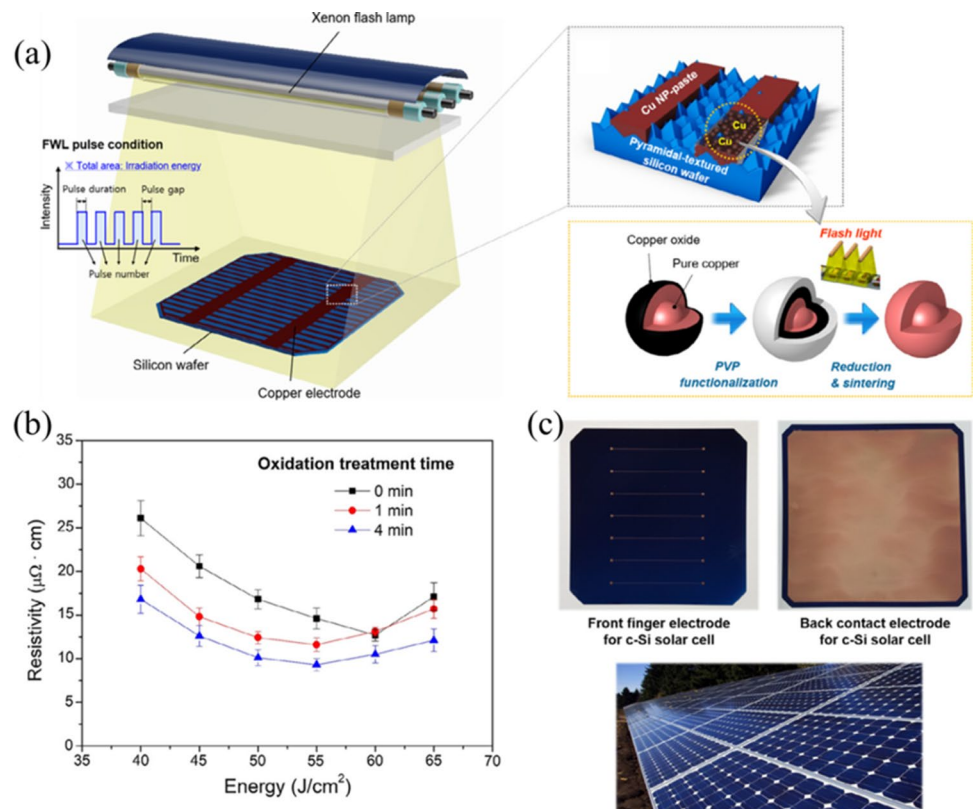


**Fig. 12** **a** Schematic showing the procedures of spray printing and flash-light-sintering to form Cu-based nanoparticle-driven electrodes [114]. Schematic diagrams of **b** the vapor self-assembled multilayers (VSAMs) technique and **c** an 1-octanethiol-coated copper nanoparticle [38]. [a] Nanoscale by National Center for Nanoscience and Tech-

nology; Royal Society of Chemistry (Great Britain), Reproduced with permission of RSC Pub in the format Journal/magazine via Copyright Clearance Center; **b, c** Reprinted from Son et al. [38], Copyright (2018), with permission from Elsevier]

**Fig. 13** **a** Schematics of flash white light sintering process of PVP functionalized Cu NP-pastes on the pyramidal-textured silicon wafer substrate, **b** the resistivity of the bimodal Cu NP-paste with the oxidized Cu NPs, **b** The IPL sintered Cu front finger electrode and back contact electrode for crystalline silicon solar cells [39]. [Reprinted from Hwang et al. [39], Copyright (2018), with permission from Elsevier]



## 2.2 Silver (Ag) Based Conductive Ink/Paste For IPL Sintering

In spite of the low cost of the copper particles, it still has weak resistance of oxidation [115]. Therefore, silver nanoparticles, which are cheaper than gold and more conductive than copper, are suited for the fabrication of ink and has been studied widely.

In 2011, Kang et al. used the intense pulsed light (IPL) to sinter the inkjet-printed silver nanoparticles ink at room temperature [115]. The silver nanoparticles with sizes from 20 to 40 nm in diameter were prepared to fabricate silver inks with a solid content of 50 wt%. The temperature of the printed silver nanoparticles ink pattern increased by 500 °C when the IPL was irradiated with light energy of 50 J/cm<sup>2</sup>. As a result, it was confirmed that the grain size of silver nanoparticles increased three times ( $86.3 \pm 7.2$  nm) after sintering compared to before sintering. The sintered silver nanoparticles film had an average resistivity of  $49 \pm 3$  nΩ · m, and it was suitable for printing electronic technologies such as RFID tags.

Niittynen et al. investigated the three alternative sintering methods, which were plasma, IPL, and laser sintering method and compared their sintering performance [116]. Table 1 showed the qualitative feasibility comparison of the characteristics of each sintering method. IPL method had better conductivity and mechanical performance than that of other sintering due to a more uniform and denser nanostructure as shown in Fig. 14a. The IPL sintered silver film had a resistivity from 3.3–13.6 μΩ · cm and these values were 2.5–5 times the values of bulk silver resistivity. Overall, it was reported that IPL sintering showed the best performance among the methods that could replace traditional thermal sintering.

Galagan et al. showed that the resistivity of silver nanoparticles had a value of 7 times bulk silver after conventional thermal sintering for 6 h at 130 °C [48]. The resistivity of nine times bulk silver was obtained only within 5 s using IPL sintering and this value was similar to that of thermal sintered film (Fig. 14b).

Chung et al. investigated the IPL sintering process of silver nanoparticles inks on PET substrates [16]. The in-situ monitoring was performed for studying IPL sintering

mechanism. As shown in Fig. 14c, the sheet resistance decreased for each pulse until the fourth pulse was irradiated, but there was almost no sheet resistance change after the fourth pulse in ten-pulse case. Therefore, the four pulses were applied in the sintering of printed Ag film. As a result, the IPL sintered silver nanoparticles film was showed 0.95 Ω /sq of sheet resistance, which is two times lower than that (2.03 Ω/sq) of the thermally sintered one for 1 h at 120 °C. Also, there were no damages of PET substrate in case of IPL sintering because of the very short sintering time [17].

The morphology and microstructure of the IPL sintered silver film according to IPL sintering conditions were investigated [7, 18]. As shown in Fig. 15a, it was reported that consecutive light pulsed could induce the delamination of the printed silver nanoparticles during IPL sintering process [7]. It is because the internal vaporization induced from the thermal decomposition of the organic additives at this time could not be exhausted. As shown in Fig. 15b, the microstructures such as film delamination and porosity affect the resistance of sintered silver nanoparticles ink. Also, the cracks formation of nanoparticle film can be critical issue. Several studies have been reported that crack formation and resistivity of the sintered Ag film were affected depending on the substrate [8, 17, 49, 117]. When the Au-nanoparticles ink was IR-sintered, the crack formation was observed in the case of the glass substrate, but not in the paper substrate [117]. The conductivity of film printed on the glass substrate was not measured due to this crack formation, but the resistivity of 25 μΩ cm was measured in film printed on the paper substrate. The adhesion to the paper substrate was better compared to the glass substrate because it was also influenced because of the crack formation of nanoparticles film. Also, the resistivity of silver nanoparticles ink printed on paper was lower than that of the Au nanoparticles ink. This was because there was no crack formation in sintered silver nanoparticles film as shown in Fig. 15c.

Therefore, it is important to reduce or prevent crack formation in order to improve the quality of the sintered silver nanoparticles film. Park et al. investigated the two steps IPL sintering process to reduce crack formation (Fig. 15d) [18]. The first step was preheating step before the main sintering, and 15 rectangular pulses were irradiated having 5 ms on-time with a 30 ms gap between pulses. The second step was

**Table 1** Qualitative feasibility comparison of the resulting conductivity, adhesion, suitability for roll-to-roll processing, temperature and degree of process control for the four tested sintering [116]

Sintering method	Conductivity	Mechanical performance	Roll-to-roll compatibility	Temperature	Controllability
Thermal	+++	+++	--	--	+
Plasma	+	---	---	+++	+
Laser	++	---	++	-	+++
Photonic	+++	+++	+++	---	++

Reprinted from Niittynen et al. [115], Copyright (2014), with permission from Elsevier

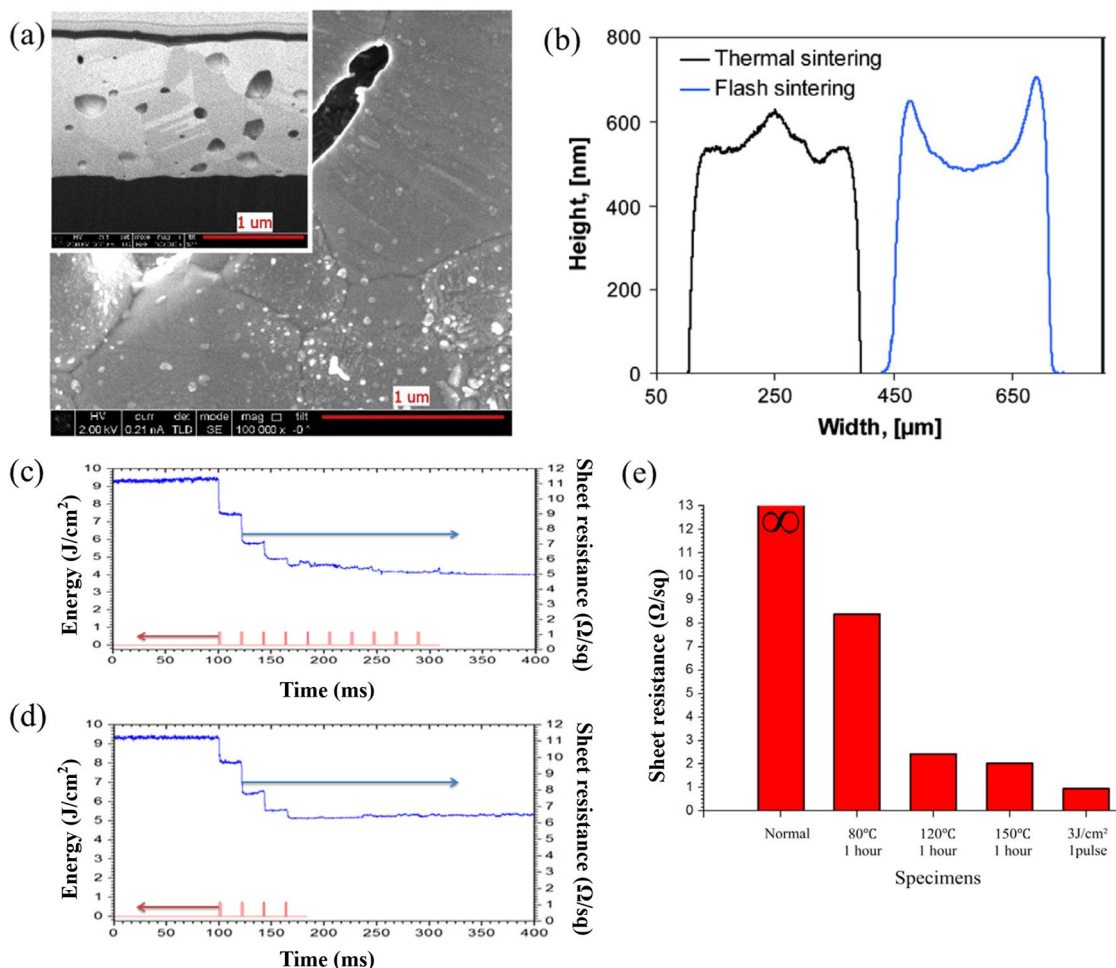


**Fig. 14** **a** Top-view and cross-section SEM images of IPL sintered Ag ink samples. Uniform structure is presented [116]. **b** Typical cross-section profiles of inkjet printed silver lines after thermal (30 min at 130 °C) and flash sintering (5 s) on glass substrate [48]. Comparison of the cases for pulse number 10 and 4 (energy: 0:75 J cm<sup>-2</sup> per pulse). **c** In situ monitoring result for the ten-pulse case. **d** In situ monitoring result for the four-pulse case. **e** The sheet resistances of normal silver nano-inks, thermally sintered silver nano-

inks and IPL sintered silver nano-inks [16]. [**a** Reprinted from Niitynen et al. [115], Copyright (2014), with permission from Elsevier; **b** Reprinted from Galagan et al. [48], Copyright (2013), with permission from Elsevier; **c–e** Nanotechnology by Institute of Physics (Great Britain); American Institute of Physics Reproduced with permission of IOP Publishing in the format Journal/magazine via Copyright Clearance Center.]

the main sintering step, which the single pulse was used, and the total energy was varied from 10 to 20 J/cm<sup>2</sup>. When the 15 J/cm<sup>2</sup> preheating–20 J/cm<sup>2</sup> sintering was performed, the delamination was observed while in the case of the 10 J/cm<sup>2</sup> preheating and 20 J/cm<sup>2</sup>, the silver film was uniformly sintered without pores and became more densely packed because the organic binder was removed smoothly during the preheating step. The silver film showed the resistivity (36.32 nΩ · m) through the optimal two-step IPL sintering process, and it was lower than that of silver film thermally sintered (40.84 nΩ · m).

The multi-pulses sintering method was investigated by Moon et al. to improve the characteristic of the sintered silver mesh film because the maximum temperature was

varied depending on the width of the mesh [19]. Figure 16a, b showed that as the mesh width decreased, the maximum temperature increased with the same sintering energy. The defects such as micro-pores and delamination were observed in the film because the surface of the film was sintered faster than the inside due to the high energy. Thus, the evaporated organic material was trapped in the film and it caused interfacial defects. To remove these defects, a preheating step was performed with multi-pulses and each pulse was irradiated with 5 J/cm<sup>2</sup> energies for 1 ms. As the number of pulses was increased from 5 to 15, the defects like micro-pores and delamination disappeared as shown in Fig. 16c–g. As a result, the sintered 3 μm-mesh-width film showed the sheet resistance

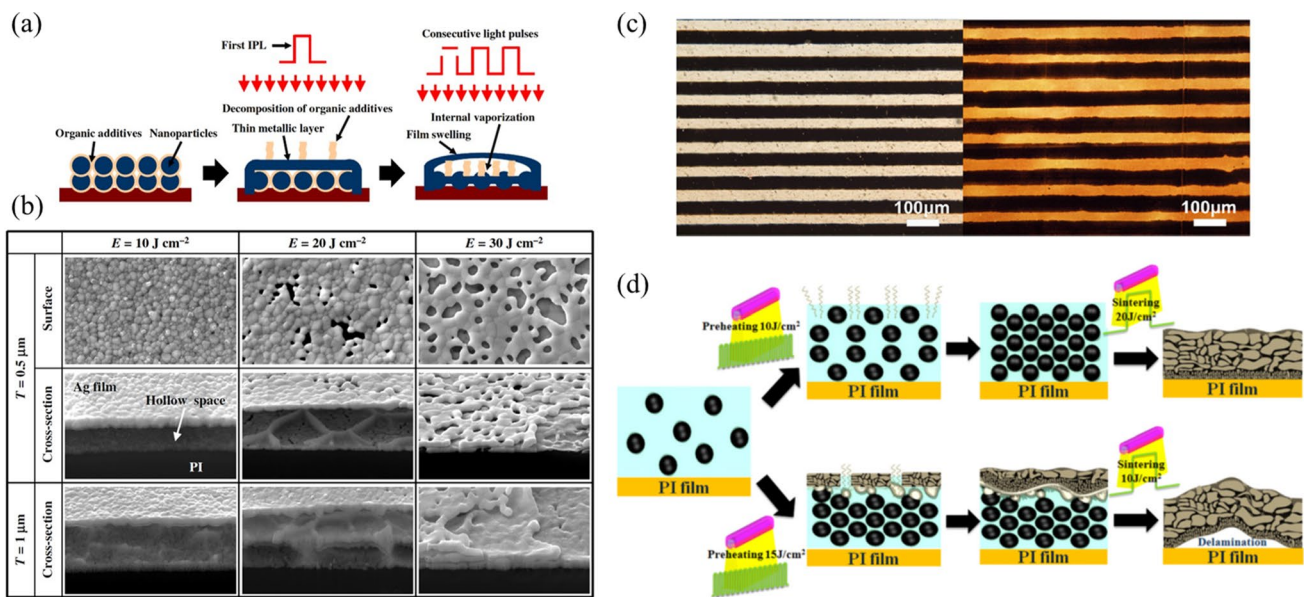


**Fig. 15** **a** Schematic of film swelling phenomena induced by IPL sintering with consecutive light pulses. **b** Microstructures of IPL-sintered nanosilver films ( $W=150 \mu\text{m}$ ) as a function of film thickness and light energy [7]. **c** Optical microscope images of inkjetted interdigitated Ag-contacts are shown on a PET (to the left) and on a paper (to the right) substrate after thermal annealing at  $120^\circ\text{C}$  for 30 min and exposure to the IR-lamp A for 15 s, respectively. The black color of the printed lines is due to the illumination from below the substrates that were used in order to enhance the contrast [117]. **d** A schematic of the two-step IPL sintering process with two different energy combinations [18]. [**a**, **b** Journal of micromechanics and

microengineering: structures, devices, and systems by Institute of Physics (Great Britain); American Institute of Physics Reproduced with permission of INSTITUTE OF PHYSICS PUBLISHING in the format Journal/magazine via Copyright Clearance Center; **c** Reprinted from Tobjörk et al. [116], Copyright (2012), with permission from Elsevier; **d** Journal of micromechanics and microengineering: structures, devices, and systems by Institute of Physics (Great Britain); American Institute of Physics Reproduced with permission of INSTITUTE OF PHYSICS PUBLISHING in the format Journal/magazine via Copyright Clearance Center.]

of  $27 \Omega/\text{sq}$  having an optical transmittance of 84.7%. A more selective approach about IPL irradiation condition was performed by Chung et al. [16]. The printed silver nano inks were sintered using IPL sintering with various IPL irradiation condition (Fig. 17a). During sintering process, the resistance change was measured in real time. Also, the scanning electron microscope analysis was performed to observe microstructure of IPL sintered silver nano inks. As a result, using the optimized white light irradiation conditions, it showed lower sheet resistance than the thermal sintering method without damaging the PET substrate. In the silver nanoparticles case, multiple pulses did not show a better result than a single pulse [16]. On the contrary, in the copper nanoparticles case, multiple pulses give smoother morphologies, because the multi pulses process prevents the excessive vaporization of organic binder of inks and disruption of the coherent conductive network [4, 5]. Kwak et al. sintered printed silver electrode on the transparent PET substrate using back-irradiation [118]. Back-irradiation means that a IPL is irradiated on the opposite side of the electrode printed side. This method prevents vapor trapping and enables effective vapor venting which makes defects in the electrode. Kwak et al.

performed back-irradiation IPL sintering of inkjet-printed Ag patterns of PET substrates (Fig. 18). Back irradiation sintering method showed defect-free high conductivity Ag patterns on transparent plastic substrates that prevents vapor trapping with effective vapor venting. Therefore, high conductivity of  $2.3 \times 10^7 \text{ S/m}$  under  $10 \text{ J/cm}^2$  could be obtained within a few milliseconds [118].

The characteristic of IPL sintered silver nanoparticles ink printed on the different substrate was also studied by Yung et al. [17]. The nanoparticles were 8–15 nm and its solid content was 14 wt%. Nanoparticles of this size grew to 100–200 nm IPL sintering. After flashing two times, the silver nanoparticle ink was the most significant melting when printed on photonic paper as shown in Fig. 17b–e. In the case of film printed on PI and paper substrate, crack and voids were observed, but they were not found when printed on PET and silver nanoparticles were densely packed. These cracks affected the resistivity of sintered silver film and the sintered silver film on photonic paper showed higher resistivity compared to other cases as shown in Fig. 17f. Therefore, the optimal resistivity was  $6.2 \mu\Omega \text{ cm}$  after the flash sintering of silver nanoparticles film printed on the PET.

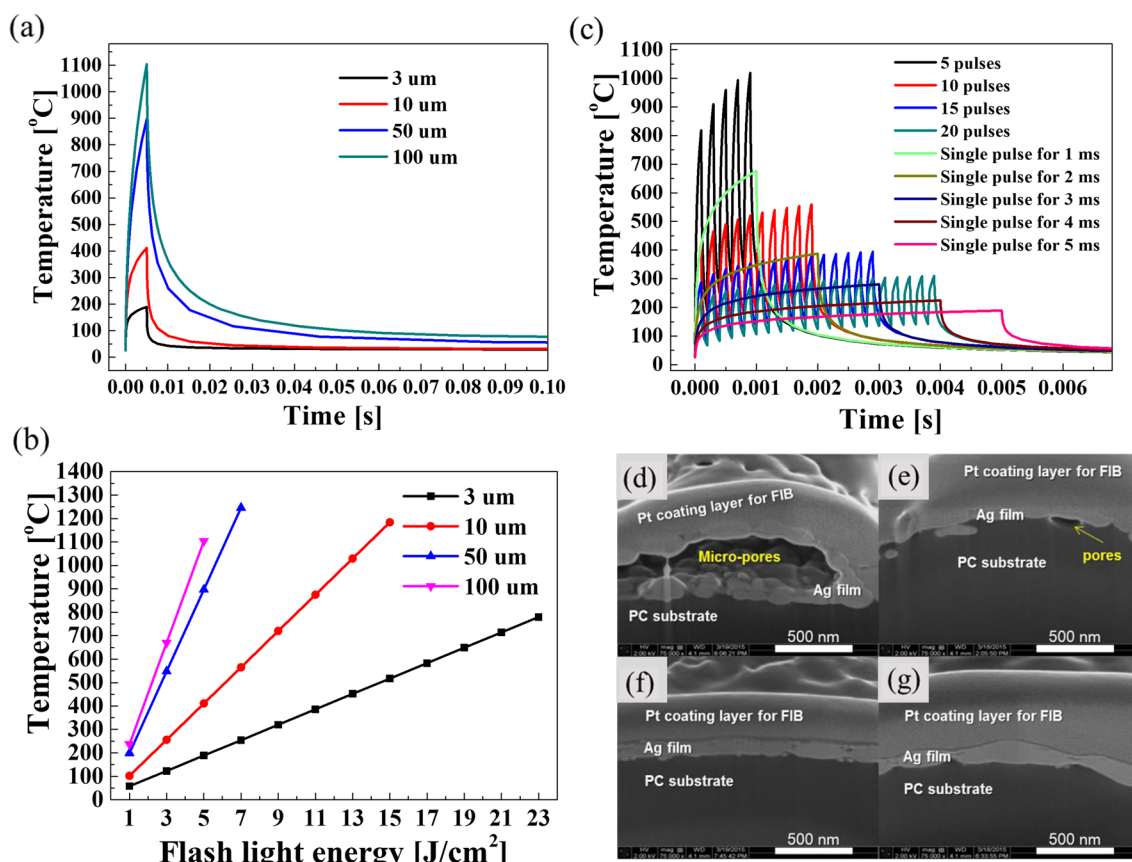


**Fig. 16** a Calculated temperature in the Ag layers with respect to sintering time and line width when a single-pulsed IPL was irradiated with a pulse duration time of 5 ms and a light energy of 5 J/cm<sup>2</sup>. b Maximum peak temperature of a IPL sintered Ag layer with respect to light energy and line width [19]. c Calculated temperature of 3- $\mu$ m wide Ag lines with respect to pulse numbers and pulse duration time,

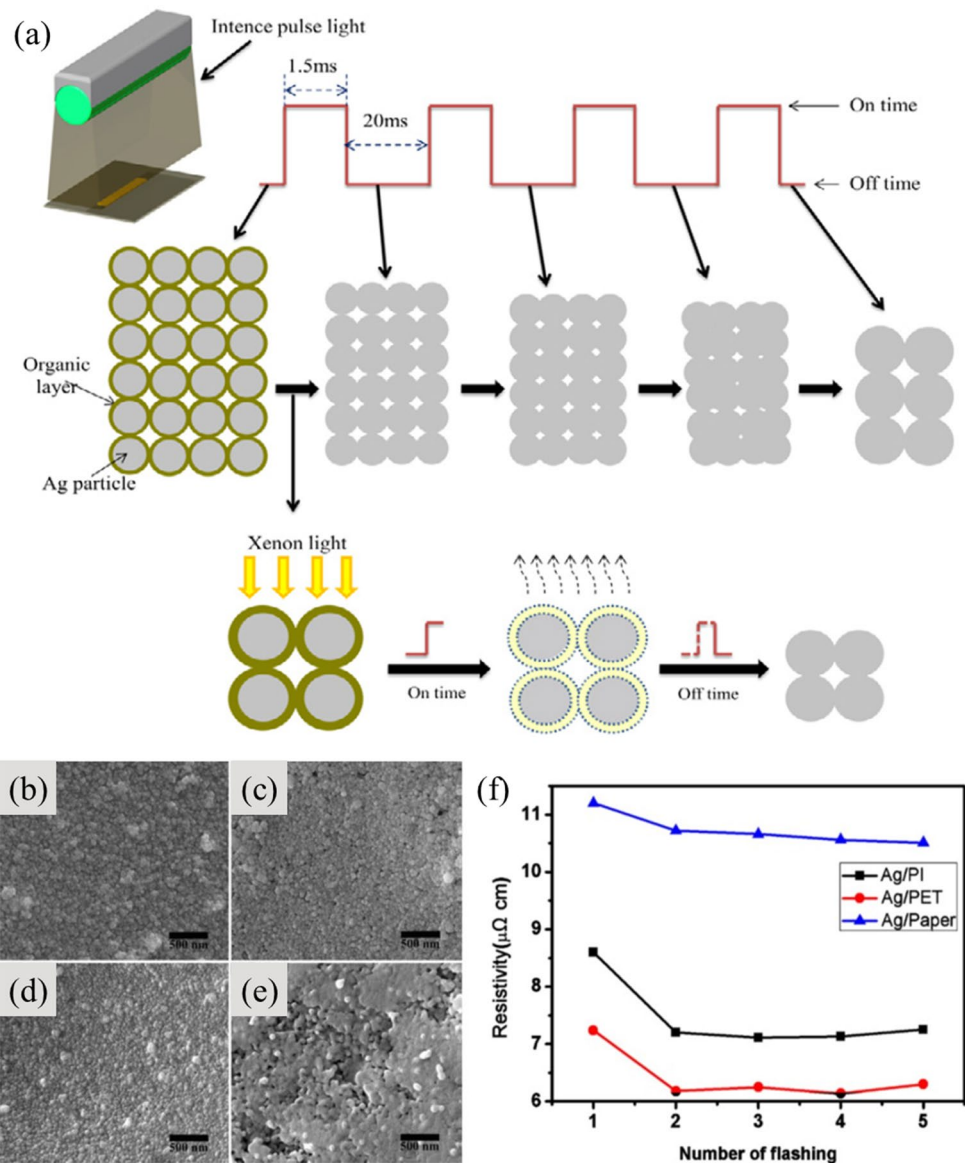
and the cross-sectional SEM images of the Ag lines treated with the two-step IPL sintering method. A preheating step composed of d 5 pulses, e 10 pulses, f 15 pulses or g 20 pulses, and a main sintering step with a single rectangular pulse of 5 J/cm<sup>2</sup> for 1 ms was consecutively conducted [19]. [Reprinted from Moon et al. [19], Copyright (2017), with permission from Elsevier]

### 2.3 Silver(Ag) and Copper(Cu) Hybrid Conductive Ink/Paste for IPL Sintering

Recently, Silver(Ag) nanoparticles(NPs) have been used most extensively because of their high electrical conductivity and oxidation stability [69, 119]. However, the high cost of Ag materials limits their use on a commercial scale [120]. As an alternate material to Ag, copper(Cu) has been actively studied due to its low cost (about one percent of Ag cost) and high electrical conductivity (only 6% less than that of Ag) [121]. Despite these advantage, Cu was not used alone in printing electronic processes. It was because that Cu easily oxidized in ambient conditions as mentioned before. In particular, nano-sized Cu can be more easily oxidized than bulk Cu due to higher surface activity [122–125]. Therefore, synergistic combinations of two-type materials were the solution that can compensate for the shortcomings of the materials. Among the various combinations of two-type materials, the structure of Ag coated Cu core-shell NPs has

been developed and explored [127–130]. To synthesis the Ag coated Cu core-shell NPs, thin Ag shell can be deposited on the surface of a Cu core. The simple method of formation Ag shell was heterogeneous nucleation [131]. The Ag-amino complex composed of Ag(I)  $\beta$ -ketocarboxylate [132] and 2-ethylhexylamine solvent was used to form seeds on the surface of Cu particles. Ag-amino complex and Cu NPs and ethanol were combined to form a conductive nano-ink. To adjust the thickness of Ag shell, Ag-amino complex and Cu particles were introduced at different mass ratio. As mass ratio of Cu particle was decreased, resulting in thick Ag shell of core-shell NPs. The formed conductive ink was printed at PI film and precured at a temperature of 140 °C to form a core-shell having a uniform thickness in Fig. 19a–c. It can be seen that the thickness of Ag shell of core-shell NPs varied depending on the ratio of Ag in Fig. 19d. The sintering energy, the resistivity after sintering were greatly changed depending on the thickness of the shell. Among the core-shell nano-ink films, Cu–Ag core-shell nano-ink films

**Fig. 17** **a** Schematic for the sintering processes for silver nanoparticles about pulse numbers [16]. SEM images of ink-jet printed tracks on various substrates: **b** on PI substrate before sintering, **c** on PI substrate after flashing two times, **d** on PET substrate after flashing two times, and **e** on photographic paper after flashing two times. **f** The relationship between electrical resistivity and the number of flashings for tracks ink-jet printed on to various substrates [17]. [a Nanotechnology by Institute of Physics (Great Britain); American Institute of Physics Reproduced with permission of IOP Publishing in the format Journal/magazine via Copyright Clearance Center; **b–f** Reprinted from Yung et al. [17], Copyright (2010), with permission from Elsevier]



exhibited the lowest resistivity of  $3.4 \mu\Omega \text{ cm}$  upon applying an IPL energy of  $4.9 \text{ J/cm}^2$  for  $2100 \mu\text{s}$ , this being even lower than that of sintered pure silver films ( $5.3 \mu\Omega \text{ cm}$ ) and the sintered Cu/Ag combined nano-ink films ( $4.06 \mu\Omega \text{ cm}$ ) [20]. It was because in situ-formed Ag nanoparticles help bond the Cu particles, and enough connection between these Cu particles can enable them to endure high energies/thermal shock while retaining a good surface [133]. Compared with the pure Cu film abruptly increased owing to oxidation after 2 h [20], while the sintered core-shell nanoink film did not exhibit significant changes in resistivity more than 60 h in Fig. 19e [133]. The high oxidation resistance of core-shell nano-ink films was explained by the free energy of the metal. The Ag-rich phase at the surface can be more stable than the Cu-rich phase because of the higher surface energy of Cu ( $1.85 \text{ J/m}^2$ ) compared to that of Ag ( $1.25 \text{ J/m}^2$ ) [134].

Therefore, Core shell nano-ink films with appropriate Ag shell thickness had high oxidation resistance at high temperature conditions. Therefore, structure of core-shell NPs can be widely used to generate printed electronics for low-cost, reliable, high electrical conductivity.

In order to take advantage of the high electrical conductivity of silver and the low cost of copper, Chu et al. fabricated a hybrid ink for IPL sintering by mixing Ag and Cu [135]. The Ag/Cu hybrid ink must penetrate into the via-hole that connects the circuit formed on both sides of the substrate. When the IPL is irradiated, not only the circuits on both sides of the substrate but also ink in the via-hole must be sintered. Therefore, the rheological analysis and the optimization of the sintering process were performed together. As shown in Fig. 19f–h, the unsintered Cu/Ag hybrid ink showed Cu MPs/Ag NPs covered with binders. After single-pulse sintering,

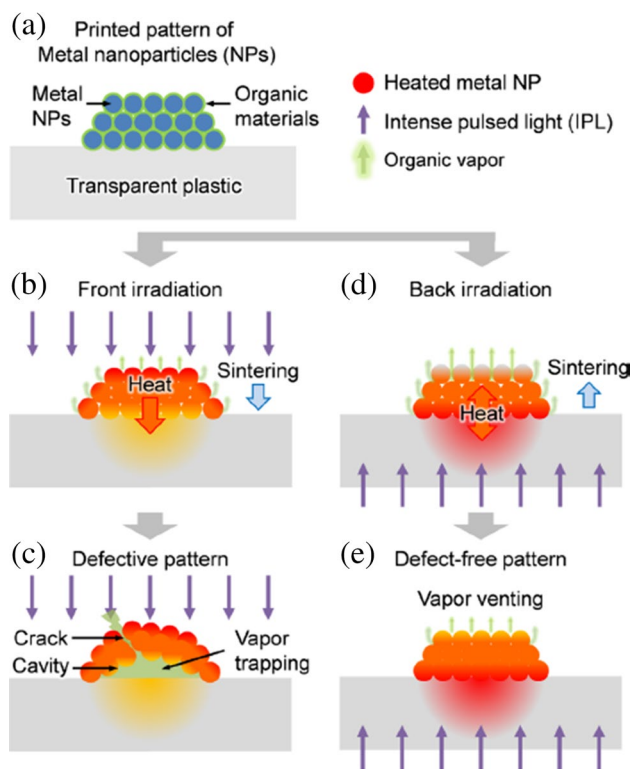


**Fig. 18** a Schematic of a metal NP pattern printed on a transparent substrate. b, c During front irradiation with IPL, sintering starts from the top of the pattern, frequently leading to a defective pattern. d, e During back irradiation, sintering starts from the bottom of the pattern, leading to a defect-free pattern [118]. [Reprinted from Kwak et al. [117], with the permission of AIP Publishing]

reduction of the Cu MP oxide shell with removal of binders and necking between Cu MPs/Ag NPs occurred (Fig. 19g). However, there is a difference of grain size between the surface and inside of the via-hole due to the thickness difference of the ink between the pattern area and the via-hole section, which resulted in differences of resistivity and grain size after IPL sintering. Meanwhile, 20-pulse sintered case showed improved necking between Cu MPs/Ag NPs compared to the single-pulse case because of the sufficient time for sintering of Cu MPs/Ag NPs with removal of the Cu MP oxide shell. Moreover, the overall grain size significantly increased, affecting the surface area and inside of the via-hole simultaneously. From the results, the multi-pulse sintering method enables a dense structure with minimized resistivity difference between pattern area and via-hole section.

### 3 IPL Welding of Nanowires

Transparent electrodes technology is one of the fastest growing area in the printed electronics market. Recently, demand for various electronics devices such as solar cells [136,

137], organic emitting diodes (OLED) [138, 139], wearable devices [45, 140], touch screens [141, 142], and transparent displays [143, 144] have been increased due to the development of electronic and communication technologies. Most of transparent electrodes are formed with Indium Tin Oxide (ITO)-based electrodes, however the ITO electrodes have some problems such as a brittleness properties, indium scarcity, and high cost [146–147]. The demand for ITOs is gradually reduced as bendable and rollable electronic devices become popular. Recently, carbon materials such as carbon nanotubes (CNTs) [141, 144, 148] and grapheme [149, 150], which have ductile properties, or metal nanowires [152–153] have attracted great interest to apply in flexible transparent conducting electrodes (FTCEs). Among these, there is an increasing tendency to use metal nanowires which have high electrical conductivity, are usable in flexible substrates and can maintain high transmittance. These metal nanowires, which have high conductivity, transmittance and good bending properties on a flexible substrate, are subjected to a welding process to ensure better electrode characteristics. This section will focus on the metal nanowire FTCEs which are welded via IPL irradiation.

Silver nanowire (Ag NW) is one of the most attracted material of the FTCEs in recent years, and has a high conductivity and transmittance intrinsically. Because of the ductile nature of Ag NWs, they have excellent mechanical properties when applied to flexible substrates. Generally, Ag NWs were synthesized by the polyol process and produced by the reaction of Ag precursor such as  $\text{AgNO}_3$  with Polyvinylpyrrolidone (PVP) and some chlorides such as  $\text{CuCl}_2$ ,  $\text{NaCl}$ , and  $\text{FeCl}_2$ . The synthesized Ag NWs were washed, dispersed and coated on a flexible transparent substrate such as polyethylene terephthalate (PET), poly (vinyl-butryal) (PVB), and polycarbonate (PC) film in the form of ink. Various coating process such as drop coating, aerosol-jet nozzle printing, bar coating, spray coating was applied to fabricate Ag NWs FTCEs. In order to enhance the electrical, optical, and mechanical properties of the Ag NWs FTCEs, various welding processes such as heat [154], laser [155], plasma [156], cold [105], IPL welding [21, 157] have been studied. Especially, IPL welding process was continuously developed because it has a fast processing time, large process area and can be applied in ambient condition at room temperature.

Chung et al. used Ag NW inks with hydroxypropyl methylcellulose (HPMC) binders coated on polyethylene terephthalate (PET) substrates and welded via IPL and ultraviolet C (UV-C) irradiation to produce highly conductive transparent electrodes [22]. In order to remove the HPMC binder and weld the AgNWs, UV-C light assisted two-step IPL welding process was conducted. The sheet resistance of the films after the UV-C pre-treatment and main flash white light welding process decreased as the irradiation energy of the UV-C light was increased. This was because



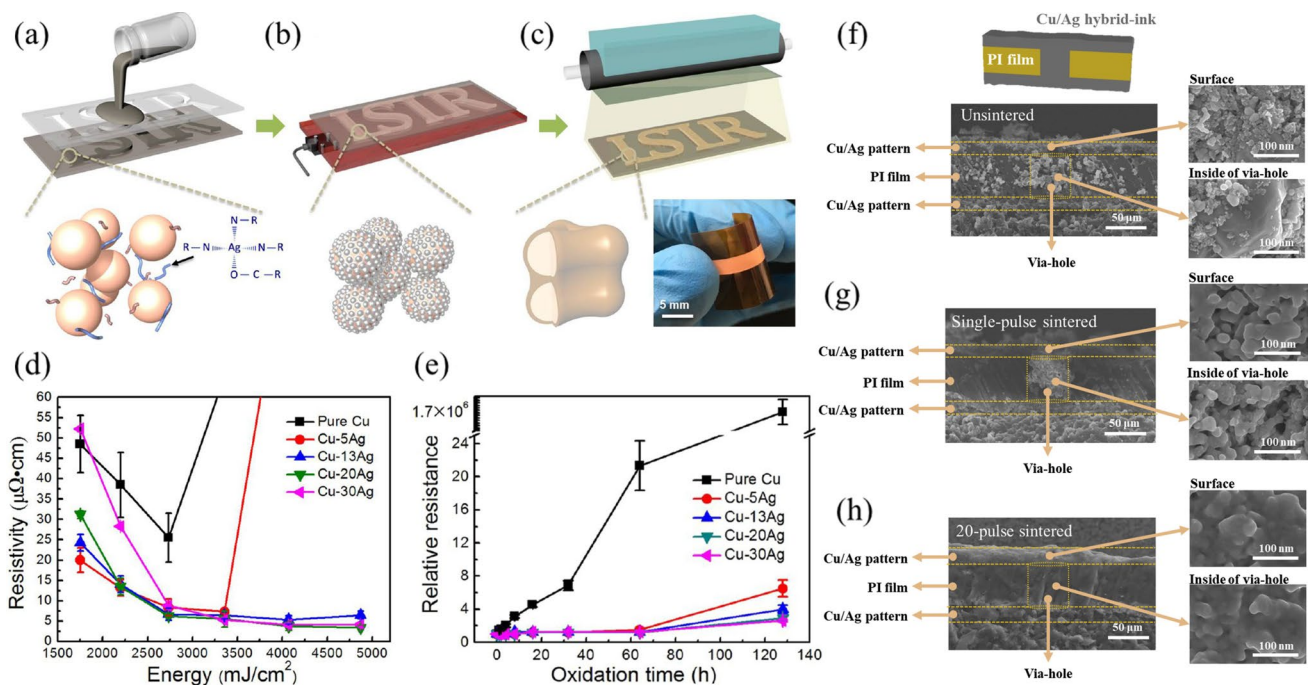


**Fig. 19** Schematic diagram: **a** Mask printing and fabrication of Cu–Ag alloy electrodes or circuits by **b** low-temperature precuring and **c** rapid-sintering (LTRS) under an air atmosphere. (Inset) Photograph of flexible Cu–Ag alloy electrode on a polyimide (PI). **d** Resistivity evolution of a printed pure Cu electrode and Cu–Ag electrodes as a function of supplied energy of photonic sintering **e** Relative resistance of electrode prepared from pure Cu, Cu–5Ag, Cu–13Ag, Cu–

20Ag, Cu–30Ag at 180 °C [133]. Cross-sectional SEM images of Cu/Ag hybrid ink: **f** unsintered, **g** single- and **h** 20-pulse sintered cases (irradiation energy: 7 J/cm<sup>2</sup>) [135]. [**a–e** Reprinted with permission from Li et al. [132]]. Copyright (2017) American Chemical Society; **f–h** Reprinted from Chu et al. [134], Copyright (2019), with permission from Elsevier]

the photo-catalytic effect of UV-C light irradiation could decompose the HPMC binder, thereby inducing closer contact among the Ag NWs as shown in Fig. 20a. From the study, they reported successful welded and embedded Ag NW films achieved by the optimal combined light welding process, shows an excellent mechanical reliability, transmittance (98.76%) and sheet resistance of a film (77.93 Ω/sq).

On the other hand, it was also reported that the flash-induced plasmonic interactions of Ag NWs for exceptionally low sheet resistance ( $\approx 5 \Omega/\text{sq}$ ), high transparency (90%), and strong adhesion on plastic substrates [23]. Localized heat energy with a self-limited photo thermal reaction could be generated at the junctions of NWs, resulting in ultrafast and completely welded Ag NWs. In addition, it was found that the spectral peaks in the near-infrared (NIR) region could locally melt the interface between the Ag NW network and a polyethylene terephthalate (PET) substrate by surface plasmon polaritons (SPPs), and 310% higher adhesion force of Ag NWs to the PET than that of pristine Ag NW/PET film was demonstrated. The mechanism underlying effective welding and adhesion strengthening for the AgNW network was theoretically investigated by a 3D finite-difference time-domain (FDTD) analysis. Interestingly, the high EHG peaks were observed in ultraviolet (UV, wavelength in 400 nm) and

NIR (wavelength in 830 and 900 nm) frequencies, indicating that intensive thermal energy can be generated by the UV and NIR light (Fig. 20d). It can be seen that the UV frequency (wavelength in 400 nm) generated the heat on the gap between the Ag NWs, and NIR frequency (wavelength in 830 and 900 nm) generated the heat on the surface of the Ag NWs. From these heat generations from surface plasmon resonances on the Ag NWs, top and bottom Ag NWs could be welded each other.

These results were also reported in other studies. Garnett et al. introduced finite element method simulations of optical heat generation at Ag NW junctions during the IPL welding process [152]. From Fig. 21a it is clear that heating is most efficient when the illumination wavelength is close to the localized surface plasmon (LSP) resonance of an individual Ag NW and when the polarization direction is correct to effectively drive such a resonance in the top NW, as determined by polarization selection rules. In short, when flash light in the wavelength region around 400 nm was irradiated to the Ag NWs, the heat generated by the LSP was the largest at the junction between the Ag NWs.

Also, Jang et al. studied selective wavelength plasmonic welding of silver nanowire film. Figure 21b–f shows that the sheet resistance of the Ag NW film was greatly reduced

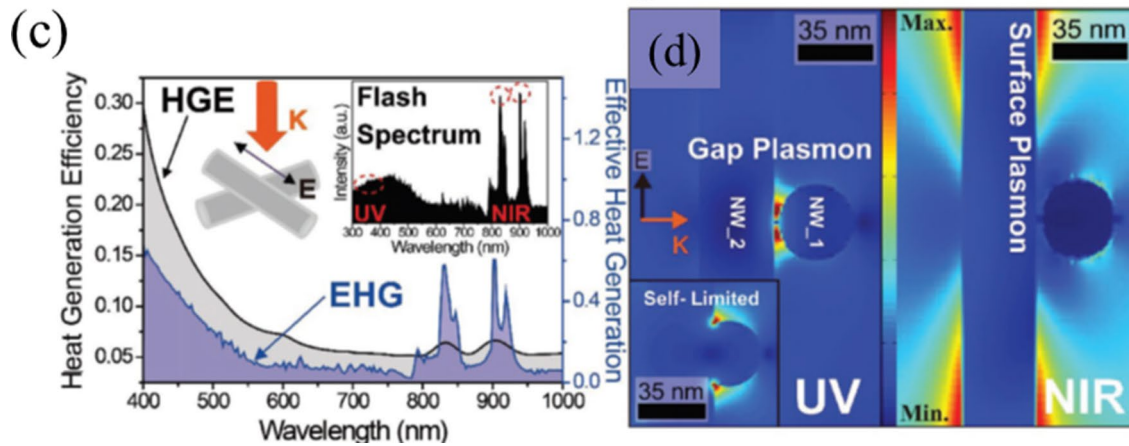
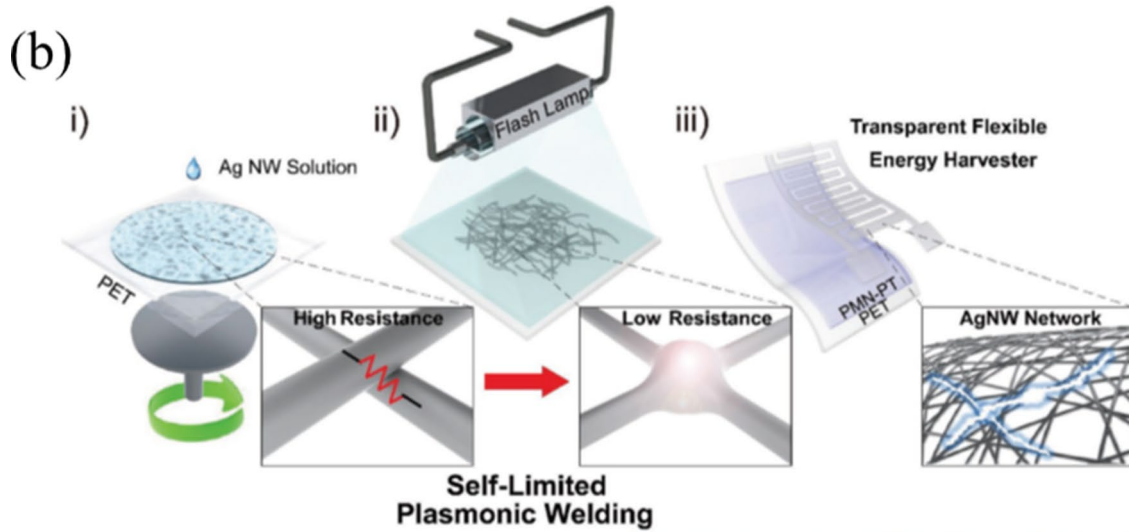
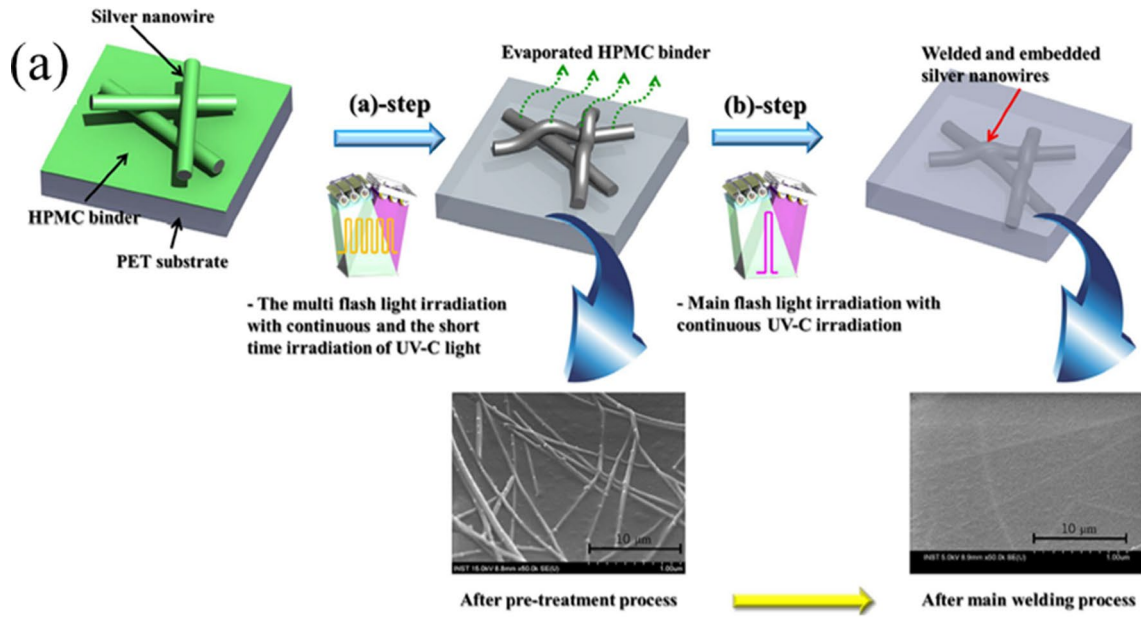


**Fig. 20** **a** The schematic diagram for welding mechanism of silver nanowire using combined flash white light irradiation [22]. **b** Schematic illustration of the AgNW FPW procedure and conceptual application towards a transparent flexible energy harvester. **c** The FDTD simulation results of HGE and EHG for light polarized parallel to the first NW. The inset shows the spectrum of the xenon flash lamp. **d** The local field distribution at a NW junction. The field enhancement response under the UV spectrum (400 nm) at the NW gap (left image). The inset shows FDTD simulation results that exhibit the self-limiting nature of the FPW. The field distribution caused by SPP (right image) under 800 nm electromagnetic wavelength [23]. [a This work is licensed under the Creative Commons Attribution 4.0 International License. To view a copy of this license, visit <https://creativecommons.org/licenses/by/4.0/> or send a letter to Creative Commons, PO Box 1866, Mountain View, CA 94,042, USA; **b–d** Reprinted by permission from Park et al. [23]]

when only the 400–500 nm wavelength region was irradiated in the IPL welding experiments [157]. As a result of the scanning electron microscope (SEM) analysis as well as the change of the sheet resistance, it was confirmed that the Ag NWs were completely welded and the substrate was not damaged. In addition, as shown in Fig. 21g–m, the heat generation of junctions between Ag NWs at each wavelength was simulated to support the experimental results by COMSOL multiphysics [157]. As shown in Fig. 21h, the heat generated by the absorbed light was concentrated around the junction area. This indicates that a local hot spot known as the plasmon-enhanced area occurred at the spherical nanowire junction point [158, 159]. Meanwhile, when the incident light with the wavelength over 500 nm was irradiated, the surface plasmonic resonance happened on the overall silver nanowire (not on the junction points). Therefore, by these phenomenon, the Ag NWs and PET substrate might be damaged because the temperature of the overall Ag NW was increased. Thus, the conductivity and the transmittance of the Ag NW film was decreased. Therefore, to improve the welding characteristic of Ag NW, the flash light with a wavelength from over 400 to under 500 nm should be irradiated.

On the other hand, there have been attempts to predict generated heat and resistance changes that occur when the Ag NWs coated on a polymer substrate are welded by IPL irradiation. Dexter et al. develops a multiphysical approach for predicting evolution of conductivity, NW fusion and nanoscale temperature gradients on the substrate during pulsed light sintering of Ag NWs on polycarbonate [160]. Their approach can predict the change in sheet resistance after IPL when the NW material, NW diameter and initial optical absorption of the as-deposited NW network are known. In addition, the MD simulations was conducted that the kinetics of fusion between Ag NWs is significantly dependent on the NW diameter, with the rate of sintering reducing faster beyond a critical NW diameter ( $\approx 20$  nm here for Ag). Finally, using a thermal Finite Element Analysis (FEA), new insight into temperature gradients in the

substrate during IPL was provided. It shows that the ratio of NW temperature to substrate temperature reduces with increasing pulse fluence because increasing pulse fluence, via greater pulse duration, results in the heat diffusing to a greater extent into the substrate.

Research for improving the adhesion of Ag NW film with the substrate has been carried out. A conductive, uniform, and ultra-smooth flexible transparent composite film was produced by embedding silver nanowires (Ag NWs) into poly(vinyl-butylal) (PVB) without pressure or high-temperature annealing [161]. The adhesion of Ag NWs was greatly improved by embedding them in PVB, and surface roughness and sheet resistance ( $R_s$ ) improvements were achieved through the use of the intense pulsed light (IPL) method, which welded the interconnections among Ag NWs in a short time without heat or pressure treatment. When exposed to an IPL energy of  $4 \text{ J/cm}^2$  for only  $500 \mu\text{s}$ , the sheet resistance of PVB/Ag NWs with the IPL (PAI) composite film reached  $12.6 \Omega/\text{sq}$  with a transmittance of 85.7% (at 550 nm) (Fig. 22a–c); no clear changes in the sheet resistance were observed after a substrate bending and tape test, suggesting excellent flexibility. In the case of PAI, the change in sheet resistance was only 2.6% after a 2000-bend test, and the resulting bending radius was less than 1 mm. The transparent and flexible embedded Ag NWs fabricated using spin-coating, IPL exposure, and transfer method were successfully used in OLEDs. From these results, it was found that a transparent electrode having strong adhesion with the substrate can be manufactured when the Ag NW was embedded into the PC substrate.

Some researches were reported to use IPL sintering for welding of AgNW on PET substrates. In 2012, Jiu et al. found that AgNW can be adhered strongly on PET substrate by a high intensity pulsed light sintering technique [162]. They performed adhesive tests and bending tests were performed with an adhesive tape (3 M, USA) and automatic bending apparatus, respectively. Figure 22d shows the relative resistance of the electrode at the different number of peeling test cycles. The sheet resistance was maintained constantly when the light intensity was higher than  $1.14 \text{ J/cm}^2$  while the films and its resistance could not withstand the peeling test when light energy was low. In sequence, bending test was performed because the flexibility is also one of the important factor on flexible devices. When irradiation energy was higher than  $0.74 \text{ J/cm}^2$ , the resistance change did not occur before 1000 cycles as shown in Fig. 22e. Also, the transparency has increased as the sheet resistance decreased as shown in Fig. 22f, because the high transparency means that the amounts of AgNWs are small. This paper suggested that various films can be designed for various applications by optimizing the light sintering parameters.

Additionally, to improve the electrical conductivity of the Ag NWs, graphene layer can encapsulate silver nanowires

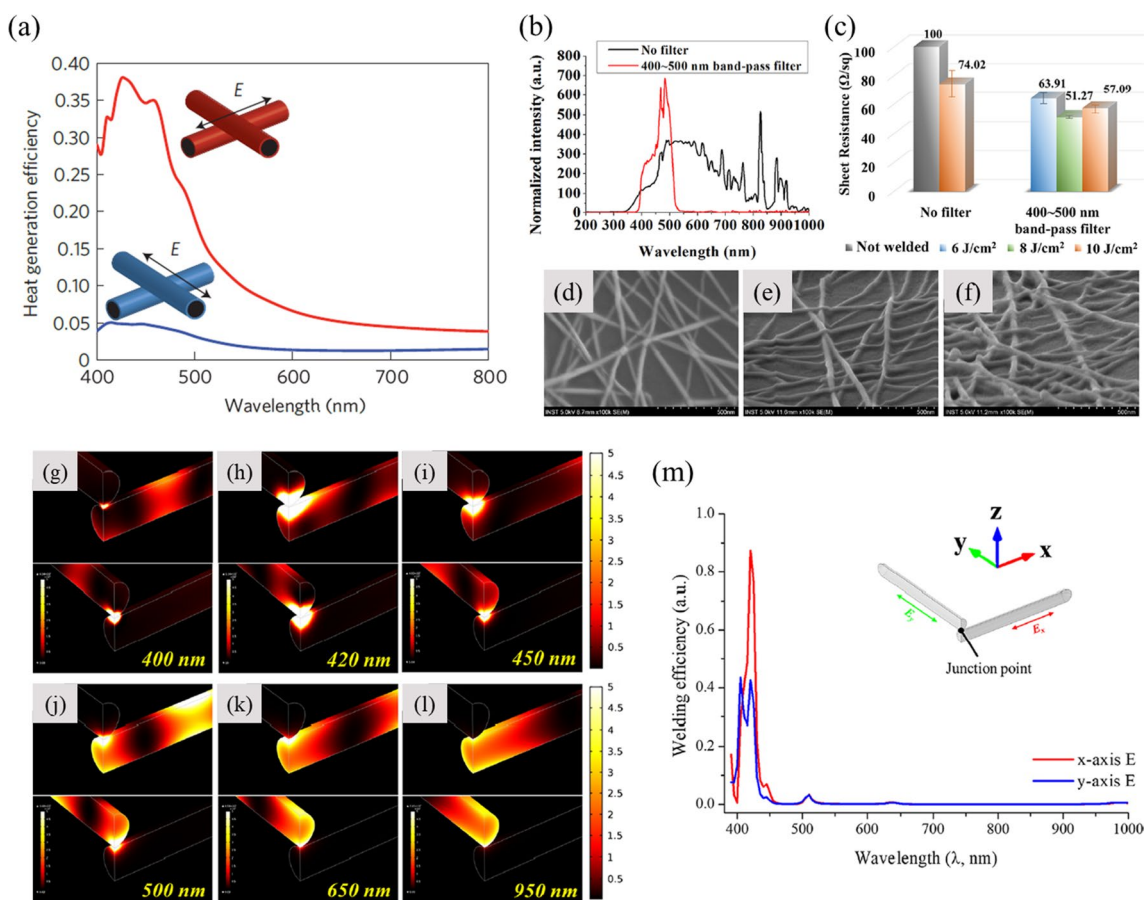


**Fig. 21** **a** Finite element method simulations of optical heat generation at silver nanowire junctions during the nanowelding process. Heat generation efficiency as a function of wavelength for light polarized perpendicular (red) or parallel (blue) to the top nanowire for a junction with a 2 nm gap [152]. **b** The wavelength spectrum of flash white light passed by 400–500 nm band-pass filter compared with the spectrum of flash white light without optical filter. **c** Sheet resistance of the AgNWs without filter and with low-pass filter (irradiation

energy, 6–10 J/cm<sup>2</sup>; pulse number, 1; on-time, 10 ms), SEM images of the AgNWs films welded by IPL using 400–500 nm band-pass filter with the irradiation energy of **d** 6, **e** 8, and **f** 10 J/cm<sup>2</sup>. Heat generation at the junction point when the wavelength was **g** 400, **h** 420, **i** 450, **j** 500, **k** 650, and **l** 950 nm. **m** The averaged heat generation value at the junctions of the Ag NWs [157]. [**a** Reprinted by permission Garnett et al. [151]; **b–m** Reprinted with permission from Jang et al. [156]. Copyright (2018) American Chemical Society]

(AgNWs) using the intense pulsed light (IPL) method was reported and shown in Fig. 23a–f [163]. This result in approximately a four-fold reduction in the sheet resistance of IPL-treated graphene/AgNWs compared to that of IPL-treated AgNWs providing fast welding of Ag wire-to-wire junctions in stacked electrodes of graphene/AgNWs, enhanced conductivity and long-term stability under oxygen and sulfur atmospheres. In addition to graphene, there have been attempts to construct electrodes by mixing silver nanowires with other materials. Hwang et al. compared and analyzed the degree of necking when silver nanowires (NWs) and silver nanospheres (NSs) were mixed at each ratio (Fig. 23g) [164]. This work combines experiments, mass transfer simulations, and electromagnetic simulations to understand how neck growth kinetics during sintering and self-damping optical behavior in IPL is affected by the nanostructure shape (specifically NWs and NSs here). Neck

growth kinetics at Ag NW–NS interfaces is substantially anisotropic, greater than that at NW–NW interfaces, and lesser than that at NS–NS interfaces. The dominant mechanism behind this difference is an interface specific change in dislocation generation during sintering. Too high NS content causes stronger self-damping behavior along with lesser neck growth rate, which limits the optical absorption capacity before low enough resistivity is reached. Excessive NW content reduces optical absorption efficiency to such an extent that it overwhelms the accompanying advantages of increased neck growth kinetics and more sustained optical absorption. Mixing NWs and NSs in an optimal ratio (50:50 here) reaches a balance between neck growth kinetics, optical absorption efficiency, and sustained temperature in multiple pulses. The ideal nanostructure shapes to be mixed should concurrently reduce self-damping, increase or retain high optical absorption efficiency, and increase or

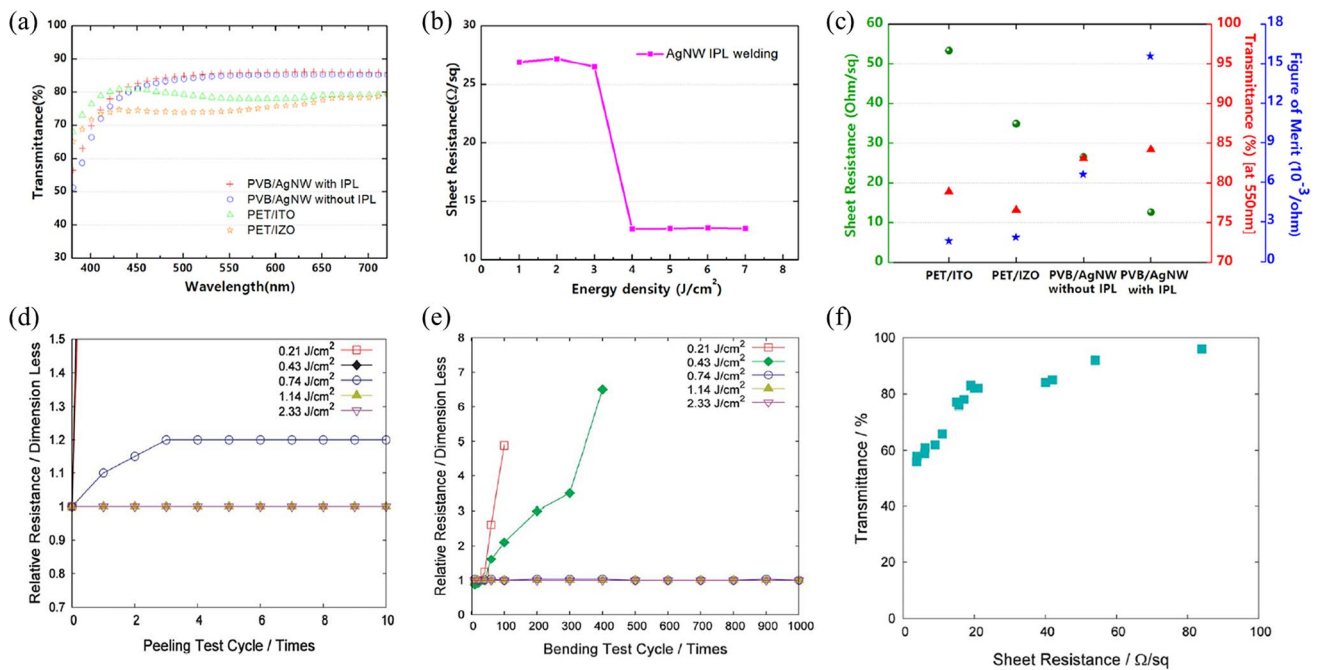


**Fig. 22** **a** Transmittance spectrum of IPL-treated and non-treated pristine PVB/AgNWs, PET/ITO, and PET/IZO films. **b** Sheet resistance response to the intense pulsed light method induced welding. **c** Figure of merit values for relative sheet resistance and transmittance values of the PET/ITO, PET/IZO, and PVB/AgNWs films with and without IPL [161]. Variations in sheet resistance of AgNW films as a function of **d** peeling and **e** bending cycles, **f** Transmission spectra of AgNW films before and after high intensity pulsed light sintering

[162]. [a–c] This work is licensed under the Creative Commons Attribution 4.0 International License. To view a copy of this license, visit <https://creativecommons.org/licenses/by/4.0/> or send a letter to Creative Commons, PO Box 1866, Mountain View, CA 94042, USA; **d–f** Journal of materials chemistry by Royal Society of Chemistry (Great Britain) Reproduced with permission of ROYAL SOCIETY OF CHEMISTRY, in the format Journal/magazine via Copyright Clearance Center.]

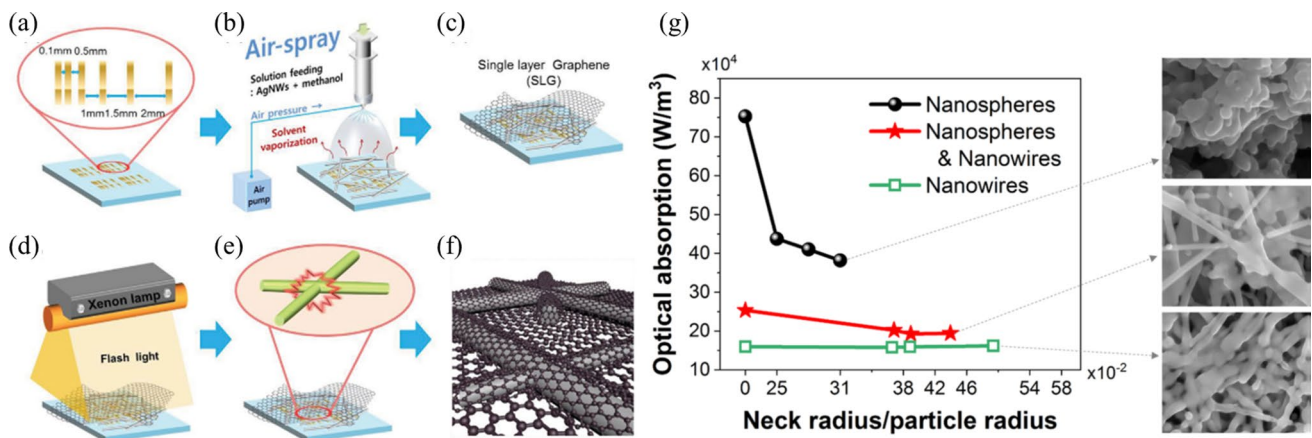


**Fig. 23** Schematic illustration for the processing steps of IPL-treated AgNWs encapsulated by a graphene layer. **a** Gold transfer lines patterned on a glass substrate. **b** Air-spray coating of AgNWs. **c** Graphene transfer onto AgNWs coated on a glass substrate. **d** IPL optical sintering using a Xenon flash lamp on AgNWs encapsulated by graphene sheets. **e** Nanowelding at junctions of AgNWs encapsulated by graphene sheets. **f** Schematic image of single-layer graphene (SLG)/AgNWs after IPL exposure. Graphene is tightly attached to welded

AgNWs [163]. **g** The self-damping coupling and optical absorption, which drive temperature evolution in IPL, are tunable by nanostructure shape. The introduction of NWs into a NS ensemble reduces the dependence of optical absorption on neck growth [164]. [a–f] Reprinted by permission from Yang et al. [162]; **g** Reprinted with permission from Hwang et al. [163]. Copyright (2018) American Chemical Society]

retain similar levels of neck growth rates as the unmixed nanostructures.

On the other hand, as the above research, a study was conducted to analyze the mechanism during the IPL process with the theme of mixing nanoparticles and nanowires. Dexter et al. investigated the effect of nanomaterial shape distribution in Ag NW–NP composite films on sintering temperatures and sintered material properties in IPL, yielding the following insights and implications on process performance and material properties [165]. Mixing nanowires with nanoparticles can reduce the maximum sintering temperatures to around 150 °C, while retaining film resistivity within 4–5 times that of bulk silver. This has significant implications on reducing substrate distortion and damage when using thermally sensitive substrates like polymers and paper, without compromising on process throughput or sintered material conductivity. Based on these experiments choosing a NW content of 50% will minimize materials cost while retaining the low processing temperatures, high processing speed and low film resistivity achieved here. In addition, electromagnetic simulations were performed to determine the inherent dependence of the self-damping behavior in the IPL process on the nanomaterial shape distribution of the deposited film. This approach implies that the processing temperature of IPL can be controlled according to the type of nanomaterial through the prediction of self-damping behavior.

In addition, the study on self-damping nature of densification and neck growth during IPL sintering of nanoparticles was studied by MacNeill et al. in 2015 [166]. Similarly, the temperature change of the optical absorption and densification of nanoparticles during IPL sintering was studied by Bansal et al. [167]. These papers used a coupling method to investigate the self-damping nature of nanoparticles. Nanoparticle densification, neck growth, and optical absorption are interrelated and determine the temperature during IPL process. It is not constantly changing, but it has a property of being maintained when certain conditions are established. This has been demonstrated through experimental and analytical results, and various studies have been conducted [152, 164, 168]. All of these phenomena are closely related to a study of self-limited plasmonic welding of Ag NWs by Garnett, E. C., et al., in 2012, mentioned with Fig. 21a. They have demonstrated an optical method for welding together Ag NWs selectively at junction points by taking advantage of the extreme field concentration offered by plasmonics. The process is naturally self-limited owing to the very strong dependence of the plasmonic light concentration on the distance between the wires during IPL process. These papers basically explain that as IPL is irradiated on nanomaterials, necks grow between them, which changes the distance between them. As the sintering proceeds, the plasmonic phenomenon is reduced to suppress itself so that the sintering no longer proceeds. This is likely to have a greater impact when

applied not only to polymer substrates, but also to silicon and ceramic substrates, where the CTE is high and IPL has to be irradiated for a relatively long time.

Copper nanowire (Cu NW)-based flexible transparent conducting electronics (FTCEs) represent an enormous breakthrough for the development of efficient, scalable and facile processing techniques. From the standpoint of commercialization, a cost-effective and eco-friendly procedure for welding nanowires is imperative to fabricate Cu NW network-based transparent electrodes. However, the oxide shells that form on Cu NWs are difficult to be eliminated under ambient conditions using conventional sintering methods like mechanical pressing, conventional thermal sintering, plasma sintering, and microwave sintering.

To overcome these limitation, IPL welding process was adopted for welding of ultra-long Cu NW networks. The IPL irradiation which has a pulse on-time of 5 ms, energy of 1 J/cm<sup>2</sup> per 1 pulse was conducted on the Cu NWs film. The sheet resistance of the Cu NWs electrode was gradually decreased as the irradiation light energy increased to 3 J/cm<sup>2</sup> because neck-like junctions were formed successfully and they grew larger as the irradiation light energy increased. The Cu NWs were welded at the junctions due to local heat generation derived from absorption of IPL irradiation energy with respect to the Zipper effect of metal nanowire [152, 169]. Wide angle XRD measurements were conducted to determine the structure of the percolated Cu NWs on a PET substrate before and after IPL irradiation. After welding with IPL irradiation, complete absence of the Cu oxide peaks was observed, and Cu became more crystalline, as the reflections appear to be more prominent in the XRD patterns.

On the other hand, as an extension of the welding of Cu NWs, a research has been carried out to achieve strong adhesion strength to substrates that can be used in FTCEs applications [170]. The prepared NW film was shielded by a disposable, thick paper mask carved with a star shaped pattern for selective IPL irradiation. Then, the film covered with the mask was irradiated by IPL at 710 V for 520 μs. After irradiation, the non-irradiated NWs were selectively wiped away by fabric soaked with isopropanol (IPA), which was used as the main solvent for the Cu NW ink (Fig. 24a). For all star-shaped conducting patterns, uniform RS values were observed, with only slight changes in the average RS and its deviation before (17.8 Ω/sq ± 1.8 Ω/sq) and after (17.4 Ω/sq ± 1.8 Ω/sq) wiping, indicating that there was little damage on IPL irradiated NWs after R2R wiping process. In addition, it was successfully demonstrated that high efficient flexible phosphorescent organic light-emitting diode (PhOLED) and transparent heater with uniform heating and a fast response time can be achievable using R2R-patterned Cu NW FTCEs.

In addition, Cu NW film is considered to be an amazing candidate for next generation of flexible, transparent and

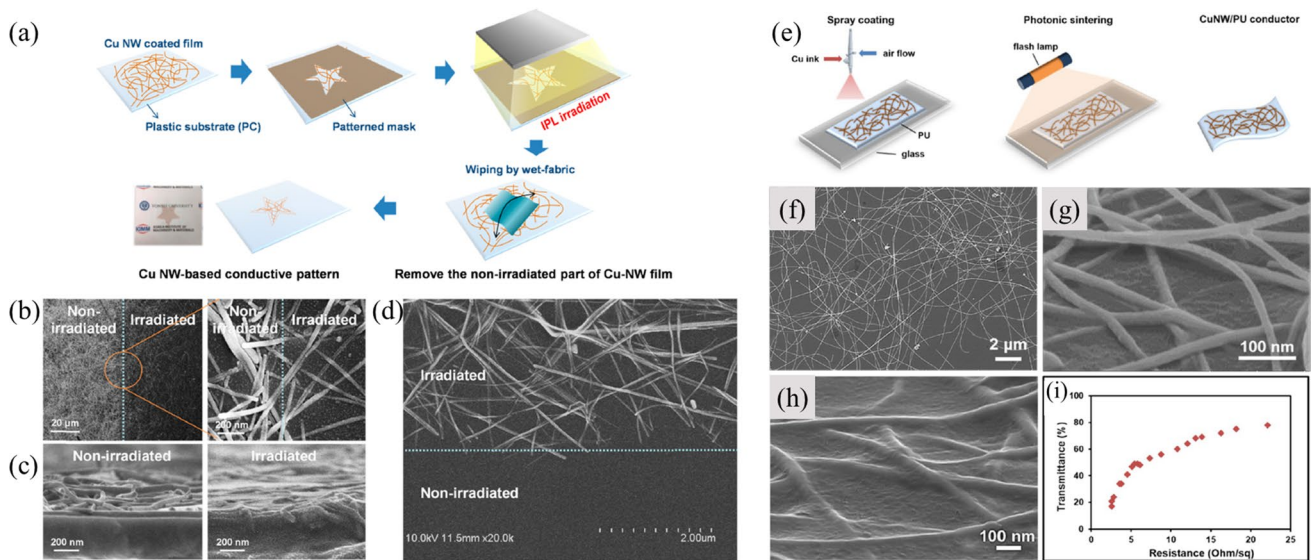


**Fig. 24** **a** Schematic illustration of the patterning method for Cu NW FTCEs using a mask for selective IPL irradiation. SEM images show the **b** surface and **c** cross section of Cu NW-coated areas with and without IPL irradiation. The left side shows the nonirradiated area, and the right side presents the irradiated area. **d** Surface image of the boundary between the nonirradiated area and the irradiated area after removal of NWs (wiped away by wet fabric). The NWs in the non-irradiated area are clearly eliminated [170]. **e** Schematic illustration

of the fabrication process of CuNW/PU conductors. **f** SEM image of as prepared CuNWs. Tilted SEM images of CuNW networks on PU matrix **g** before and **h** after photonic sintering. **i** Plot of transmittance ( $\lambda = 550$  nm) versus sheet resistance for photonic sintering CuNW conductors [45]. [**a–d** Reprinted with permission from Zhong et al. [169]. Copyright (2016) American Chemical Society; **e–i** Reprinted with permission from Ding et al. [45]. Copyright (2016) American Chemical Society]

stretchable conductors. A stretchable conductors with Cu NW percolation network on poly urethane (PU) flexible substrate were fabricated using a simple IPL welding technique at room temperature in air within only one-step [45]. It is clear that Cu NWs were almost completely embedded in PU after the IPL welding with irradiation energy of  $272 \text{ mJ/cm}^2$  for only  $20 \mu\text{s}$  on-time (Fig. 24h). Repeated stretching test and bending test were carried out to confirm the mechanical properties of Cu NW/PU conductor. While stretching and releasing the Cu NW/PU conductor to 10% strain for 1000 cycles, the resistance change was very small compared to other reference results. The bending performance was also investigated by curving the Cu NW/PU conductors along a cylinder with diameter of 20 mm from  $0^\circ$  to  $180^\circ$ . The resistance of Cu NW/PU conductors kept superior stability against deformation even after 100 bending cycles. The excellent mechanical properties were corresponding to the strong adhesion between CuNWs and PU substrates by IPL irradiation. This process provides an effective method for fabricating simple, low-cost, large-scalable patterned conductive electrodes on flexible plastic substrates.

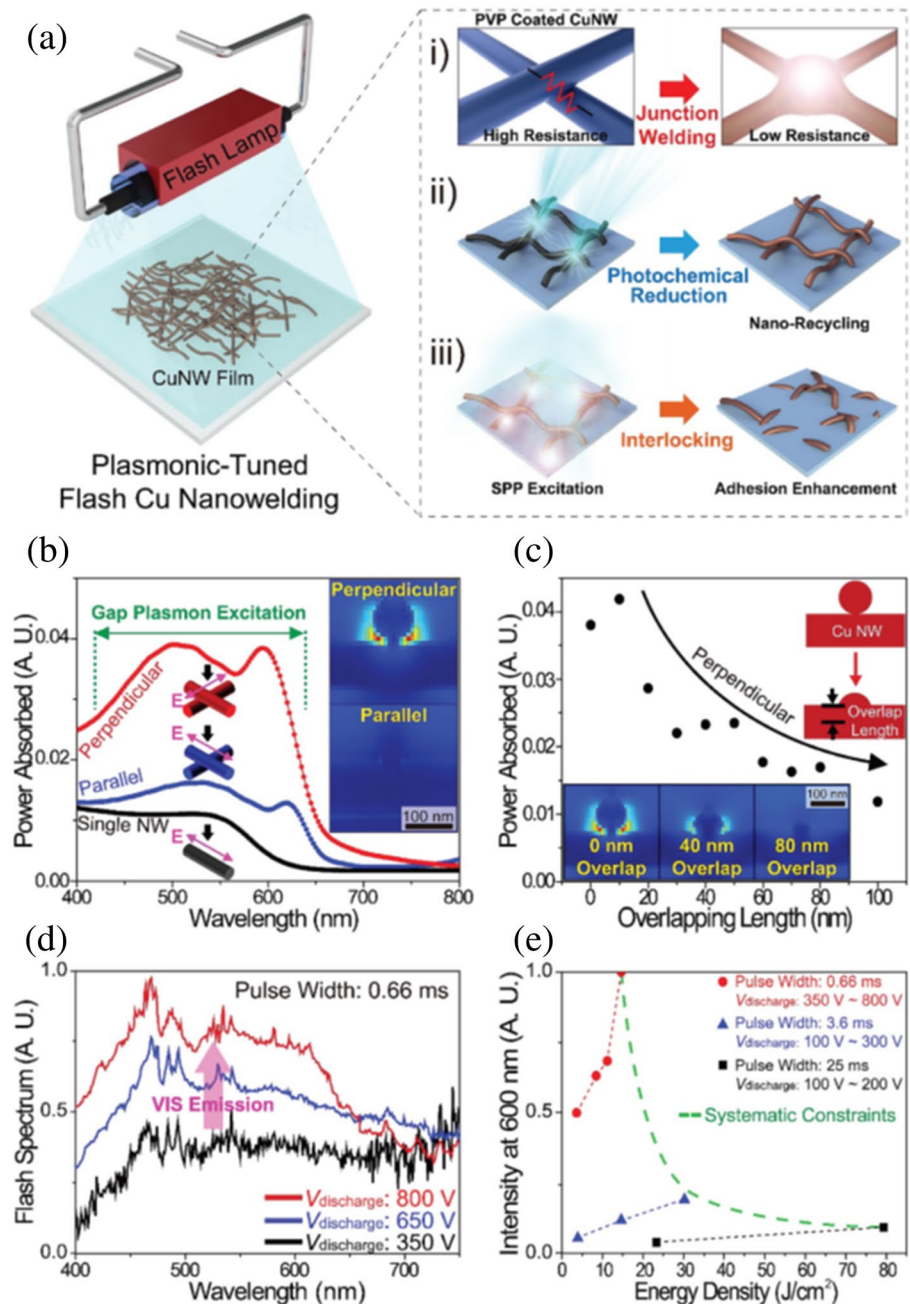
On the other hand, a high-performance copper nanowire (Cu NW) network (sheet resistance  $\approx 17 \Omega/\text{sq}$ , transmittance 88%) fabricated by plasmonic-tuned flash welding (PFW) with ultrafast interlocking and photochemical reducing is reported, which greatly enhance the mechanical and chemical stability of Cu NWs (Fig. 25) [171]. High intensity

visible light is emitted by the plasmonic-tuned flash, which strongly improves Cu nano welding without oxidation. Near-infrared spectrum of the flash induced an interlocking structure of NW/polyethylene terephthalate interface by exciting Cu NW surface plasmon polaritons (SPPs), increasing adhesion of the Cu nanonetwork by 208%. This strong adhesion of Cu NWs provided considerable bending stability over 30,000 cycles. The finite-difference time-domain (FDTD) simulations theoretically confirmed that junction nanowelding and adhesion strengthening of Cu NWs could occur by visible (wavelength from 600 to 650 nm) and NIR (wavelength from 900 to 975 nm) light, respectively.

#### 4 Applications Of Intense Pulsed Light (IPL) Sintered Conductive Electrodes

For the fabrication of small electronic devices, multi-layered structuring became important for application in industrial field [172]. Krivec et al. successfully demonstrated multilayering of via-free conductive structure (Fig. 26a). Ag nano-ink was printed firstly on  $200 \mu\text{m}$  thick PET substrate, then dielectric layer and Ag pattern were subsequently printed. The printed Ag patterns and dielectric layer were sintered using IPL method, sintering condition of each layer was slightly adjusted to find appropriate sintering condition. The fabricated multilayer planar coil structure were successfully

**Fig. 25** **a** Schematic illustration of the Cu NW PFW process. **b** Spectral and polarization-dependent simulations of local light absorption for the Cu NW junction from 400 to 800 nm wavelength. The inset shows the field enhancement response under the visible light (wavelength of 600 nm) for light polarized perpendicular/parallel to the first NW. **c** Local heat generation as a function of Cu NW overlap length, which shows the self-limiting nature of the PFW process. The insets show field distribution simulations as a function of Cu NW overlap length. **d** Normalized flash light spectrum emitted by discharging voltage of 350, 650, and 800 V at a pulse width of 0.66 ms. **e** Normalized flash intensity at 600 nm wavelength emitted by various discharging voltages and pulse widths. The green dashed line indicates the systematic constraints caused by the limited power supply and capacitance of the flash lamp [171]. [Reprinted by permission from Park et al. [170]]



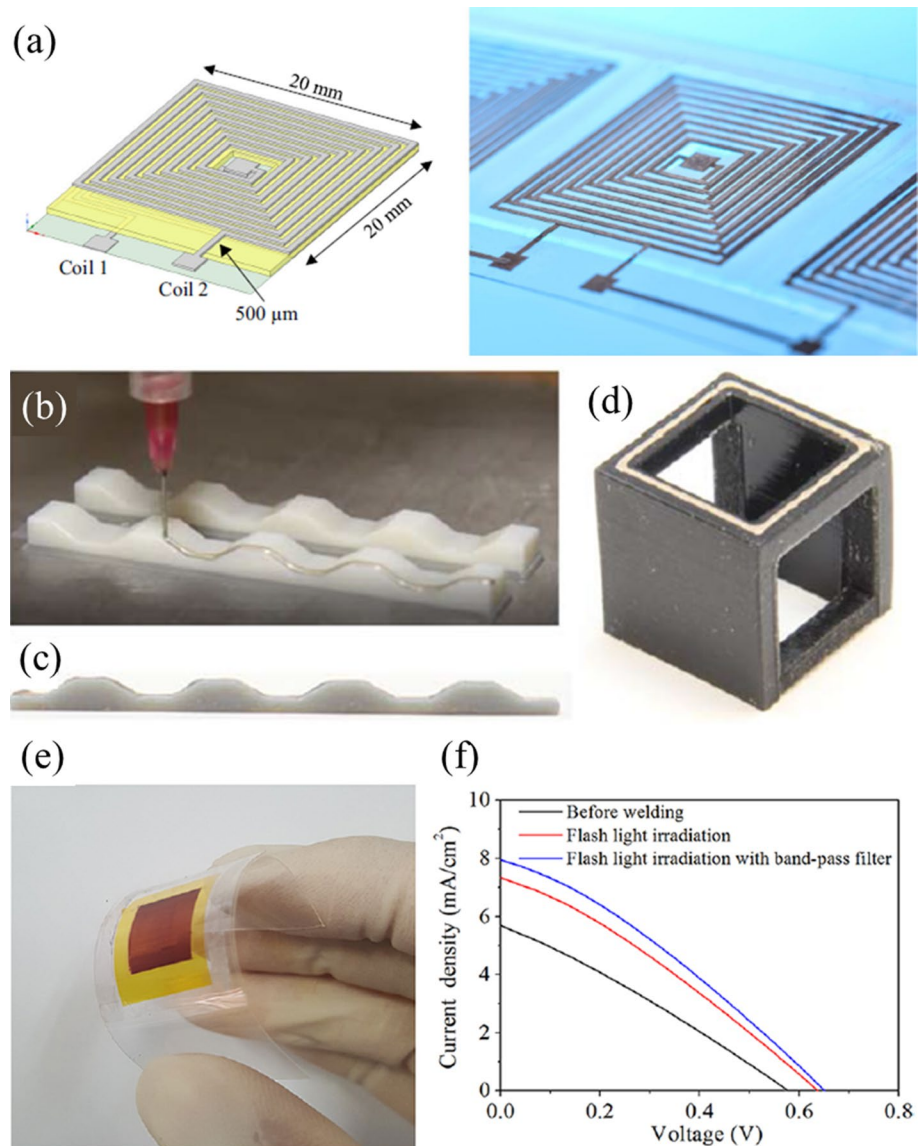
tested and verified by comparing several experiments and finite element method simulations [173].

Mu et al. investigated IPL sintering conditions of a thick direct-ink-write (DIW) Ag wire on 3D printed light absorbing substrates. Since printed pattern with DIW showed much thicker than other printing methods, multi-cycle sintering method was studied to obtain optimized sintering condition (Fig. 26b–d). By controlling sintering parameters, optimally IPL sintered case (light exposure duration: 8 s, total light exposure: 40 s) showed the resistivity of comparable to oven sintered cases [174]. Therefore, it is reliable, fast, and can be easily combined with 3D printing systems. In addition, 3-D

printing technique is suitable for polymer system processing technology [175–188]. Polymers that are easy to mold and can be used in various devices can be applied to complex applications through 3-d printing technique. In addition, polymers can be applied to not only substrates of the various electrodes but also one material of polymer-metal composite structure. These applications can be directly applied to IPL process. On the other hand, Devaraj et al. investigated a new process that can transform planar printed circuits on thermoplastic sheets into freeform interconnect–polymer assemblies for facile integration with a desired 3D surface [189]. Importantly, IPL-induced inter-NW neck growth



**Fig. 26** **a** Schematic presentation and the corresponding macro image of the double-layered coiled coil Ag structure [173]. **b** Conformal printing silver trace on the surface of 3D printed VeroWhite; **c** side view of IPL-sintered silver wire on 3D printed no-planar Gray60; **d** the IPL-sintered silver wire on 3D printed TangoBlack hollow cubic [174]. **e** An image of flexible DSSC fabricated with Ag NW films. **f** Photocurrent density voltage curves for DSSCs with Ag nanowire transparent electrodes before and after flash white light irradiation (energy, 8 J/cm<sup>2</sup>; on-time, 10 ms; pulse number, 1) with band-pass filter (wavelength range from 400 to 500 nm) [157]. [a Reprinted by permission from Krivec et al. [172]; b–d Smart Materials and Structures by Society of Photo-optical Instrumentation Engineers; American Institute of Physics; Institute of Physics (Great Britain) Reproduced with permission of IOP Publishing in the format Journal/magazine via Copyright Clearance Center. e, f Reprinted with permission from Jang et al. [156]. Copyright (2018) American Chemical Society.]



significantly compensates for crack growth induced reduction in resistance during thermoforming and IPL. With the optimal parameters found here, this process achieved interconnect resistance of  $< 10 \Omega/\text{cm}$  within 90.8 s at 100% maximum strain over a 1 square inch forming area. The potential of this approach to enable surface size and material insensitivity, robust integration, and easy replaceability for conformal circuit fabrication was discussed.

A solar cell converts the energy of light directly into electricity by the photovoltaic effect that is a physical and chemical phenomenon. Jang et al. fabricated DSSC with IPL sintering of Ag NWs film on PET substrate and selective wavelength filter (400–500 nm with a band-pass filter). The selective wavelength filter improved welding phenomena between Ag NWs, which resulted in high conductivity ( $51.275 \Omega/\text{sq}$ ) with high transparency (95.343%). The optimally IPL sintered transparent electrode was applied

to DSSC, which exhibited 1.6% of efficiency by improved welding phenomena of Ag NWs (Fig. 26e, f) [157].

TFTs were conventionally fabricated by depositing thin films of active semiconductor layers, the dielectric layers, and metallic contacts over a non-conducting substrate. Sarkar et al. fabricated TFT by changing from deposition of Ag electrodes to printing and IPL sintering of Ag nano-ink (Fig. 27a–c) [40]. IPL sintering condition of inkjet printed Ag nano-ink on PET substrate was optimized, the optimized condition was applied as source/drain contacts in the fabrication of flexible TFTs, which showed field effect mobility of  $0.09 \text{ cm}^2/\text{V}\cdot\text{s}$  and ON/OFF ratio of  $10^6$  which are similar with the value obtained for TFTs with conventional Ag deposited cases.

With the increasing demand of electronic devices, demand of transparent conductive films instead of expensive and brittle sputtered indium tin oxide (ITO) films was

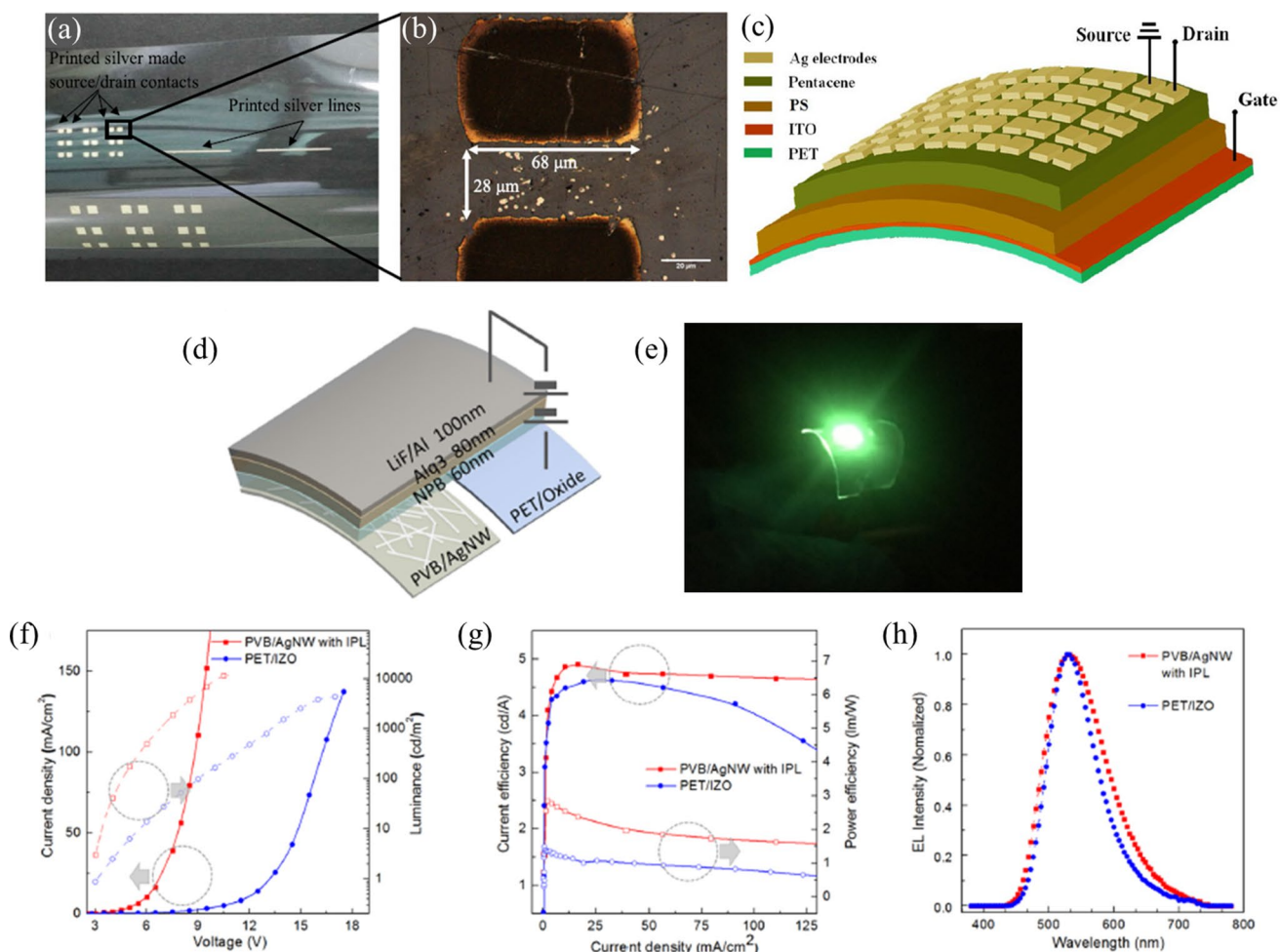


**Fig. 27** **a** Optical image of various printed patterns on PET sheet, **b** Enlarged optical microscopic image of printed silver source/drain contacts, **c** Schematic of fabricated flexible OTFTs with printed silver source/drain [40]. Characteristics of OLED devices with PVB/AgNWs with IPL composite and IZO anode. **d** Schematic section of the OLED device. **e** Photographic images of operating PVB/AgNWs-based OLEDs in flexible modes, compressive stress. **f** Current density–voltage–luminance characteristics. **g** Current efficiency and

power efficiency as a function of luminance. **h** Normalized EL intensity versus wavelength [161]. [a–c © [2017] IEEE. Reprinted, with permission, from Sarkar et al. [40]; d–h This work is licensed under the Creative Commons Attribution 4.0 International License. To view a copy of this license, visit <https://creativecommons.org/licenses/by/4.0/> or send a letter to Creative Commons, PO Box 1866, Mountain View, CA 94042, USA.]

increased. It stimulated the development of transparent conductive materials having 90% in the visible spectrum and a sheet resistance under  $20 \Omega/\text{sq}$ . However, a high temperature ( $300\text{--}500 \text{ }^\circ\text{C}$ ) is needed to achieve better crystallization of the metal oxide [190]. Lee et al. reported that a flexible transparent conducting Ag NWs film fabricated by embedding Ag NWs at the surface of a transparent PVB (Fig. 27d–h). The Ag NWs networks can be improved by using the IPL irradiation, sheet resistance was decreased to  $12.6 \Omega/\text{sq}$  with a transmittance of 85.7% (at 550 nm). It was applied to OLEDs application, which exhibited comparable or higher electro luminescent feature than known flexible electrodes (e.g., indium-zinc-oxide on polymer plastic) [161].

A purpose of sensor is to perceive any changes related to object and convey the relevant information to a computer by electrical output. Among them, thin film flexible sensors increasingly received attention because they are easy to apply any structure. Han et al. reported that ultrathin transparent and conformable pressure-induced bending sensor with high flexibility and stretchability (Fig. 28a–g). Ag NWs were printed on PET substrate, and IPL sintered Ag NWs showed extremely flexible and stretch-compatible up to 100% uniaxial strain [19]. Kim et al. IPL sintered Ag flake/Ag nanocrystal (NC) hybrid materials incorporated into a PDMS substrate (Fig. 28h–k). The addition of NCs into an Ag flakes network greatly enhanced electrical conductivity and sensitivity of strain sensors. As a result, strain sensors

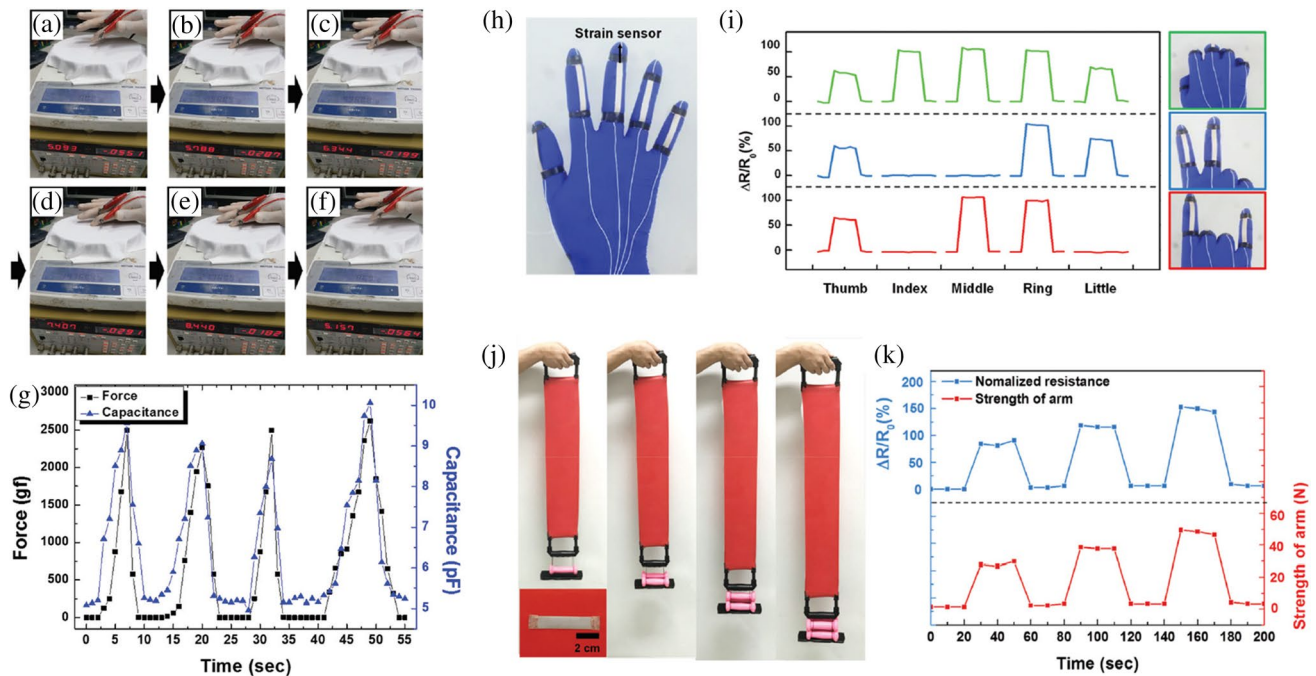


**Fig. 28** a–f Measured capacitance of the sensor attached to a gloved fingertip while applying pressure to an electronic scale. **g** Force applied to the fingertip with the capacitance formed on the sensor [211]. **h** Photograph of the smart glove with the attached strain sensors. **i** Relative resistance change in the glove under various finger gestures. **j** Photographs of the sports performance monitoring band upon applying forces with 1–4 kg dumbbells. The inset shows a photograph of the strain sensor attached to the backside of the band. **k** The relative resistance change in the sports performance monitor-

ing band when the band was stretched and released by the force of the arms [57]. [a–g] Journal of materials chemistry. **c** Materials for optical and electronic devices by Royal Society of Chemistry (Great Britain) Reproduced with permission of Royal Society of Chemistry in the format Journal/magazine via Copyright Clearance Center; **h–k** Nanoscale by National Center for Nanoscience and Technology; Royal Society of Chemistry (Great Britain) Reproduced with permission of RSC Pub in the format Journal/magazine via Copyright Clearance Center.]

had highly stretchable (up to 80%) and sensitive (gauge factor: 7.1) with high durability over 10 000 stretching under 50% strain [57]. Moreover, similar works related to stretchable sensors were extensively studied by sintering of NWs- or NPs-based inks on stretchable substrates [45, 58, 191].

Apart from the applications mentioned above, the IPL sintering method has high potential to expand various field. Takahashi et al. fabricated Ag electrode for damage sensing of carbon-fiber-reinforced plastic (CFRP) structures (Fig. 29a, b). Ag inkjet printed on CFRP substrate and sintered using IPL irradiation, sintered with  $3 \text{ J/cm}^2$  irradiation energy in 5 ms exhibited good strain sensing ability of CFRP composite, which is comparable with thermally sintered case [41]. Oh et al. newly synthesized Cu/Cu<sub>10</sub>Sn<sub>5</sub> core/shell NPs for the large-area, low-cost, flexible conductors on transparent PEN substrates (Fig. 29c–i). The low melting point of Cu<sub>10</sub>Sn<sub>3</sub> shell layer allowed highly conductive and rollable electrodes even under low IPL energy, resulted in non-damaging of PEN substrates. The fabricated electrodes were successfully demonstrated with the fabrication of a flexible touch screen and an antenna for wireless communication system [192].

In 2017, Jang et al. applied intense pulsed light sintered transparent electrodes on wearable heaters [193]. They used electrospun ultra-long metal nanofibers (mNFs) such as AgNFs on PET substrates and demonstrate their potential use as wireless wearable heaters. With a roll-based electrospinning system, continuous network of long metal nanofibers was fabricated on large area flexible polymers (Fig. 30a). They applied developed transparent electrode on a wearable heater with temperature control system using a Bluetooth of smartphone as shown in Fig. 30b. The wristband-type stretchable and flexible heating film connected to the wireless controller was attached to human skin. As shown in Fig. 30b, the heater showed stable temperature in real time even in mechanical deformation by wireless control system. As a result, wearable devices fabricated by IPL sintering are expected to present a promising strategy in many applications including flexible and stretchable heater.

To fabricate transparent electrode, copper nanowire films were also considered to be a good candidate because it is much cheaper than silver nanowires with a comparable electrical conductivity. With a IPL sintering technique, copper nanowire films could be fabricated on polymer substrate in a

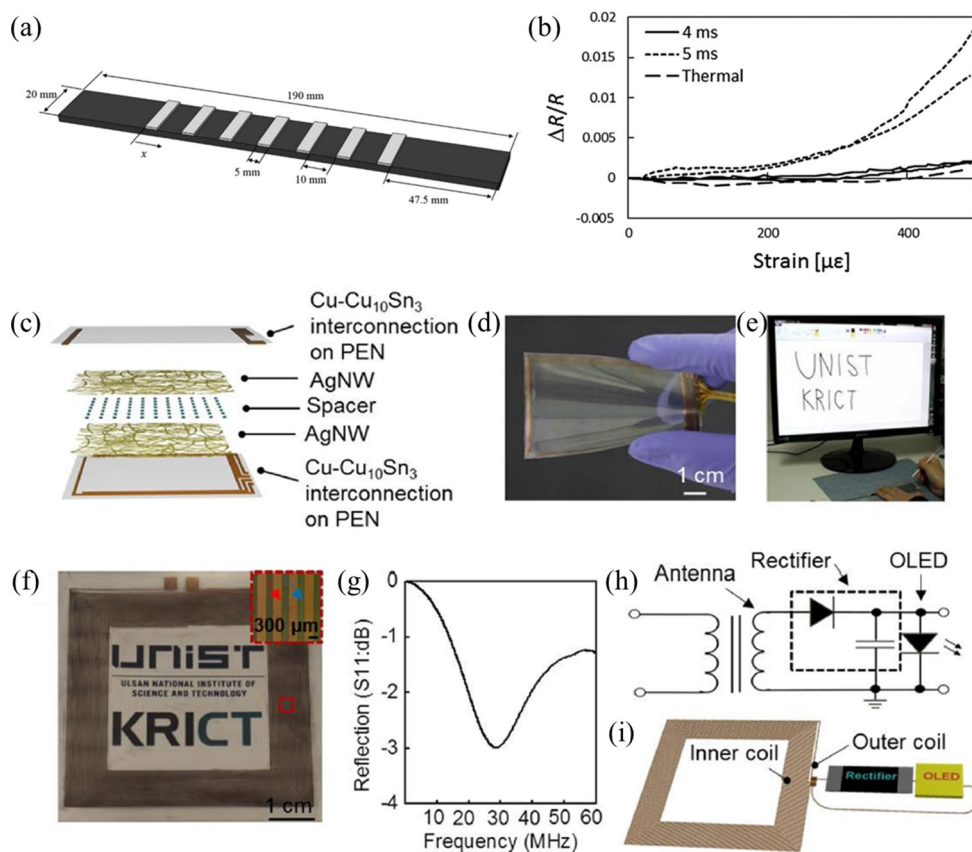


**Fig. 29** **a** Specimen dimensions and **b** the contact resistance increased as a result of deformation of the electrode sintered by IPL; the thermally sintered electrode showed negligible changes in contact resistance [41]. **c** Schematic diagram of the TSP, including Cu/Cu<sub>10</sub>Sn<sub>3</sub> interconnections, Ag nanowires (NWs), and spacers, fabricated on PEN substrates. **d** Photo of the fabricated, flexible TSP and **e** phot of the result of the TSP operation. The letters “UNIST KRICT” were written on the TSP. **f** Photograph and optical microscopic image (in the inset, red and blue arrows denote the Cu/Cu<sub>10</sub>Sn<sub>3</sub> electrode

and the PEN substrate, respectively) of the antenna fabricated on the PEN substrate. This image is reproduced with the permission of the copyright owner. **g** Frequency response of the reflection coefficient (S<sub>11</sub>) of the Cu/Cu<sub>10</sub>Sn<sub>3</sub> antenna. **h** Circuit diagram and **i** schematic diagram of the wireless operable OLED with the Cu/Cu<sub>10</sub>Sn<sub>3</sub> antenna [192]. [**a**, **b** Reprinted from Takahashi et al. [41], Copyright (2015), with permission from Elsevier; **c**–**i** Reprinted with permission from Oh et al. [191]. Copyright (2016) American Chemical Society]

very short time with reducing oxidation problems [45, 194]. Ding et al. developed stretchable conductors with CuNW percolation network on PU flexible substrate using IPL sintering technique [45]. Intense pulsed light welded the CuNWs at contact spots and also reducing the oxides on the surface of CuNWs. Additionally, the CuNW network was embedded into the surface of PU matrix with great adhesion by softening phenomenon of the PU surface. Finally, they applied metal nanowires as heater and good performance with small applying voltage was achieved as shown in Fig. 30c. In addition, a patterned heater and a transparent heater glove were fabricated as shown in Fig. 30d, e, respectively.

On the other hand, research on IPL sintering of silver nanowire coated on the woven fabric, not on the transparent film, has been progressed. Hwang et al. investigates a scalable Intense Pulsed Light (IPL) sintering process for

fabricating silver nanowire on woven polyester heating patches (Fig. 31) [195]. Just 300 microseconds of IPL sintering results in 30% lesser electrical resistance, 70% higher thermal performance, greater durability (under bending up to 2 mm radius of curvature, washing, humidity and high temperature), with only 50% the added nanowire mass compared to state-of-the-art. Figure 31d shows the evolution of average temperature of the as-deposited and IPL sintered nanowire-fabrics under 1 V applied voltage. The temperature increases rapidly upon applying voltage, until it reaches saturation at around 120 s due to balance of thermal losses with joule heating. A higher voltage of 1.2 V led to blackening of the fabric indicating fabric damage due to excessive heating. Since heat generation in the Ag nanowire-fabrics is due to Joule heating, a lower sheet resistance leads to higher Q, which leads to higher steady-state temperature for the same applied voltage. IPL sintering enhances the

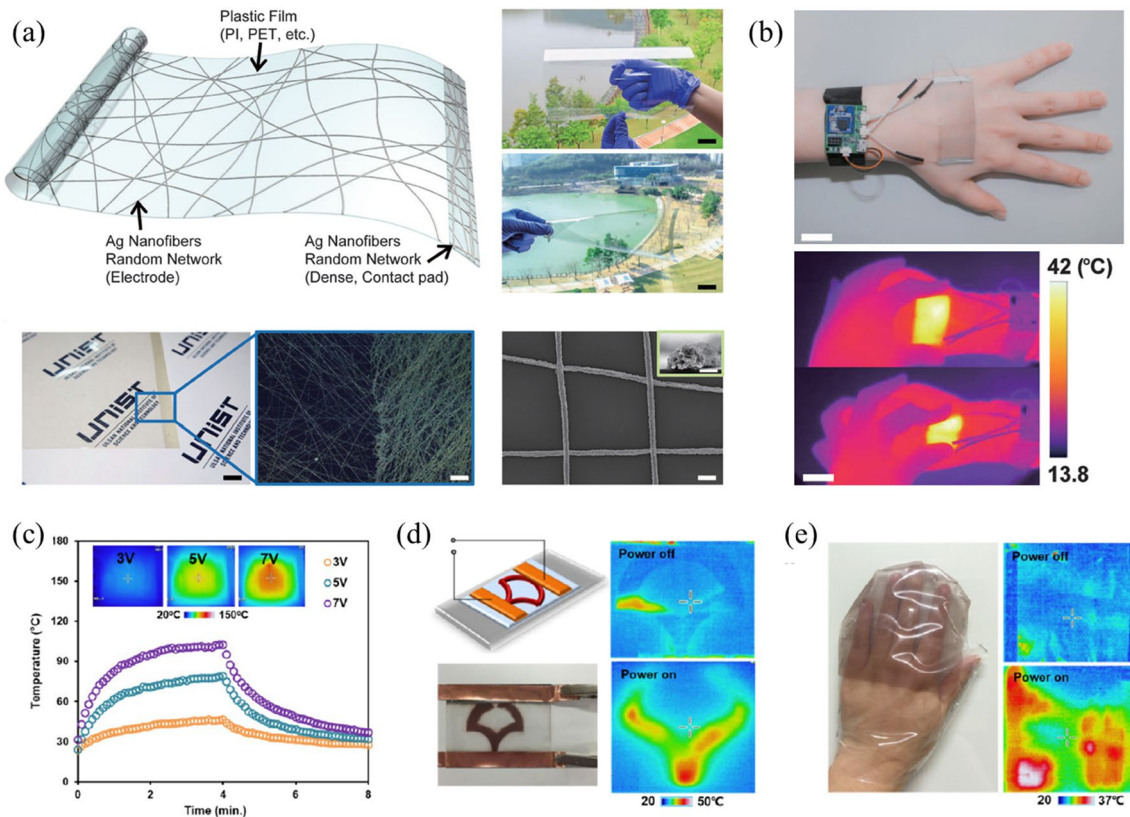


**Fig. 30** **a** Characterization of a stretchable, transparent and large-area AgNF heater. **b** A photograph and IR images of the wearable heater with a wristband-type wireless operation device [193]. Application of CuNW/PU conductors as heater. **c** Temperature under applied voltages **d** the schematic illustration and actual photo of the patterned CuNW/PU heater, infrared images of the heater when the voltage was off (above right) and on (bottom right). **e** Photo of heater glove wearing on hands (left), infrared images of the glove when the volt-

age was off (above right) and on (bottom right) [45]. [a, b This work is licensed under the Creative Commons Attribution 4.0 International License. To view a copy of this license, visit <https://creativecommons.org/licenses/by/4.0/> or send a letter to Creative Commons, PO Box 1866, Mountain View, CA 94042, USA; c–e Reprinted (adapted) with permission from Ding et al. [45]. Copyright (2016) American Chemical Society]

Joule heating by enabling an increase in the  $\Delta T$  of nearly 10 °C (26–30% increase) for both Dip-3 and Dip-5 samples (Fig. 31d). The maximum  $\Delta T$  of 32 °C, reached for IPL-sintered Dip-5 Ag nanowire-fabric, is quite close to the required value of 35 °C for personal heating patches on garments. Figure 31e shows the temperature response of the optimally IPL-sintered Dip-5 Ag nanowire-fabric, for ten repeated on/off voltage cycles with 2 min on time and 2 min off time. The heating and cooling response and the maximum saturation temperature are preserved with high repeatability, indicating high thermal stability of the IPL-sintered patches under cyclic operation. These results are expected to be used in our daily life such as wearable electronics, artificial skin and bendable sensors.

The various applications presented above are still being studied and developed. On the other hand, we will introduce several applications that have the potential to greatly improve the performance when applying the IPL

process. In addition, various fields that are currently being actively researched have a potential to be applied to the IPL process. First of all, IPL process can be applied to the high precision algorithm device such as a Micro-Electro-Mechanical System based Inertial Navigation Systems (MEMS-INS) [196], mid-wavelength infrared (MWIR) polarizer [197] and an organic magnetoresistance (OMAR) sensors [198]. In addition, it can be used to make a chemical reacting materials such as catalysts [199–201] and water splitting materials [202, 203]. Also, IPL process technology has the potential to be used to fabricate energy storage units [204–208] in line with recent development of new, clean, high efficiency energy industry. Lastly, its application in military parts [209] and antibacterial materials [210] has been outstanding. Like these potential applications, IPL process has a tremendous possibility to be applied to various research area.

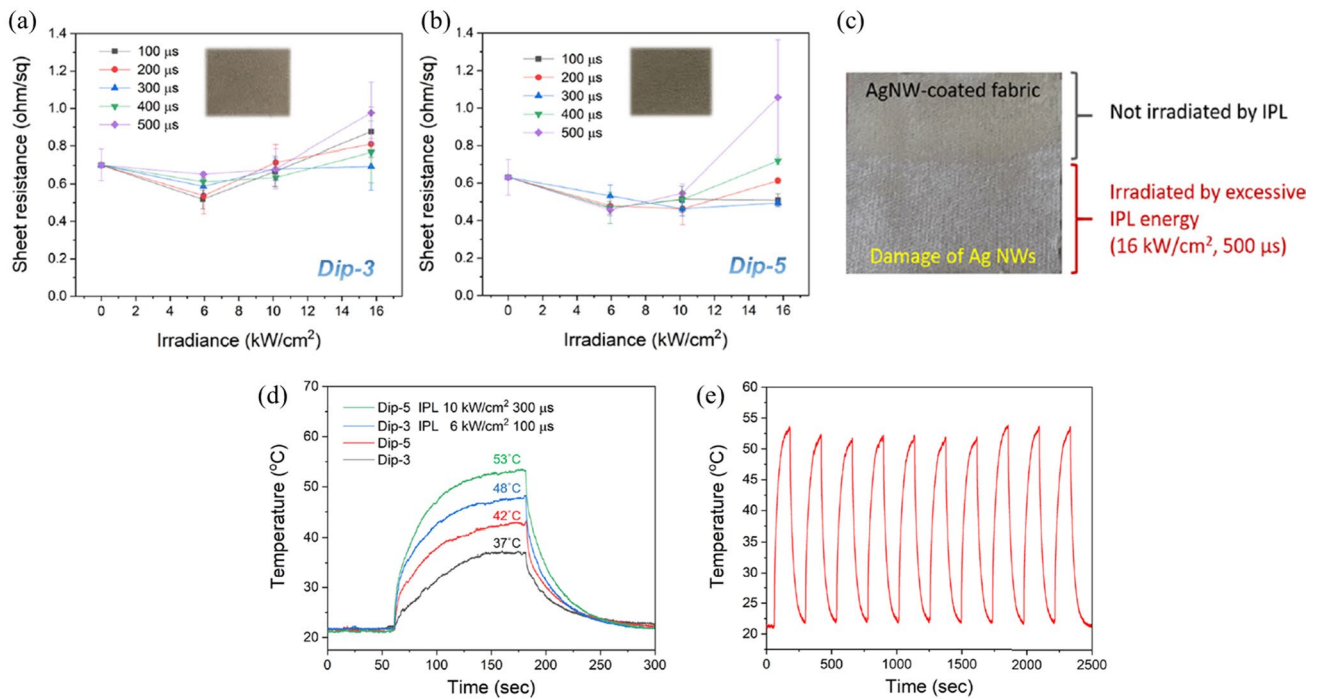


**Fig. 31** Electrical properties of IPL sintered Ag nanowire-fabrics. Sheet resistance of IPL sintered Ag nanowire-fabrics for different irradiance and pulse duration for **a** Dip-3 **b** Dip-5 cases. **c** Optical image of Ag nanowire-fabric half exposed to IPL irradiance 16 kW/cm<sup>2</sup> for 500 μs pulse duration. Joule heating test for the fabricated Ag nanowire-fabric patch. **d** Average temperature profile of the Ag nanowire-fabrics under 1 V applied voltage. **e** Average temperature

response of optimally sintered Dip-5 patches over ten on/off cycles (2 min at on state and 2 min at off state) under 1 V applied voltage [195]. [This work is licensed under the Creative Commons Attribution 4.0 International License. To view a copy of this license, visit <https://creativecommons.org/licenses/by/4.0/> or send a letter to Creative Commons, PO Box 1866, Mountain View, CA 94042, USA.]

## 5 Conclusion

In this review, short history and several important research works about IPL sintering were briefly summarized and reviewed. This review focused on specifically metal ink sintering with IPL and its applications. The irradiated IPL on the materials can induce an extremely quick heating (several milliseconds) to the certain temperature by the synergetic opto-chemical, opto-thermal phenomena without damage on the low temperature substrates such as polymer and paper. IPL process is ambient and room temperature condition sintering process without damage of low-temperature substrate. The sintering quality depends much on the metal nanoink contents and substrate's property as well as IPL conditions such as light energy, pulse width/number and wavelength of the light. The IPL process can be used several nano-micro metal particles, flake or wire ink as well as semi-conductor ink or energy harvesting/storage materials, which will be our next review work. It is certain that the IPL process will provide a paved route to revolutionary eco-benign and low-cost manufacturing process for many applications in near future.

**Acknowledgements** This work was supported by a National Research Foundation of Korea (NRF), funded by the Ministry of Education (2012R1A6A1029029, 2018R1D1A1A09083236).

## References

- Kim, H.-S., Dhage, S. R., Shim, D.-E., & Hahn, H. T. (2009). Intense pulsed light sintering of copper nanoink for printed electronics. *Applied Physics A*, 97, 791.
- Kinney, L. C. & Tompkins, E. H. (1969). Method of making printed circuits. U.S. patent US3451813A.
- Ryu, J., Kim, H.-S., & Hahn, H. T. (2011). Reactive sintering of copper nanoparticles using intense pulsed light for printed electronics. *Journal of Electronic Materials*, 40, 42–50.
- Kang, H., Sowade, E., & Baumann, R. R. (2014). Direct intense pulsed light sintering of inkjet-printed copper oxide layers within six milliseconds. *ACS Applied Materials & Interfaces*, 6, 1682–1687.
- Han, W.-S., Hong, J.-M., Kim, H.-S., & Song, Y.-W. (2011). Multi-pulsed white light sintering of printed Cu nanoinks. *Nanotechnology*, 22, 395705.
- Shankar, A., Salcedo, E., Berndt, A., Choi, D., & Ryu, J. E. (2018). Pulsed light sintering of silver nanoparticles for large deformation of printed stretchable electronics. *Advanced Composites and Hybrid Materials*, 1, 193–198.

7. Lee, D. J., et al. (2011). Pulsed light sintering characteristics of inkjet-printed nanosilver films on a polymer substrate. *Journal of Micromechanics and Microengineering*, *21*, 125023.
8. Weise, D., Mitra, K. Y., Sowade, E., & Baumann, R. R. (2015). Intense pulsed light sintering of inkjet printed silver nanoparticle ink: Influence of flashing parameters and substrate. *MRS Online Proceedings Library Archive*, *1761*, 1–6.
9. Jang, K., Yu, S., Park, S.-H., Kim, H.-S., & Ahn, H. (2015). Intense pulsed light-assisted facile and agile fabrication of cobalt oxide/nickel cobaltite nanoflakes on nickel-foam for high performance supercapacitor applications. *Journal of Alloys and Compounds*, *618*, 227–232.
10. Park, C., et al. (2017). Intense pulsed white light assisted fabrication of Co-CoOx core-shell nanoflakes on graphite felt for flexible hybrid supercapacitors. *Electrochimica Acta*, *246*, 757–765.
11. Hwang, H.-J., Oh, K.-H., & Kim, H.-S. (2016). All-photonic drying and sintering process via flash white light combined with deep-UV and near-infrared irradiation for highly conductive copper nano-ink. *Scientific Reports*, *6*, 19696.
12. Oh, G.-H., Hwang, H.-J., & Kim, H.-S. (2017). Effect of copper oxide shell thickness on flash light sintering of copper nanoparticle ink. *RSC Advances*, *7*, 17724–17731.
13. Hwang, H.-J., Chung, W.-H., & Kim, H.-S. (2012). In situ monitoring of flash-light sintering of copper nanoparticle ink for printed electronics. *Nanotechnology*, *23*, 485205.
14. Joo, S.-J., Hwang, H.-J., & Kim, H.-S. (2014). Highly conductive copper nano/microparticles ink via flash light sintering for printed electronics. *Nanotechnology*, *25*, 265601.
15. Chung, W.-H., Hwang, H.-J., & Kim, H.-S. (2015). Flash light sintered copper precursor/nanoparticle pattern with high electrical conductivity and low porosity for printed electronics. *Thin Solid Films*, *580*, 61–70.
16. Chung, W.-H., Hwang, H.-J., Lee, S.-H., & Kim, H.-S. (2012). In situ monitoring of a flash light sintering process using silver nano-ink for producing flexible electronics. *Nanotechnology*, *24*, 035202.
17. Yung, K., Gu, X., Lee, C., & Choy, H. (2010). Ink-jet printing and camera flash sintering of silver tracks on different substrates. *Journal of Materials Processing Technology*, *210*, 2268–2272.
18. Park, S.-H., Jang, S., Lee, D.-J., Oh, J., & Kim, H.-S. (2012). Two-step flash light sintering process for crack-free inkjet-printed Ag films. *Journal of Micromechanics and Microengineering*, *23*, 015013.
19. Moon, C.-J., et al. (2017). Flash light sintering of ag mesh films for printed transparent conducting electrode. *Thin Solid Films*, *629*, 60–68.
20. Chung, W.-H., Hwang, Y.-T., Lee, S.-H., & Kim, H.-S. (2016). Electrical wire explosion process of copper/silver hybrid nanoparticle ink and its sintering via flash white light to achieve high electrical conductivity. *Nanotechnology*, *27*, 205704.
21. Lee, C., et al. (2018). Flash-induced nanowelding of silver nanowire networks for transparent stretchable electrochromic devices. *Scientific Reports*, *8*, 2763.
22. Chung, W.-H., Kim, S.-H., & Kim, H.-S. (2016). Welding of silver nanowire networks via flash white light and UV-C irradiation for highly conductive and reliable transparent electrodes. *Scientific Reports*, *6*, 32086.
23. Park, J. H., et al. (2017). Flash-induced self-limited plasmonic welding of silver nanowire network for transparent flexible energy harvester. *Advanced Materials*, *29*, 1603473.
24. Kang, C., Kim, H., Oh, Y.-W., Baek, K.-H., & Do, L.-M. (2016). High-performance, solution-processed indium-oxide TFTs using rapid flash lamp annealing. *IEEE Electron Device Letters*, *37*, 595–598.
25. Eom, T.-Y., et al. (2018). Investigation of the evolution of nitrogen defects in flash-lamp-annealed InGaZnO films and their effects on transistor characteristics. *Applied Physics Express*, *11*, 061104.
26. Hwang, H.-J., & Kim, H.-S. (2015). Ultra-high speed fabrication of TiO<sub>2</sub> photoanode by flash light for dye-sensitized solar cell. *Journal of Nanoscience and Nanotechnology*, *15*, 5028–5034.
27. Patil, S. A., Hwang, H.-J., Yu, M.-H., Shrestha, N. K., & Kim, H.-S. (2017). Photonic sintering of a ZnO nanosheet photoanode using flash white light combined with deep UV irradiation for dye-sensitized solar cells. *RSC Advances*, *7*, 6565–6573.
28. Park, S.-H., & Kim, H.-S. (2014). Flash light sintering of nickel nanoparticles for printed electronics. *Thin Solid Films*, *550*, 575–581.
29. Song, Y.-W., Park, S.-H., Han, W.-S., Hong, J.-M., & Kim, H.-S. (2011). Single-step high-speed nanogranulation of metal alloy around carbon nanotubes by flash light irradiation. *Materials Letters*, *65*, 2510–2513.
30. Park, S.-H., Jung, H.-M., Um, S., Song, Y.-W., & Kim, H.-S. (2012). Rapid synthesis of Pt-based alloy/carbon nanotube catalysts for a direct methanol fuel cell using flash light irradiation. *International Journal of Hydrogen Energy*, *37*, 12597–12604.
31. Park, S.-H., & Kim, H.-S. (2015). Flash light-assisted facile and eco-friendly synthesis of platinum-based alloy nanoparticle/carbon nano-tube catalysts for a direct methanol fuel cell. *Journal of the Electrochemical Society*, *162*, F204–F210.
32. Cote, L. J., Cruz-Silva, R., & Huang, J. (2009). Flash reduction and patterning of graphene oxide and its polymer composite. *Journal of the American Chemical Society*, *131*, 11027–11032.
33. Park, S.-H., & Kim, H.-S. (2015). Environmentally benign and facile reduction of graphene oxide by flash light irradiation. *Nanotechnology*, *26*, 205601.
34. Chung, W.-H., Park, S.-H., Joo, S.-J., & Kim, H.-S. (2018). UV-assisted flash light welding process to fabricate silver nanowire/graphene on a PET substrate for transparent electrodes. *Nano Research*, *11*, 2190–2203.
35. Jeon, E.-B., Joo, S.-J., Ahn, H., & Kim, H.-S. (2016). Two-step flash light sintering process for enhanced adhesion between copper complex ion/silane ink and a flexible substrate. *Thin Solid Films*, *603*, 382–390.
36. Ryu, C.-H., Joo, S.-J., & Kim, H.-S. (2016). Two-step flash light sintering of copper nanoparticle ink to remove substrate warping. *Applied Surface Science*, *384*, 182–191.
37. Hwang, Y.-T., Chung, W.-H., Jang, Y.-R., & Kim, H.-S. (2016). Intensive plasmonic flash light sintering of copper nanoinks using a band-pass light filter for highly electrically conductive electrodes in printed electronics. *ACS Applied Materials & Interfaces*, *8*, 8591–8599.
38. Son, Y.-H., Jang, J.-Y., Kang, M. K., Ahn, S., & Lee, C. S. (2018). Application of flash-light sintering method to flexible inkjet printing using anti-oxidant copper nanoparticles. *Thin Solid Films*, *656*, 61–67.
39. Hwang, H.-J., et al. (2018). Multi-pulsed flash light sintering of copper nanoparticle pastes on silicon wafer for highly-conductive copper electrodes in crystalline silicon solar cells. *Applied Surface Science*, *462*, 378–386.
40. Sarkar, S. K., Gupta, H., & Gupta, D. (2017). Flash light sintering of silver nanoink for inkjet-printed thin-film transistor on flexible substrate. *IEEE Transactions on Nanotechnology*, *16*, 375–382.
41. Takahashi, K., Namiki, K., Fujimura, T., Jeon, E.-B., & Kim, H.-S. (2015). Instant electrode fabrication on carbon-fiber-reinforced plastic structures using metal nano-ink via flash light sintering for smart sensing. *Composites Part B: Engineering*, *76*, 167–173.
42. Skorupa, W. et al. (2004). Advanced thermal processing of semiconductor materials by flash lamp annealing. *MRS Online Proceedings Library Archive*, *810*.

43. Park, J.-S., Chung, W.-H., Kim, H.-S., & Kim, Y.-B. (2017). Rapid fabrication of chemical-solution-deposited  $\text{La}_{0.6}\text{Sr}_{0.4}\text{CoO}_{3-\delta}$  thin films via flashlight sintering. *Journal of Alloys and Compounds*, 696, 102–108.
44. Schroder, K., McCool, S., & Furlan, W. (2006). Broadcast photonic curing of metallic nanoparticle films. *NSTI Nanotech*, 7, 11.
45. Ding, S., et al. (2016). One-step fabrication of stretchable copper nanowire conductors by a fast photonic sintering technique and its application in wearable devices. *ACS Applied Materials & Interfaces*, 8, 6190–6199.
46. SeonáYoon, I., & HongáKim, S. (2017). Selective photonic sintering of Ag flakes embedded in silicone elastomers to fabricate stretchable conductors. *Journal of Materials Chemistry C*, 5, 11733–11740.
47. Hösel, M., & Krebs, F. C. (2012). Large-scale roll-to-roll photonic sintering of flexo printed silver nanoparticle electrodes. *Journal of Materials Chemistry*, 22, 15683–15688.
48. Galagan, Y., et al. (2013). Photonic sintering of inkjet printed current collecting grids for organic solar cell applications. *Organic Electronics*, 14, 38–46.
49. Albrecht, A., Rivadeneyra, A., Abdellah, A., Lugli, P., & Salmerón, J. F. (2016). Inkjet printing and photonic sintering of silver and copper oxide nanoparticles for ultra-low-cost conductive patterns. *Journal of Materials Chemistry C*, 4, 3546–3554.
50. Su, B.-Y., Chu, S.-Y., Juang, Y.-D., & Chen, H.-C. (2013). High-performance low-temperature solution-processed InGaZnO thin-film transistors via ultraviolet-ozone photo-annealing. *Applied Physics Letters*, 102, 192101.
51. Gilje, S., et al. (2010). Photothermal deoxygenation of graphene oxide for patterning and distributed ignition applications. *Advanced Materials*, 22, 419–423.
52. Zhang, Y. L., et al. (2014). Photoreduction of graphene oxides: Methods, properties, and applications. *Advanced Optical Materials*, 2, 10–28.
53. Schroder, K. A. (2011). Mechanisms of Photonic Curing™: Processing high temperature films on low temperature substrates. *Nanotechnology*, 2, 220–223.
54. Gu, W. & Cui, Z. (2016). In: *Electronic System-Integration Technology Conference (ESTC), 2016 6<sup>th</sup>* (pp. 1–4). IEEE.
55. Jo, Y., et al. (2014). Extremely flexible, printable Ag conductive features on PET and paper substrates via continuous millisecond photonic sintering in a large area. *Journal of Materials Chemistry C*, 2, 9746–9753.
56. Araki, T., et al. (2013). Cu salt ink formulation for printed electronics using photonic sintering. *Langmuir*, 29, 11192–11197.
57. Kim, I., et al. (2018). A photonic sintering derived Ag flake/nanoparticle-based highly sensitive stretchable strain sensor for human motion monitoring. *Nanoscale*, 10, 7890–7897.
58. Cronin, H. M., et al. (2018). Photonic curing of low-cost aqueous silver flake inks for printed conductors with increased yield. *ACS Applied Materials & Interfaces*, 10, 21398–21410.
59. Paglia, F., et al. (2015). Photonic sintering of copper through the controlled reduction of printed CuO nanocrystals. *ACS Applied Materials & Interfaces*, 7, 25473–25478.
60. Tetzner, K., Schroder, K. A., & Bock, K. (2014). Photonic curing of sol–gel derived  $\text{HfO}_2$  dielectrics for organic field-effect transistors. *Ceramics International*, 40, 15753–15761.
61. Cui, H.-W., et al. (2014). Ultra-fast photonic curing of electrically conductive adhesives fabricated from vinyl ester resin and silver micro-flakes for printed electronics. *RSC Advances*, 4, 15914–15922.
62. Norita, S., et al. (2015). Inkjet-printed copper electrodes using photonic sintering and their application to organic thin-film transistors. *Organic Electronics*, 25, 131–134.
63. Wikipedia. <https://en.wikipedia.org/wiki/Flashtube>. Accessed 11 Jan 2020.
64. Moores, A., & Goettmann, F. (2006). The plasmon band in noble metal nanoparticles: An introduction to theory and applications. *New Journal of Chemistry*, 30, 1121–1132.
65. Kelly, K. L., Coronado, E., Zhao, L. L., & Schatz, G. C. (2003). The optical properties of metal nanoparticles: The influence of size, shape, and dielectric environment. *The Journal of Physical Chemistry B*, 107, 668–677.
66. Zhang, J. Z., & Noguez, C. (2008). Plasmonic optical properties and applications of metal nanostructures. *Plasmonics*, 3, 127–150.
67. Park, B. K., Kim, D., Jeong, S., Moon, J., & Kim, J. S. (2007). Direct writing of copper conductive patterns by ink-jet printing. *Thin Solid Films*, 515, 7706–7711.
68. Rager, M. S., Aytug, T., Veith, G. M., & Joshi, P. (2016). Low-thermal-budget photonic processing of highly conductive Cu interconnects based on CuO nanoinks: Potential for flexible printed electronics. *ACS Applied Materials & Interfaces*, 8, 2441–2448.
69. Perelaer, J., De Gans, B. J., & Schubert, U. S. (2006). Ink-jet printing and microwave sintering of conductive silver tracks. *Advanced Materials*, 18, 2101–2104.
70. Reinhold, I., et al. (2009). Argon plasma sintering of inkjet printed silver tracks on polymer substrates. *Journal of Materials Chemistry*, 19, 3384–3388.
71. Allen, M. L., et al. (2008). Electrical sintering of nanoparticle structures. *Nanotechnology*, 19, 175201.
72. Hong, S., et al. (2013). Nonvacuum, maskless fabrication of a flexible metal grid transparent conductor by low-temperature selective laser sintering of nanoparticle ink. *ACS Nano*, 7, 5024–5031.
73. Zenou, M., Ermak, O., Saar, A., & Kotler, Z. (2013). Laser sintering of copper nanoparticles. *Journal of Physics D: Applied Physics*, 47, 025501.
74. Yu, J. H., Rho, Y., Kang, H., Jung, H. S., & Kang, K.-T. (2015). Electrical behavior of laser-sintered Cu based metal-organic decomposition ink in air environment and application as current collectors in supercapacitor. *International Journal of Precision Engineering and Manufacturing-Green Technology*, 2, 333–337.
75. Allabergenov, B., & Kim, S. (2013). Investigation of electro-physical and mechanical characteristics of porous copper-carbon composite materials prepared by spark plasma sintering. *International Journal of Precision Engineering and Manufacturing*, 14, 1177–1183.
76. Luo, X.-L., et al. (2018). Microwave synthesis of hierarchical porous materials with various structures by controllable desilication and recrystallization. *Microporous and Mesoporous Materials*, 262, 148–153.
77. Luo, X., et al. (2018). In situ growth of hollow Cu<sub>2</sub>O spheres using anionic vesicles as soft templates. *Journal of Industrial and Engineering Chemistry*, 59, 410–415.
78. Pan, D., et al. (2018). Synthesis and characterization of ZnNiIn layered double hydroxides derived mixed metal oxides with highly efficient photoelectrocatalytic activities. *Industrial & Engineering Chemistry Research*, 58, 836–848.
79. Tian, J., et al. (2019). Microwave solvothermal carboxymethyl chitosan templated synthesis of TiO<sub>2</sub>/ZrO<sub>2</sub> composites toward enhanced photocatalytic degradation of Rhodamine B. *Journal of Colloid and Interface Science*, 541, 18–29.
80. Zhang, Y., et al. (2019). Facile bioactive yeast cell templated synthesis of laser stealth antimony doped tin oxide hollow microspheres. *Colloids and Surfaces A: Physicochemical and Engineering Aspects*, 583, 123965.
81. Tong, Y., et al. (2018). Thermal shock resistance of continuous carbon fiber reinforced ZrC based ultra-high temperature ceramic composites prepared via Zr-Si alloyed melt infiltration. *Materials Science and Engineering: A*, 735, 166–172.



82. Tong, Y., et al. (2018). Microstructures and properties of Si-Zr alloy based CMCs reinforced by various porous C/C performs. *Ceramics International*, *44*, 16577–16582.
83. Tong, Y., et al. (2018). Different-shaped ultrafine MoNbTaW HEA powders prepared via mechanical alloying. *Materials*, *11*, 1250.
84. Tong, Y., et al. (2018). Laser ablation resistance and mechanism of Si-Zr alloyed melt infiltrated C/C-SiC composite. *Ceramics International*, *44*, 3692–3698.
85. Zhao, Y.-H., et al. (2018). Precipitation sequence of middle Al concentration alloy using the inversion algorithm and microscopic phase field model. *Science of Advanced Materials*, *10*, 1793–1804.
86. Zhao, Z., et al. (2019). AlSi10Mg alloy nanocomposites reinforced with aluminum-coated graphene: Selective laser melting, interfacial microstructure and property analysis. *Journal of Alloys and Compounds*, *792*, 203–214.
87. Zhao, Y., et al. (2018). First-principle investigation of pressure and temperature influence on structural, mechanical and thermodynamic properties of  $Ti_3AC_2$  (A = Al and Si). *Computational Materials Science*, *154*, 365–370.
88. Yim, C., Greco, K., Sandwell, A., & Park, S. S. (2017). Eco-friendly and rapid fabrication method for producing polyethylene terephthalate (PET) mask using intensive pulsed light. *International Journal of Precision Engineering and Manufacturing-Green Technology*, *4*, 155–159.
89. Miyashita, T. (2004). Film deposition method, and film deposition system. Japan patent JP2004277832A.
90. Jiang, Z., Liu, Q., & Liu, S. (2002). Resonance scattering spectral analysis of chlorides based on the formation of (AgCl)  $n$  (Ag) s nanoparticle. *Spectrochimica Acta Part A: Molecular and Biomolecular Spectroscopy*, *58*, 2759–2764.
91. Chan, G. H., Zhao, J., Hicks, E. M., Schatz, G. C., & Van Duynne, R. P. (2007). Plasmonic properties of copper nanoparticles fabricated by nanosphere lithography. *Nano Letters*, *7*, 1947–1952.
92. de Moraes, A. C. M., Lima, B. A., de Faria, A. F., Brocchi, M., & Alves, O. L. (2015). Graphene oxide-silver nanocomposite as a promising biocidal agent against methicillin-resistant *Staphylococcus aureus*. *International Journal of Nanomedicine*, *10*, 6847.
93. Gabrion, X., Placet, V., Trivaudey, F., & Boubakar, L. J. (2016). About the thermomechanical behaviour of a carbon fibre reinforced high-temperature thermoplastic composite. *Composites Part B: Engineering*, *95*, 386–394.
94. Kim, D., & Moon, J. (2005). Highly conductive ink jet printed films of nanosilver particles for printable electronics. *Electrochemical and Solid-State Letters*, *8*, J30–J33.
95. Liu, Z., Su, Y., & Varahramyan, K. J. (2005). Inkjet-printed silver conductors using silver nitrate ink and their electrical contacts with conducting polymers. *Thin Solid Films*, *478*, 275–279.
96. Jang, S., et al. (2010). Sintering of inkjet printed copper nanoparticles for flexible electronics. *Scripta Materialia*, *62*, 258–261.
97. Rozenberg, G. G., Bresler, E., Speakman, S. P., Jeynes, C., & Steinke, J. H. (2002). Patterned low temperature copper-rich deposits using inkjet printing. *Applied Physics Letters*, *81*, 5249–5251.
98. Zhang, Z.-H., Wang, F.-C., Wang, L., & Li, S.-K. (2008). Ultrafine-grained copper prepared by spark plasma sintering process. *Materials Science and Engineering: A*, *476*, 201–205.
99. Ghosh, M., & Mittal, K. (1996). *Polyimides: Fundamentals and applications*. New York: Marcel Dekker; Tomikawa, M., Yoshida, S., Okamoto, N. (2009). *Polymer Journal*, *41*, 604.
100. Deng, D., Cheng, Y., Jin, Y., Qi, T., & Xiao, F. J. (2012). Antioxidative effect of lactic acid-stabilized copper nanoparticles prepared in aqueous solution. *Journal of Materials Chemistry*, *22*, 23989–23995.
101. Kim, Y.-J., Ryu, C.-H., Park, S.-H., & Kim, H.-S. (2014). The effect of poly (N-vinylpyrrolidone) molecular weight on flash light sintering of copper nanopaste. *Thin Solid Films*, *570*, 114–122.
102. Wang, B.-Y., Yoo, T.-H., Song, Y.-W., Lim, D.-S., & Oh, Y.-J. (2013). Cu ion ink for a flexible substrate and highly conductive patterning by intensive pulsed light sintering. *ACS Applied Materials & Interfaces*, *5*, 4113–4119.
103. Kanzaki, M., Kawaguchi, Y., & Kawasaki, H. (2017). Fabrication of conductive copper films on flexible polymer substrates by low-temperature sintering of composite Cu ink in air. *ACS Applied Materials & Interfaces*, *9*, 20852–20858.
104. Choi, Y.-H., & Hong, S.-H. (2015). Effect of the Amine concentration on phase evolution and densification in printed films using Cu (II) complex ink. *Langmuir*, *31*, 8101–8110.
105. Liu, Y., et al. (2017). Capillary-force-induced cold welding in silver-nanowire-based flexible transparent electrodes. *Nano Letters*, *17*, 1090–1096.
106. Tam, S. K., Fung, K. Y., & Ng, K. M. (2016). Copper pastes using bimodal particles for flexible printed electronics. *Journal of Materials Science*, *51*, 1914–1922.
107. Patil, S. A., Ryu, C.-H., & Kim, H.-S. (2018). Synthesis and characterization of copper nanoparticles (Cu-Nps) using rongalite as reducing agent and photonic sintering of Cu-Nps ink for printed electronics. *International Journal of Precision Engineering and Manufacturing-Green Technology*, *5*, 239–245.
108. Wong, D., Yim, C. & Park, S. S. (2019). Hybrid manufacturing of oxidation resistant cellulose nanocrystals-copper-graphene nanoplatelets based electrodes. *International Journal of Precision Engineering and Manufacturing-Green Technology*, 1–15.
109. Rosen, Y. S., Yakushenko, A., usser, A., & Magdassi, S. (2017). Self-reducing copper precursor inks and photonic additive yield conductive patterns under intense pulsed light. *ACS Omega*, *2*, 573–581.
110. Hwang, H.-J., Joo, S.-J., & Kim, H.-S. (2015). Copper nanoparticle/multiwalled carbon nanotube composite films with high electrical conductivity and fatigue resistance fabricated via flash light sintering. *ACS Applied Materials & Interfaces*, *7*, 25413–25423.
111. Joo, S.-J., Park, S.-H., Moon, C.-J., & Kim, H.-S. (2015). A highly reliable copper nanowire/nanoparticle ink pattern with high conductivity on flexible substrate prepared via a flash light-sintering technique. *ACS Applied Materials & Interfaces*, *7*, 5674–5684.
112. Yu, M.-H., Joo, S.-J., & Kim, H.-S. (2017). Multi-pulse flash light sintering of bimodal Cu nanoparticle-ink for highly conductive printed Cu electrodes. *Nanotechnology*, *28*, 205205.
113. Ryu, C.-H., Joo, S.-J., & Kim, H.-S. (2019). Intense pulsed light sintering of Cu nano particles/micro particles-ink assisted with heating and vacuum holding of substrate for warpage free printed electronic circuit. *Thin Solid Films*, *675*, 23–33.
114. Park, H. J., et al. (2018). Highly durable Cu-based electrodes from a printable nanoparticle mixture ink: Flash-light-sintered, kinetically-controlled microstructure. *Nanoscale*, *10*, 5047–5053.
115. Kang, J., Ryu, J., Kim, H., & Hahn, H. (2011). Sintering of inkjet-printed silver nanoparticles at room temperature using intense pulsed light. *Journal of Electronic Materials*, *40*, 2268.
116. Niittynen, J., et al. (2014). Alternative sintering methods compared to conventional thermal sintering for inkjet printed silver nanoparticle ink. *Thin Solid Films*, *556*, 452–459.
117. Tobjörk, D., et al. (2012). IR-sintering of ink-jet printed metal nanoparticles on paper. *Thin Solid Films*, *520*, 2949–2955.
118. Kwak, J. H., Chun, S. J., Shon, C.-H., & Jung, S. (2018). Back-irradiation photonic sintering for defect-free high-conductivity metal patterns on transparent plastic. *Applied Physics Letters*, *112*, 153103.

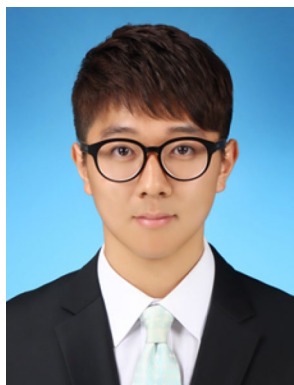
119. Ahn, B. Y., et al. (2009). Omnidirectional printing of flexible, stretchable, and spanning silver microelectrodes. *Science*, *323*, 1590–1593.
120. Woo, K., Kim, Y., Lee, B., Kim, J., & Moon, J. (2011). Effect of carboxylic acid on sintering of inkjet-printed copper nanoparticle films. *ACS Applied Materials & Interfaces*, *3*, 2377–2382.
121. Weast, R. C., & Selby, S. (1971). *Handbook of chemistry and physics* (vol. 77). Boca Raton: The Chemical Rubber Co.
122. Jeong, S., et al. (2008). Controlling the thickness of the surface oxide layer on Cu nanoparticles for the fabrication of conductive structures by ink-jet printing. *Advanced Functional Materials*, *18*, 679–686.
123. Choi, C. S., Jo, Y. H., Kim, M. G., & Lee, H. M. (2012). Control of chemical kinetics for sub-10 nm Cu nanoparticles to fabricate highly conductive ink below 150 C. *Nanotechnology*, *23*, 065601.
124. Kim, Y. H., Lee, D. K., Jo, B. G., Jeong, J. H., & Kang, Y. S. (2006). Synthesis of oleate capped Cu nanoparticles by thermal decomposition. *Colloids and Surfaces A: Physicochemical and Engineering Aspects*, *284*, 364–368.
125. Xia, X., Xie, C., Cai, S., Yang, Z., & Yang, X. (2006). Corrosion characteristics of copper microparticles and copper nanoparticles in distilled water. *Corrosion Science*, *48*, 3924–3932.
126. Chen, Y., Yang, F., Dai, Y., Wang, W., & Chen, S. (2008). Ni@Pt core-shell nanoparticles: Synthesis, structural and electrochemical properties. *The Journal of Physical Chemistry C*, *112*, 1645–1649.
127. Bala, T., Bhame, S., Joy, P., Prasad, B., & Sastry, M. (2004). A facile liquid foam based synthesis of nickel nanoparticles and their subsequent conversion to Ni core Ag shell particles: Structural characterization and investigation of magnetic properties. *Journal of Materials Chemistry*, *14*, 2941–2945.
128. Xu, X., Luo, X., Zhuang, H., Li, W., & Zhang, B. (2003). Electroless silver coating on fine copper powder and its effects on oxidation resistance. *Materials Letters*, *57*, 3987–3991.
129. Muzikansky, A., Nanikashvili, P., Grinblat, J., & Zitoun, D. (2013). Ag dewetting in Cu@Ag monodisperse core-shell nanoparticles. *The Journal of Physical Chemistry C*, *117*, 3093–3100.
130. Grouchko, M., Kamyshny, A., & Magdassi, S. (2009). Formation of air-stable copper-silver core-shell nanoparticles for inkjet printing. *Journal of Materials Chemistry*, *19*, 3057–3062.
131. Kwon, S. G., et al. (2015). Heterogeneous nucleation and shape transformation of multicomponent metallic nanostructures. *Nature Materials*, *14*, 215.
132. Hatamura, M., Yamaguchi, S., Takane, S.-Y., Chen, Y., & Suganuma, K. (2015). Decarboxylation and simultaneous reduction of silver (i)  $\beta$ -ketocarboxylates with three types of coordinations. *Dalton Transactions*, *44*, 8993–9003.
133. Li, W., et al. (2017). Printable and flexible copper-silver alloy electrodes with high conductivity and ultrahigh oxidation resistance. *ACS Applied Materials & Interfaces*, *9*, 24711–24721.
134. Malviya, K. D., & Chattopadhyay, K. (2016). Temperature- and size-dependent compositionally tuned microstructural landscape for Ag-46 atom% Cu nanoalloy prepared by laser ablation in liquid. *The Journal of Physical Chemistry C*, *120*, 27699–27706.
135. Chu, J.-H., Joo, S.-J., & Kim, H.-S. (2019). Development of a via-hole connection process via intense pulsed light sintering with Cu micro/Ag nano-hybrid ink for a multi-layered flexible printed circuit board. *Thin Solid Films*, *680*, 1–11.
136. Leem, D. S., et al. (2011). Efficient organic solar cells with solution-processed silver nanowire electrodes. *Advanced Materials*, *23*, 4371–4375.
137. Zou, J., Yip, H.-L., Hau, S. K., & Jen, A. K.-Y. (2010). Metal grid/conducting polymer hybrid transparent electrode for inverted polymer solar cells. *Applied Physics Letters*, *96*, 96.
138. Yang, Y., & Heeger, A. J. (1994). Polyaniline as a transparent electrode for polymer light-emitting diodes: Lower operating voltage and higher efficiency. *Applied Physics Letters*, *64*, 1245–1247.
139. Haight, R. A., & Troutman, R. R. (1998). Optically transparent diffusion barrier and top electrode in organic light emitting diode structures. U.S. patent US5714838A.
140. Trung, T. Q., Ramasundaram, S., Hwang, B. U., & Lee, N. E. (2016). An all-elastomeric transparent and stretchable temperature sensor for body-attachable wearable electronics. *Advanced Materials*, *28*, 502–509.
141. Hecht, D. S., et al. (2009). Carbon-nanotube film on plastic as transparent electrode for resistive touch screens. *Journal of the Society for Information Display*, *17*, 941–946.
142. Madaria, A. R., Kumar, A., & Zhou, C. (2011). Large scale, highly conductive and patterned transparent films of silver nanowires on arbitrary substrates and their application in touch screens. *Nanotechnology*, *22*, 245201.
143. Yamamoto, N., et al. (2012). Development of Ga-doped ZnO transparent electrodes for liquid crystal display panels. *Thin Solid Films*, *520*, 4131–4138.
144. Fu, W., Liu, L., Jiang, K., Li, Q., & Fan, S. (2010). Super-aligned carbon nanotube films as aligning layers and transparent electrodes for liquid crystal displays. *Carbon*, *48*, 1876–1879.
145. Lee, J.-Y., Connor, S. T., Cui, Y., & Peumans, P. (2008). Solution-processed metal nanowire mesh transparent electrodes. *Nano letters*, *8*, 689–692.
146. Rathmell, A. R., & Wiley, B. J. (2011). The synthesis and coating of long, thin copper nanowires to make flexible, transparent conducting films on plastic substrates. *Advanced Materials*, *23*, 4798–4803.
147. Guo, H., et al. (2013). Copper nanowires as fully transparent conductive electrodes. *Scientific Reports*, *3*, 2323.
148. Van De Lagemaat, J., et al. (2006). Organic solar cells with carbon nanotubes replacing  $\text{In}_2\text{O}_3$ : Sn as the transparent electrode. *Applied Physics Letters*, *88*, 233503.
149. Kim, K. S., et al. (2009). Large-scale pattern growth of graphene films for stretchable transparent electrodes. *Nature*, *457*, 706.
150. Pang, S., Hernandez, Y., Feng, X., & Müllen, K. (2011). Graphene as transparent electrode material for organic electronics. *Advanced Materials*, *23*, 2779–2795.
151. Hu, L., Kim, H. S., Lee, J.-Y., Peumans, P., & Cui, Y. (2010). Scalable coating and properties of transparent, flexible, silver nanowire electrodes. *ACS Nano*, *4*, 2955–2963.
152. Garnett, E. C., et al. (2012). Self-limited plasmonic welding of silver nanowire junctions. *Nature Materials*, *11*, 241.
153. Kholmanov, I. N., et al. (2013). Reduced graphene oxide/copper nanowire hybrid films as high-performance transparent electrodes. *ACS Nano*, *7*, 1811–1816.
154. Qian, F., et al. (2017). Ultralight conductive silver nanowire aerogels. *Nano Letters*, *17*, 7171–7176.
155. Spechler, J. A., & Arnold, C. B. (2012). Direct-write pulsed laser processed silver nanowire networks for transparent conducting electrodes. *Applied Physics A*, *108*, 25–28.
156. Zhu, S., et al. (2013). Transferable self-welding silver nanowire network as high performance transparent flexible electrode. *Nanotechnology*, *24*, 335202.
157. Jang, Y.-R., et al. (2018). Selective wavelength plasmonic flash light welding of silver nanowires for transparent electrodes with high conductivity. *ACS Applied Materials & Interfaces*, *10*, 24099–24107.
158. Wang, Z., et al. (2008). The influences of particle number on hot spots in strongly coupled metal nanoparticles chain. *The Journal of Chemical Physics*, *128*, 094705.
159. Wei, H., & Xu, H. (2013). Hot spots in different metal nanostructures for plasmon-enhanced Raman spectroscopy. *Nanoscale*, *5*, 10794–10805.

160. Dexter, M., et al. (2018). Modeling nanoscale temperature gradients and conductivity evolution in pulsed light sintering of silver nanowire networks. *Nanotechnology*, 29, 505205.
161. Lee, D. J., Oh, Y., Hong, J.-M., Park, Y. W., & Ju, B.-K. (2018). Light sintering of ultra-smooth and robust silver nanowire networks embedded in poly (vinyl-butylal) for flexible OLED. *Scientific Reports*, 8, 14170.
162. Jiu, J., et al. (2012). Strongly adhesive and flexible transparent silver nanowire conductive films fabricated with a high-intensity pulsed light technique. *Journal of Materials Chemistry*, 22, 23561–23567.
163. Yang, S. B., et al. (2015). Improved optical sintering efficiency at the contacts of silver nanowires encapsulated by a graphene layer. *Small (Weinheim an der Bergstrasse, Germany)*, 11, 1293–1300.
164. Hwang, H.-J., & Malhotra, R. (2018). Shape-tuned junction resistivity and self-damping dynamics in intense pulsed light sintering of silver nanostructure films. *ACS Applied Materials & Interfaces*, 11, 3536–3546.
165. Dexter, M., Bhandari, R., Chang, C., & Malhotra, R. (2017). Controlling processing temperatures and self-limiting behaviour in intense pulsed sintering by tailoring nanomaterial shape distribution. *RSC Advances*, 7, 56395–56405.
166. MacNeill, W., Choi, C.-H., Chang, C.-H., & Malhotra, R. (2015). On the self-damping nature of densification in photonic sintering of nanoparticles. *Scientific Reports*, 5, 14845.
167. Bansal, S., & Malhotra, R. (2016). Nanoscale-shape-mediated coupling between temperature and densification in intense pulsed light sintering. *Nanotechnology*, 27, 495602.
168. Meng, F., & Huang, J. (2019). Evolution mechanism of photonic sintered nano-silver conductive patterns. *Nanomaterials*, 9, 258.
169. Sun, Y., Jin, S., Yang, G., Wang, J., & Wang, C. (2015). Germanium nanowires-in-graphite tubes via self-catalyzed synergetic confined growth and shell-splitting enhanced Li-storage performance. *ACS Nano*, 9, 3479–3490.
170. Zhong, Z., et al. (2016). Continuous patterning of copper nanowire-based transparent conducting electrodes for use in flexible electronic applications. *ACS Nano*, 10, 7847–7854.
171. Park, J. H., et al. (2017). Plasmonic-tuned flash Cu nanowelding with ultrafast photochemical-reducing and interlocking on flexible plastics. *Advanced Functional Materials*, 27, 1701138.
172. Kim, D., Lee, S. H., Jeong, S., Moon, J. J. E., & Letters, S.-S. (2009). All-ink-jet printed flexible organic thin-film transistors on plastic substrates. *Electrochemical and Solid-State Letters*, 12, H195–H197.
173. Krivec, M., et al. (2018). Inkjet printing of multi-layered, via-free conductive coils for inductive sensing applications. *Microsystem Technology*, 24, 2673–2682.
174. Mu, Q., et al. (2018). Intense pulsed light sintering of thick conductive wires on elastomeric dark substrate for hybrid 3D printing applications. *Smart Materials and Structures*, 27, 115007.
175. Gu, H., et al. (2019). Carbon nanospheres induced high negative permittivity in nanosilver-polydopamine metacomposites. *Carbon*, 147, 550–558.
176. Guo, Y., et al. (2019). Constructing fully carbon-based fillers with hierarchical structure to fabricate highly thermally conductive polyimide nanocomposites. *Journal of Materials Chemistry C*, 7, 7035–7044.
177. Guo, Y., et al. (2019). Reduced graphene oxide heterostructured silver nanoparticles significantly enhanced thermal conductivities in hot-pressed electrospun polyimide nanocomposites. *ACS Applied Materials & Interfaces*, 11, 25465–25473.
178. He, Y., et al. (2019). Friction and wear of MoO<sub>3</sub>/graphene oxide modified glass fiber reinforced epoxy nanocomposites. *Macromolecular Materials and Engineering*, 304, 1900166.
179. Huang, C., et al. (2019). Boosted selectivity and enhanced capacity of As (V) removal from polluted water by triethylenetetramine activated lignin-based adsorbents. *International Journal of Biological Macromolecules*, 140, 1167–1174.
180. Jiang, D., et al. (2019). Flexible sandwich structural strain sensor based on silver nanowires decorated with self-healing substrate. *Macromolecular Materials and Engineering*, 304, 1900074.
181. Liu, M., et al. (2017). Extraordinary rate capability achieved by a 3D “skeleton/skin” carbon aerogel–polyaniline hybrid with vertically aligned pores. *Chemical Communications*, 53, 2810–2813.
182. Ma, L., et al. (2019). Reinforcing carbon fiber epoxy composites with triazine derivatives functionalized graphene oxide modified sizing agent. *Composites Part B: Engineering*, 176, 107078.
183. Ma, L., et al. (2019). Enhancing interfacial strength of epoxy resin composites via evolving hyperbranched amino-terminated POSS on carbon fiber surface. *Composites Science and Technology*, 170, 148–156.
184. Shi, Z., et al. (2019). Synthesis and characterization of porous tree gum grafted copolymer derived from Prunus cerasifera gum polysaccharide. *International Journal of Biological Macromolecules*, 133, 964–970.
185. Xu, G., et al. (2019). Structural characterization of lignin and its carbohydrate complexes isolated from bamboo (*Dendrocalamus sinicus*). *International Journal of Biological Macromolecules*, 126, 376–384.
186. Yang, J., et al. (2019). Synergistically toughening polyoxymethylene by methyl methacrylate–butadiene–styrene copolymer and thermoplastic polyurethane. *Macromolecular Chemistry and Physics*, 220, 1800567.
187. Zhang, Y., et al. (2019). Metal-free energy storage systems: Combining batteries with capacitors based on a methylene blue functionalized graphene cathode. *Journal of Materials Chemistry A*, 7, 19668–19675.
188. Zhu, G., et al. (2019). Poly (vinyl butyral)/graphene oxide/poly (methylhydrosiloxane) nanocomposite coating for improved aluminum alloy anticorrosion. *Polymer*, 172, 415–422.
189. Devaraj, H., & Malhotra, R. (2019). Scalable forming and flash light sintering of polymer-supported interconnects for surface-conformal electronics. *Journal of Manufacturing Science and Engineering*, 141, 041014.
190. Gaynor, W., Burkhard, G. F., McGehee, M. D., & Peumans, P. J. A. M. (2011). Smooth nanowire/polymer composite transparent electrodes. *Advanced Materials*, 23, 2905–2910.
191. Kwon, Y.-T., et al. (2018). Ultrahigh conductivity and superior interfacial adhesion of a nanostructured, photonic sintered copper membrane for printed flexible hybrid electronics. *ACS Applied Materials & Interfaces*, 10, 44071–44079.
192. Oh, S.-J., et al. (2016). Newly designed Cu/Cu<sub>10</sub>Sn<sub>3</sub> core/shell nanoparticles for liquid phase-photonic sintered copper electrodes: Large-area, low-cost transparent flexible electronics. *Chemistry of Materials*, 28, 4714–4723.
193. Jang, J., et al. (2017). Rapid production of large-area, transparent and stretchable electrodes using metal nanofibers as wirelessly operated wearable heaters. *NPG Asia Materials*, 9, e432.
194. Ding, S., et al. (2015). Fast fabrication of copper nanowire transparent electrodes by a high intensity pulsed light sintering technique in air. *Physical Chemistry Chemical Physics*, 17, 31110–31116.
195. Hwang, H.-J., et al. (2018). Rapid pulsed light sintering of silver nanowires on woven polyester for personal thermal management with enhanced performance, durability and cost-effectiveness. *Scientific Reports*, 8, 17159.
196. Shen, C., et al. (2019). Brain-like navigation scheme based on MEMS-INS and place recognition. *Applied Sciences*, 9, 1708.
197. Berndt, A. J., et al. (2019). Poly (sulfur-random-(1, 3-diisopropenylbenzene)) based mid-wavelength infrared polarizer:

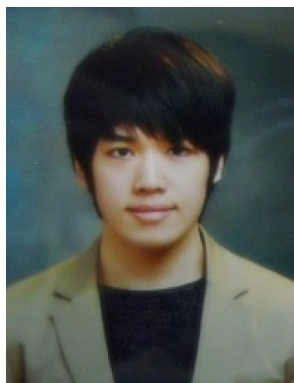
Optical property experimental and theoretical analysis. *Polymer*, 176, 118–126.

198. Gu, H., et al. (2019). Controllable organic magnetoresistance in polyaniline coated poly (p-phenylene-2, 6-benzobisoxazole) short fibers. *Chemical Communications*, 55, 10068–10071.
199. Yang, P., et al. (2019). Anchoring carbon nanotubes and post-hydroxylation treatment enhanced Ni nanofiber catalysts towards efficient hydrous hydrazine decomposition for effective hydrogen generation. *Chemical Communications*, 55, 9011–9014.
200. Shi, Z., et al. (2019). Optimization of epoxy-pinane synthesis by silicotungstic acid supported on SBA-15 catalyst using response surface methodology. *Science of Advanced Materials*, 11, 699–707.
201. Shi, Z., et al. (2019). Preparation and characterization of mesoporous CuO/ZSM-5 catalysts for automotive exhaust purification. *Science of Advanced Materials*, 11, 1198–1205.
202. Lin, B., et al. (2019). Surface intercalated spherical MoS<sub>2</sub> (1-x) nanocatalysts for highly efficient and durable hydrogen evolution reactions. *Dalton Transactions*, 48, 8279–8287.
203. Lin, Z., et al. (2019). Facile preparation of 1T/2H-Mo (S1-xSex) 2 nanoparticles for boosting hydrogen evolution reaction. *ChemCatChem*, 11, 2217–2222.
204. Zhai, Y., et al. (2019). Highly efficient cobalt nanoparticles anchored porous N-doped carbon nanosheets electrocatalysts for Li-O<sub>2</sub> batteries. *Journal of Catalysis*, 377, 534–542.
205. Le, K., et al. (2019). MOF-derived hierarchical core-shell hollow iron-cobalt sulfides nanoarrays on Ni foam with enhanced electrochemical properties for high energy density asymmetric supercapacitors. *Electrochimica Acta*, 323, 134826.
206. Ren, J., et al. (2019). Suppressing charge recombination and ultraviolet light degradation of perovskite solar cells using silicon oxide passivation. *ChemElectroChem*, 6, 3167–3174.
207. Le, K., et al. (2019). Sandwich-like NiCo layered double hydroxide/reduced graphene oxide nanocomposite cathodes for high energy density asymmetric supercapacitors. *Dalton Transactions*, 48, 5193–5202.
208. Ma, Y., et al. (2019). Three-dimensional core-shell Fe<sub>3</sub>O<sub>4</sub>/Polyaniline coaxial heterogeneous nanonets: Preparation and high performance supercapacitor electrodes. *Electrochimica Acta*, 315, 114–123.
209. Liang, T., et al. (2019). Experimental study on thermal expansion coefficient of composite multi-layered flaky gun propellants. *Composites Part B: Engineering*, 166, 428–435.
210. Sun, H., et al. (2019). Zinc oxide/vanadium pentoxide heterostructures with enhanced day-night antibacterial activities. *Journal of Colloid and Interface Science*, 547, 40–49.
211. Han, C. J., Park, B.-G., Oh, M. S., Jung, S.-B., & Kim, J.-W. (2017). Photo-induced fabrication of Ag nanowire circuitry for invisible, ultrathin, conformable pressure sensors. *Journal of Materials Chemistry C*, 5, 9986–9994.

**Publisher's Note** Springer Nature remains neutral with regard to jurisdictional claims in published maps and institutional affiliations.



**Yong-Rae Jang** He is currently a Ph.D. Candidate in the Department of Mechanical Engineering at Hanyang University in South Korea. His research interests include printed electronics, transparent electrodes, and semiconductor manufacturing & packaging technology.



**Sung-Jun Joo** He received his Ph.D. degree of the Department of Mechanical Engineering at Hanyang University in South Korea in 2019. His research interests include printed electronics, composite modeling & analysis, and semiconductor manufacturing & packaging technology.



**Ji-Hyeon Chu** He received his Master's degree in the Department of Mechanical Engineering at Hanyang University in South Korea in 2019. His research interests include printed electronics, and silicon solar cells.



**Hui-Jin Uhm** She is currently a Master's degree Candidate in the Department of Mechanical Engineering at Hanyang University in South Korea. Her research interests include printed electronics, composite modeling & analysis.



**Jong-Whi Park** He is currently a Ph.D Candidate in the Department of Mechanical Engineering at Hanyang University in South Korea. His research interests include printed electronics, transparent electrodes and flexible semiconductor manufacturing.



**Myeong-Hyeon Yu** He is currently a Ph.D. Candidate in the Department of Mechanical Engineering at Hanyang University in South Korea. His research interests include printed electronics, composite modeling and nuclear fuel performance.



**Chung-Hyeon Ryu** He received his Master's degree in the Department of Mechanical Engineering at Hanyang University in South Korea in 2015. He also received his Ph.D. degree of the Department of Mechanical Engineering at Hanyang University in South Korea in 2019. His research interests include printed electronics, solar cells, and semiconductor manufacturing & packaging technology.



**Hak-Sung Kim** He is a professor in the Department of Mechanical Engineering at Hanyang University in South Korea since 2010. His research interests include structural composite, printed electronics, nondestructive evaluation with terahertz and semiconductor packaging technology.